J. Fluid Mech. (2014), *vol.* 753, *pp.* 307–359. © Cambridge University Press 2014
doi:10.1017/jfm.2014.365

The generalized Onsager model for a binary gas mixture

V. Kumaran[1,†] and S. Pradhan[2,‡]

[1]Department of Chemical Engineering, Indian Institute of Science, Bangalore 560 012, India

[2]Chemical Technology Group, Bhabha Atomic Research Centre, Mysore 571 130, India

(Received 31 August 2013; revised 20 November 2013; accepted 24 June 2014;
first published online 23 July 2014)

The Onsager model for the secondary flow field in a high-speed rotating cylinder is extended to incorporate the difference in mass of the two species in a binary gas mixture. The base flow is an isothermal solid-body rotation in which there is a balance between the radial pressure gradient and the centrifugal force density for each species. Explicit expressions for the radial variation of the pressure, mass/mole fractions, and from these the radial variation of the viscosity, thermal conductivity and diffusion coefficient, are derived, and these are used in the computation of the secondary flow. For the secondary flow, the mass, momentum and energy equations in axisymmetric coordinates are expanded in an asymptotic series in a parameter $\epsilon = (\Delta m/m_{av})$, where Δm is the difference in the molecular masses of the two species, and the average molecular mass m_{av} is defined as $m_{av} = (\rho_{w1}m_1 + \rho_{w2}m_2)/\rho_w$, where ρ_{w1} and ρ_{w2} are the mass densities of the two species at the wall, and $\rho_w = \rho_{w1} + \rho_{w2}$. The equation for the master potential and the boundary conditions are derived correct to $O(\epsilon^2)$. The leading-order equation for the master potential contains a self-adjoint sixth-order operator in the radial direction, which is different from the generalized Onsager model (Pradhan & Kumaran, *J. Fluid Mech.*, vol. 686, 2011, pp. 109–159), since the species mass difference is included in the computation of the density, viscosity and thermal conductivity in the base state. This is solved, subject to boundary conditions, to obtain the leading approximation for the secondary flow, followed by a solution of the diffusion equation for the leading correction to the species mole fractions. The $O(\epsilon)$ and $O(\epsilon^2)$ equations contain inhomogeneous terms that depend on the lower-order solutions, and these are solved in a hierarchical manner to obtain the $O(\epsilon)$ and $O(\epsilon^2)$ corrections to the master potential. A similar hierarchical procedure is used for the Carrier–Maslen model for the end-cap secondary flow. The results of the Onsager hierarchy, up to $O(\epsilon^2)$, are compared with the results of direct simulation Monte Carlo simulations for a binary hard-sphere gas mixture for secondary flow due to a wall temperature gradient, inflow/outflow of gas along the axis, as well as mass and momentum sources in the flow. There is excellent agreement between the solutions for the secondary flow correct to $O(\epsilon^2)$ and the simulations, to within 15 %, even at a Reynolds number as low as 100, and length/diameter ratio as low as 2, for a low stratification parameter $\mathscr{A}$ of 0.707, and when the secondary flow velocity is as high as 0.2 times the maximum base flow velocity, and the ratio $2\Delta m/(m_1 + m_2)$ is as high as 0.5. Here, the Reynolds number $Re = \rho_w \Omega R^2/\mu$, the

† Email address for correspondence: kumaran@chemeng.iisc.ernet.in

‡ This work forms part of the PhD Thesis of Sahadev Pradhan, Indian Institute of Science, 2014.

https://doi.org/10.1017/jfm.2014.365 Published online by Cambridge University Press

stratification parameter $\mathscr{A} = \sqrt{m\Omega^2R^2/(2k_BT)}$, R and Ω are the cylinder radius and angular velocity, m is the molecular mass, ρ_w is the wall density, μ is the viscosity and T is the temperature. The leading-order solutions do capture the qualitative trends, but are not in quantitative agreement.

Key words: compressible flows, molecular dynamics, rarefied gas flow

1. Introduction

Centrifugal gas separation processes effect separation by utilizing the difference in the mole fraction in a high-speed rotating cylinder caused by the difference in molecular mass, and consequently the centrifugal force density. These have been widely used in isotope separation because chemical separation methods cannot be used to separate isotopes of the same chemical species. An important application is the separation of trace radioactive isotopes of metals (molybdenum, tellurium, iridium, cadmium, technetium, indium, etc.) for medical imaging, as well as use in non-destructive testing using gamma cameras. These are also used in the nuclear industry in the separation of uranium isotopes for power generation, as well as zinc isotopes for corrosion resistance. More recently, centrifugal separation has also been explored for the separation of gases such as carbon dioxide and methane. This separation is of great commercial importance in the natural gas industry, because natural gas reserves are often contaminated with small amounts of carbon dioxide and hydrogen sulphide, and gas reserves with even 10 % carbon dioxide and 1 % hydrogen sulphide cannot be economically exploited. Even though this separation involves different gas species that can be chemically separated, chemical separation typically involves organic solvents for scrubbing one of the species, and these solvents are expensive and are not environmentally friendly. Moreover, the large mass difference increases the difference in the centrifugal force density between the two species, and thereby the efficiency of the centrifugal separation process. Current studies seem to indicate that centrifugal separation is still not an economical option, though the feasibility studies are hindered by the lack of good analytical models for the centrifugal separation of gases of very different molecular masses.

As discussed below, the Onsager model traditionally used for centrifugal separation assumes equal molecular masses for the two species in the flow analysis. This is a good assumption for isotope separation, where the difference in molecular masses is typically 100 times less than the average molecular mass, but is not a good assumption for separation of dissimilar gases such as carbon dioxide and methane. The objective of the present analysis is to examine the approximations in the Onsager model due to the assumption of equal mass, and propose a method for systematically correcting these approximations in order to make the model applicable to the separation of dissimilar gases. The analysis is compared with results from molecular simulations for hard-sphere gases using the direct simulation Monte Carlo (DSMC) procedure (Bird 1994).

The Onsager model is extensively used for the simulation of high-speed rotating flows (Wood & Morton 1980; Gunzburger & Wood 1982; Viecelli 1983; Wood & Sanders 1983; Gunzburger, Wood & Jordan 1984; Wood, Jordan & Gunzburger 1984; Wood, Mason & Soubbaramayer 1996; Pradhan & Kumaran 2011) owing to its clever reduction of the complicated mass, momentum and energy equations to a relatively

https://doi.org/10.1017/jfm.2014.365 Published online by Cambridge University Press

simple sixth-order equation for the 'master potential'. In a high-speed rotating cylinder, the base flow is a solid-body rotation, where the angular velocity is a constant throughout the cylinder, and the pressure gradient for each gas species is balanced by the centrifugal force density. The difference in the centrifugal force densities due to the molecular mass difference causes a variation in the mole fraction across the cylinder, with the higher-molecular-weight species preferentially concentrated near the wall. However, for separation of the two species, it is necessary to have inserts for inflow/outflow of gas, and there typically are temperature gradients at the wall as well. These different types of external forcing cause a secondary flow in the cylinder. This secondary flow has a strong effect on the efficiency of separation, and it is important to formulate accurate models for the secondary flow.

A complete flow simulation involves the solution of the compressible mass, momentum and energy equations for the gas velocity in the cylinder, along with the ideal gas equation of state. There have been previous numerical simulations of axisymmetric flows in a high-speed rotating cylinder (Lahargue & Soubbaramayer 1978; Soubbaramayer & Billet 1980; Berger 1987). Apart from the complicated formulation of the differential equations for five variables (density, three components of velocity and temperature), there are two important conceptual difficulties in the numerical solution of the continuum equations. The flow in the cylinder is usually at high Mach number, where the secondary flow is restricted to a region of thickness $Re^{-1/3}R$ smaller than the cylinder diameter, where $Re = \rho_w \Omega R^2/\bar{\mu}$ is the Reynolds number based on the mean density at the wall ρ_w, the cylinder radius R and angular velocity Ω and the viscosity for the base state μ. While the continuum approximation is valid in the radial boundary layer, the density in the central region is sufficiently small that the flow is in the free-molecular regime. There is no simple way to determine the boundary between the continuum and free-molecular regimes, and to prescribe boundary conditions at this boundary. Another important issue is the modelling of the wall slip in the simulations. While the no-slip conditions are applicable to low-Mach-number flows, there is usually a substantial slip velocity at the wall, which needs to be modelled in continuum simulations.

An alternative is to use a molecular simulation procedure. In the DSMC procedure, the Boltzmann equation is simulated using a probabilistic Monte Carlo procedure to obtain the velocity distribution function, and the density, velocity and temperature are obtained by taking moments of the distribution function. Here, one 'simulated' molecule represents a large number of real molecules, and the collision probability is chosen in such a manner that the collision frequency, mean free path and temperature of the simulated molecules are equal to those for the real molecules. This procedure can be used for the simulation of both the rarefied gas regime and the continuum regime, and this has been used previously for centrifugal flows (Roberts 1985; Roberts & Hausman 1988; Pradhan & Kumaran 2011). However, these simulations are computationally intensive, owing to the requirement of having a large number of simulated molecules in each differential volume in order to reduce statistical fluctuations.

The Onsager model, which is considerably simpler than the solution of the continuum equation, even admits analytical solutions in some cases, and can be solved using separation of variables in the cases of sources and sinks within the flow. The analytical solution is in error, of course, in the high-Knudsen-number regime owing to the breakdown of the continuum approximation. However, the density and the secondary mass flux decrease as the inverse of the exponential of the distance from the wall where the local Knudsen number (proportional to the inverse of the

https://doi.org/10.1017/jfm.2014.365 Published online by Cambridge University Press

number density) is large, resulting in a negligible contribution to the secondary flux in the cylinder from the high-Knudsen-number regions where the analytical solution is not valid. So the analytical solution has the advantage of being accurate in the low-Knudsen-number regions where the secondary flux is largest, while at the same time giving a uniform approximation throughout the domain. The starting point for the Onsager model is the mass, momentum and energy conservation equations for a rotating gas. The solid-body rotation with a constant angular velocity and temperature is considered to be the base state, and the equations are linearized about the base state on the assumption that the secondary flow velocity is much smaller than the velocity of rotation of the cylinder. The equations for an axisymmetric flow are reduced to one sixth-order equation for the 'master potential' for the radial boundary layer. Since the operator, with the prescribed boundary conditions, is self-adjoint, it can be solved using the separation-of-variables procedure, leading to an eigenfunction expansion (Wood & Morton 1980; Pradhan & Kumaran 2011). It is also possible to solve the equation using the finite-difference (Viecelli 1983) or finite-element (Gunzburger & Wood 1982; Gunzburger *et al.* 1984) methods.

The Onsager model is not valid at the end-caps of the cylinder where there is a radial flow in a thin axial boundary layer. Here, procedures similar to derivation of the Onsager model, but with the assumption that the 'axial boundary layer' is much smaller than the cylinder radius, have been used to derive the 'Carrier–Maslen' model (Olander 1981), which is a fourth-order differential equation for the stream function. This has been solved to obtain the flow profiles at the end-caps.

Though the Onsager and Carrier–Maslen models are simple and elegant, there are significant approximations. It is assumed that the length of the cylinder is much greater than the diameter, so that the axial variations can be neglected away from the end-caps. The model is restricted to the limit of high Reynolds number and high stratification parameter (stratification parameter based on rotation velocity and speed of sound based on gas density and temperature at the wall), where the radial boundary layer thickness is small compared to the cylinder radius. Here, the stratification parameter $\mathscr{A} = \sqrt{m\Omega^2R^2/(2k_BT)}$ and the Reynolds number $Re = \rho_w\Omega R^2/\mu$, where m is the molecular mass, Ω is the angular velocity of the cylinder, R is the cylinder radius, ρ_w is the wall density, μ is the viscosity and T is the temperature. The difference in molecular masses of the two species is neglected in the secondary flow calculation, though the predicted flow velocities are subsequently used in the equations for the species mole fractions. When the difference in molecular mass is neglected and the temperature is considered a constant in the base state, the thermal conductivity and viscosity are also a constant, and the pressure decreases exponentially with distance from the wall.

The generalized Onsager and Carrier–Maslen models (Pradhan & Kumaran 2011) were formulated where the approximation of high stratification parameter was relaxed. In this case, a generalized sixth-order operator was derived, which is applicable even when the stratification parameter is $O(1)$, though the assumption of high Reynolds number was made. This operator is also self-adjoint, with real eigenvalues and orthogonal eigenfunctions, though these have to be determined numerically. For the secondary flow, it was found that the predictions of the generalized Onsager model were in very good agreement with DSMC results even when the Reynolds number is as low as 100 and the length/diameter ratio is as low as 2. However, this model retains the assumption that the molecular masses of the two species are equal while calculating the secondary flow.

https://doi.org/10.1017/jfm.2014.365 Published online by Cambridge University Press

Here, we examine how the species mass difference can be incorporated into the Onsager model to make it applicable to systems where the difference in molecular masses is not much smaller than the average molecular mass. In the base state, the flow is considered to be a solid-body rotation with constant temperature, but the variation in the mole fraction is taken into account. Because of this, there is a variation in the viscosity and thermal conductivity in the radial direction. In addition, the total pressure is written as the sum of the partial pressures of the two species, and is not approximated as an exponential function of the distance from the wall. The dilute gas equation of state is used for the pressure, while the Chapman–Enskog expressions (Chapman & Cowling 1970) for hard-sphere gases are used for the thermal conductivity and viscosity.

In the analysis of the secondary flow, the equation for the master potential is expanded in an asymptotic series in the parameter $\epsilon = \Delta m/m_{av}$, where Δm is the difference in the molecular masses of the two species, and m_{av} is a suitably defined average molecular mass. The leading-order equation and boundary conditions for the master potential are nearly identical to the sixth-order differential equation of the generalized Onsager model (Pradhan & Kumaran 2011). The important differences are that the density is not assumed to decrease exponentially from the wall, but the actual species densities are used, and the radial variation in the viscosity and thermal conductivity due to the variation in mole fraction are incorporated. The mean velocity and temperature obtained by solving the leading-order equations are used in the species balance equations for the mole fractions of the two species, and the corrections for the number density and mass density of the two species due to the secondary flow are obtained. These appear as inhomogeneous terms in the equation for the $O(\epsilon)$ correction for the master potential; this equation is solved with appropriate boundary conditions to obtain the $O(\epsilon)$ correction to the master potential and flow velocity. This is then used in the $O(\epsilon)$ contribution to the species balance equation, and the hierarchical procedure is repeated until the $O(\epsilon^2)$ correction to the secondary flow velocity and mole fraction are calculated. A similar hierarchical procedure is used for the Carrier–Maslen model for the end-cap boundary layers.

The results of the Onsager hierarchy, up to $O(\epsilon^2)$, are compared with the results of DSMC simulations for the axisymmetric flow of a two-species hard-sphere molecular gas. The constitutive relations for mass diffusion, viscosity and heat conduction predicted by the DSMC simulations are compared with the Chapman–Enskog expressions (Chapman & Cowling 1970) in order to validate the constitutive relations used in the analysis. After this, the results of the $O(\epsilon^2)$ Onsager hierarchy for the secondary flow are compared with DSMC simulations for three types of forcing, a wall temperature gradient, inflow/outflow of gas along the axis, and mass/momentum input due to inserts within the flow.

2. Formulation

A cylindrical (r, θ, z) coordinate system is used to analyse the flow in a rotating cylinder of radius R and height Z with constant angular velocity Ω. The flow is assumed to be axisymmetric, and there is no dependence on the meridional coordinate θ. We consider a binary gas mixture with number densities (n_1, n_2) and molecular masses (m_1, m_2). The mole fractions are denoted $N_1 = (n_1/n)$ and $N_2 = (n_2/n)$. The densities of the two species are $\rho_1 = m_1 n_1$ and $\rho_2 = m_2 n_2$, while the total density is $\rho = \rho_1 + \rho_2$. The flux of species 1 in a binary mixture is given by (Chapman & Cowling 1970)

$$\boldsymbol{j}_1 = -\frac{D_{12} n m_1 m_2}{N_1 m_1 + N_2 m_2}(\boldsymbol{d}_{12} + k_T \boldsymbol{\nabla}(\log_e T)), \tag{2.1}$$

https://doi.org/10.1017/jfm.2014.365 Published online by Cambridge University Press

where k_T is the thermal diffusion coefficient, and $\boldsymbol{d}_{12}$ is,

$$\boldsymbol{d}_{12} = \nabla N_1 + \frac{N_1 N_2 (m_2 - m_1)}{\rho k_B T} \nabla p. \tag{2.2}$$

It is appropriate to express $D_{12} = (D'_{12}/n)$, since D_{12} is proportional to the inverse of the total number density, to obtain

$$\boldsymbol{j}_1 = -\frac{m_1 m_2 D'_{12}}{N_1 m_1 + N_2 m_2} (\boldsymbol{d}_{12} + k_T \nabla (\log_e T)), \tag{2.3}$$

where D'_{12} is a function only of temperature, and is independent of the total number density.

The flux is written as the sum of the mean flux in the absence of secondary flow $\bar{\boldsymbol{j}}$, and the perturbation due to the secondary flow, $\hat{\boldsymbol{j}}$. In the following analysis, the overbar $\bar{\star}$ always represents the mean quantities in the absence of secondary flow, and the hat $\hat{\star}$ is the perturbation due to the secondary flow. The base flow is a solid-body rotation about the axis, with a radial gradient in the density and the mole fractions due to the centrifugal forces. The fluxes are zero, and the gradient of the pressure is given by the centrifugal force density, $\bar{\rho}\Omega^2 r$. The expression for the flux in the base state is

$$\bar{\boldsymbol{j}}_1 = -\frac{m_1 m_2 D'_{12}}{\bar{N}_1 m_1 + \bar{N}_2 m_2} \left(\nabla \bar{N}_1 - \frac{\bar{N}_1 \bar{N}_2 \Delta m}{\bar{\rho} k_B \bar{T}} \nabla \bar{p} \right), \tag{2.4}$$

where $\Delta m = m_1 - m_2$. In the base state, the fluxes are zero, and the gradient of the pressure is given by the centrifugal force density, $\bar{\rho}\Omega^2 r$. Since there are only radial variations in the base state, the zero-flux condition reduces to

$$\frac{\mathrm{d}\bar{N}_1}{\mathrm{d}r} - \frac{\bar{N}_1 \bar{N}_2 \Delta m \Omega^2 r}{k_B \bar{T}} = 0, \tag{2.5}$$

where the radial momentum balance equation

$$\frac{\partial \bar{p}}{\partial r} = \bar{\rho}\Omega^2 r \tag{2.6}$$

is used to substitute for the pressure gradient.

Equation (2.5) is solved to obtain the mole fraction of the two components, subject to the condition for the total holdup for each component,

$$2\pi \int_0^R r \, \mathrm{d}r \, m_i \bar{n}_i = \mathscr{M}_i, \tag{2.7}$$

where $\mathscr{M}_i$ is the mass holdup of the ith component per unit length of the cylinder. With this condition, the expressions for the molar and mass densities and the mole fraction are

$$\bar{n}_i = \bar{n}_{wi} \exp(-m_i \Omega^2 (R^2 - r^2)/2k_B \bar{T}), \tag{2.8}$$

$$\bar{\rho}_i = \bar{\rho}_{wi} \exp(-m_i \Omega^2 (R^2 - r^2)/2k_B \bar{T}), \tag{2.9}$$

$$\bar{N}_i = \frac{\bar{n}_{wi} \exp(-m_i \Omega^2 (R^2 - r^2)/2k_B \bar{T})}{\sum_{j=1}^{2} \bar{n}_{wj} \exp(-m_j \Omega^2 (R^2 - r^2)/2k_B \bar{T})}, \tag{2.10}$$

https://doi.org/10.1017/jfm.2014.365 Published online by Cambridge University Press

where

$$\bar{n}_{wi} = \frac{\mathscr{M}_i \Omega^2 \exp\left(m_i \Omega^2 R^2 / 2k_B \bar{T}\right)}{2\pi k_B \bar{T}\left(\exp\left(m_i \Omega^2 R^2 / 2k_B \bar{T}\right) - 1\right)}, \tag{2.11}$$

$$\bar{\rho}_{wi} = \frac{\mathscr{M}_i m_i \Omega^2 \exp\left(m_i \Omega^2 R^2 / 2k_B \bar{T}\right)}{2\pi k_B \bar{T}\left(\exp\left(m_i \Omega^2 R^2 / 2k_B \bar{T}\right) - 1\right)}. \tag{2.12}$$

The calculation of the number density for a multi-component system is a little more complicated. However, it can easily be verified that the solutions (2.10) and (2.12) are still valid for a multi-component system, when the summations are taken over all components.

Expressions for the mixture viscosity, thermal conductivity, diffusion coefficient and thermal diffusion coefficient (Chapman & Cowling 1970) are listed in equations (A 1) in appendix A. In the base state, the temperature is a constant and all the coefficients in (A 1) (which are listed in (A 4) to (A 21)) are independent of position. Therefore, the position dependence of the transport coefficients in (A 1) is due only to the dependence of the mole fractions N_1 and N_2 on position in the base state.

In the following analysis, the species masses are defined in terms of the average mass and the mass difference,

$$m_{av} = b_1 m_1 + b_2 m_2, \tag{2.13}$$

$$\Delta m = m_1 - m_2 = \epsilon m_{av}. \tag{2.14}$$

Here, the parameter $\epsilon = \Delta m / m_{av}$ is used as the small parameter for the asymptotic expansion of the Onsager equation. The individual masses can now be represented in terms of the average mass and the mass difference,

$$m_1 = m_{av} + b_2 \Delta m, \tag{2.15}$$

$$m_2 = m_{av} - b_1 \Delta m. \tag{2.16}$$

The above expressions for the individual molecular masses are used to obtain corrections to the Onsager equation and the flux equations in the parameter Δm. The expression (2.13) for the average mass can be used for different averages, such as the arithmetic average ($b_1 = b_2 = 0.5$), mass average ($b_1 = m_1 \bar{N}_1 / (m_1 \bar{N}_1 + m_2 \bar{N}_2)$, $b_2 = m_2 \bar{N}_2 / (m_1 \bar{N}_1 + m_2 \bar{N}_2)$) or mole average ($b_1 = \bar{N}_1$, $b_2 = \bar{N}_2$), or any other type of average depending on the situation, where $\bar{N}_1$ and $\bar{N}_2$ are the average mole fractions. The only restriction is that the averages should be based on the total mass/molar holdup, and not on the local mass/mole fractions, with the restriction $b_1 + b_2 = 1$. Here, we define the average mass as $m_{av} = (\rho_{w1} m_1 + \rho_{w2} m_2)/\rho_w$, where ρ_{w1} and ρ_{w2} are the mass densities of the two species at the wall, and $\rho_w = \rho_{w1} + \rho_{w2}$. The reason for this choice is discussed after (3.27).

In the generalized Onsager model, the difference in molecular mass is neglected, and the number and mass densities for the solid-body rotation (2.10) are independent of the radial position. Since the temperature is also uniform, the viscosity and thermal conductivity in (A 1) are independent of radial position. In most of the analysis, we do not explicitly expand $\bar{\mu}$, $\bar{K}$, $\bar{\rho}$, $\bar{\rho}_i$ and $\bar{N}_i$ in a series in ϵ, since it is easier to solve the equation for the master potential using the forms (2.10) for the mass density and mole fraction, and (A 1) for the viscosity and thermal conductivity. However, at select locations in the analysis, an expansion is used in order to recover an equation similar in form to the generalized Onsager equation as the leading approximation of the hierarchy of equations. In all cases where the expansion is used, terms correct to $O(\epsilon^2)$ in the expansion are retained in the analysis.

https://doi.org/10.1017/jfm.2014.365 Published online by Cambridge University Press

The dimensionless parameters used in the analysis are as follows. The stratification parameter is defined on the basis of the average mass and the mean temperature, and is proportional to the ratio of the linear wall velocity and the speed of sound at the wall,

$$\mathscr{A} = \sqrt{\frac{m_{av}\Omega^2 R^2}{2k_B\bar{T}}} \propto \frac{R\Omega}{c_s}, \tag{2.17}$$

where $c_s = \sqrt{\gamma k_B \bar{T}/m_{av}}$. The wall density and viscosity at the wall are used to define the Reynolds number,

$$Re = \frac{\bar{\rho}_w \Omega R^2}{\bar{\mu}_w}, \tag{2.18}$$

where $\bar{\mu}_w$ is the viscosity at the wall in the base state. The other dimensionless groups used are the Prandtl number, Schmidt number and the ratio of specific heats,

$$Pr = \frac{C_p \bar{\mu}_w}{\bar{K}_w}, \tag{2.19}$$

$$Sc = \frac{\bar{\mu}_w}{m_{av}\bar{D}'_w}, \tag{2.20}$$

$$\gamma = \frac{C_p}{C_v}, \tag{2.21}$$

which are $O(1)$ for an ideal gas. Here, $\bar{K}_w$ is the thermal conductivity in the base flow at the wall, $\bar{D}'_w$ is the value of the diffusion coefficient D'_{12} at the temperature $\bar{T}$ in the base state, and at the mole fraction N_{1w} at the wall, and C_p and C_v are the specific heats at constant pressure and volume, respectively. Finally, the scaled radial coordinate in the analysis is defined as

$$\xi = \frac{m_{av}\Omega^2(R^2 - r^2)}{2k_B\bar{T}} = \mathscr{A}^2\left(1 - \frac{r^2}{R^2}\right), \tag{2.22}$$

where $\mathscr{A}$ is the stratification parameter (2.17).

In all the following analysis, all variables are expressed as $\star = \bar{\star} + \hat{\star}$, where $\bar{\star}$ is the value in the base flow (solid-body rotation), and $\hat{\star}$ is the additional contribution due to the secondary flow. All equations are then linearized in the perturbation variables $\hat{\star}$. In the base flow, the mean velocity $\bar{\boldsymbol{v}} = R\Omega \boldsymbol{e}_\theta$, where $\boldsymbol{e}_\theta$ is the unit vector in the θ direction. The flux $\bar{\boldsymbol{j}}_i = 0$ for the solid-body rotation reduces to (2.5) for the radial flux, and the solution is (2.10) for the mass density and mole fraction. The equation for the perturbation to the flux due to the secondary flow is

$$\boldsymbol{\nabla} \cdot \hat{\boldsymbol{j}}_1 + \boldsymbol{\nabla} \cdot (\bar{\rho}_1 \hat{\boldsymbol{v}}) = 0, \tag{2.23}$$

where the linear approximation for the perturbation to the flux is

$$\hat{\boldsymbol{j}}_1 = -\frac{m_1 m_2 \bar{D}'_{12}}{\bar{N}_1 m_1 + \bar{N}_2 m_2}\left(\boldsymbol{\nabla}\hat{N}_1 - \frac{\Delta m \Omega^2 r \boldsymbol{e}_r}{k_B\bar{T}}\left((\bar{N}_2 - \bar{N}_1)\hat{N}_1 - \frac{\hat{T}}{\bar{T}} - \frac{\hat{\rho}}{\bar{\rho}}\right) - \frac{\Delta m \bar{N}_1 \bar{N}_2 \boldsymbol{\nabla}\hat{p}}{\bar{\rho} k_B \bar{T}} + \frac{k_T \boldsymbol{\nabla}\hat{T}}{\bar{T}}\right), \tag{2.24}$$

where $\bar{D}'_{12}$ is the value of D'_{12} for $T = \bar{T}$. Here, we have used the pressure gradient $\boldsymbol{\nabla}\bar{p} = \bar{\rho}\Omega^2 r \boldsymbol{e}_r$ in the base state, where $\boldsymbol{e}_r$ is the unit vector in the radial direction.

https://doi.org/10.1017/jfm.2014.365 Published online by Cambridge University Press

The perturbation (2.24) is inserted into the balance (2.23), and the mass difference is defined in terms of the small parameter $\epsilon = \Delta m/m_{av}$, to obtain

$$\frac{1}{r}\frac{\partial}{\partial r}\left[\frac{m_1 m_2 \bar{D}'_{12} r}{m_1\bar{N}_1 + m_2\bar{N}_2}\left(\frac{\partial \hat{N}_1}{\partial r} + \frac{\epsilon m_{av}\bar{N}_1\bar{N}_2}{\bar{\rho}k_B\bar{T}}\frac{\partial \hat{p}}{\partial r} - \frac{k_T}{\bar{T}}\frac{\partial \hat{T}}{\partial r}\right.\right.$$
$$\left.\left. + \frac{\epsilon m_{av}\Omega^2 r}{k_B\bar{T}}\left(-(\bar{N}_2 - \bar{N}_1)\hat{N}_1 + \frac{\hat{T}}{\bar{T}} + \frac{\hat{\rho}}{\bar{\rho}}\right)\right)\right]$$
$$+ \frac{m_1 m_2 \bar{D}'_{12}}{\bar{N}_1 m_1 + \bar{N}_2 m_2}\left(\frac{\partial^2 \hat{N}_1}{\partial z^2} + \frac{\epsilon m_{av}\bar{N}_1\bar{N}_2}{\bar{\rho}k_B\bar{T}}\frac{\partial^2 \hat{p}}{\partial z^2} - \frac{k_T}{\bar{T}}\frac{\partial^2 \hat{T}}{\partial z^2}\right)$$
$$- \frac{1}{r}\frac{\partial(r\hat{v}_r\bar{\rho}_1)}{\partial r} - \frac{\partial(\hat{v}_z\bar{\rho}_1)}{\partial z} = 0. \tag{2.25}$$

The differential equation (2.25) can be solved using zero-flux boundary conditions at the solid boundary to obtain the correction to the mole fraction $\hat{N}_1$, provided the perturbation to the velocity $\hat{\boldsymbol{v}}$, temperature $\hat{T}$, pressure $\hat{p}$ and density $\hat{\rho}$ are known.

3. Equations of motion

The compressible axisymmetric mass, momentum and energy equations (listed in appendix B) are expressed in terms of the density ρ, the three components of the velocity v_r, v_θ, v_z, the pressure p and the temperature T. The disturbance to the base state due to a temperature gradient at the walls, or due to a flux of mass, momentum or energy, is incorporated by perturbing the base velocity and pressure profile as follows:

$$\rho = \bar{\rho} + \hat{\rho}, \tag{3.1}$$
$$p = \bar{p} + \hat{p}, \tag{3.2}$$
$$T = \bar{T} + \hat{T}, \tag{3.3}$$
$$v_r = \hat{v}_r, \tag{3.4}$$
$$v_\theta = r\Omega + \hat{v}_\theta, \tag{3.5}$$
$$v_z = \hat{v}_z. \tag{3.6}$$

Perturbations of the form given in (3.6) are substituted into the mass, momentum and energy conservation equations, and the resulting equations are linearized in the perturbation (hatted) quantities. Steady state is assumed, so that all the time derivatives are zero. After subtracting the corresponding base state equations, and noting that the density, viscosity and thermal conductivity in the base state are functions of r and independent of z, we obtain the following equations for the mass and momentum:

$$\frac{1}{r}\frac{\partial}{\partial r}(r\bar{\rho}\hat{v}_r) + \frac{\partial}{\partial z}(\bar{\rho}\hat{v}_z) = \mathscr{S}_m, \tag{3.7}$$
$$-\hat{\rho}\Omega^2 r - 2\bar{\rho}\Omega\hat{v}_\theta = -\frac{\partial \hat{p}}{\partial r} + \bar{\mu}\left(\nabla^2\hat{v}_r - \frac{\hat{v}_r}{r^2}\right) + \frac{\bar{\mu}}{3}\left(\frac{\partial(\boldsymbol{\nabla}\cdot\hat{\boldsymbol{v}})}{\partial r}\right)$$
$$- \frac{2}{3}\boldsymbol{\nabla}\cdot\hat{\boldsymbol{v}}\frac{\partial\bar{\mu}}{\partial r} + 2\frac{\partial\hat{v}_r}{\partial r}\frac{\partial\bar{\mu}}{\partial r} + f_r, \tag{3.8}$$

https://doi.org/10.1017/jfm.2014.365 Published online by Cambridge University Press

$$2\bar{\rho}\Omega\hat{v}_r = \frac{1}{r^2}\frac{\partial}{\partial r}\left(r^3\bar{\mu}\frac{\partial}{\partial r}\left(\frac{\hat{v}_\theta}{r}\right)\right) + \bar{\mu}\frac{\partial^2\hat{v}_\theta}{\partial z^2} + f_\theta, \tag{3.9}$$

$$0 = -\frac{\partial\hat{p}}{\partial z} + \bar{\mu}\nabla^2\hat{v}_z + \frac{\bar{\mu}}{3}\frac{\partial(\boldsymbol{\nabla}\cdot\hat{\boldsymbol{v}})}{\partial z} + \frac{\partial\bar{\mu}}{\partial r}\left(\frac{\partial\hat{v}_z}{\partial r} + \frac{\partial\hat{v}_r}{\partial z}\right) + f_z. \tag{3.10}$$

Here we have considered a mass source density $\mathscr{S}_m$ (mass input per unit volume per unit time) in the mass conservation equation (3.7), and force densities f_r, f_θ and f_z in the r, θ and z directions, respectively, in (3.8)–(3.10). The term on the left in (3.8) is the contribution to the r momentum equation due to the centrifugal force, while the term on the left in (3.9) represents the contribution to the θ momentum equation due to the Coriolis force. The energy equation is

$$0 = -\bar{p}\boldsymbol{\nabla}\cdot\hat{\boldsymbol{v}} + \left(\frac{1}{r}\frac{\partial}{\partial r}\left(r\bar{K}\frac{\partial\hat{T}}{\partial r}\right) + \bar{K}\frac{\partial^2\hat{T}}{\partial z^2}\right) + \mathscr{S}_e, \tag{3.11}$$

where $\mathscr{S}_e$ is the energy input per unit volume per unit time. The above equation can be simplified using the mass conservation equation,

$$\begin{aligned}\boldsymbol{\nabla}\cdot\hat{\boldsymbol{v}} &= \frac{\mathscr{S}_m}{\bar{\rho}} - \bar{\rho}^{-1}\hat{\boldsymbol{v}}\cdot\boldsymbol{\nabla}\bar{\rho} \\ &= \frac{\mathscr{S}_m}{\bar{\rho}} - \frac{\hat{v}_r}{\bar{\rho}}\frac{\partial\bar{\rho}}{\partial r},\end{aligned} \tag{3.12}$$

to give

$$0 = \frac{\bar{p}\hat{v}_r}{\bar{\rho}}\frac{\partial\bar{\rho}}{\partial r} + \left(\frac{1}{r}\frac{\partial}{\partial r}\left(r\bar{K}\frac{\partial\hat{T}}{\partial r}\right) + \bar{K}\frac{\partial^2\hat{T}}{\partial z^2}\right) + \mathscr{S}'_e. \tag{3.13}$$

Here, $\mathscr{S}'_e = \mathscr{S}_e - (\bar{p}\mathscr{S}_m/\bar{\rho})$, and $\mathscr{S}_e$ is the energy source. In the energy equation (3.11), the first term on the right is the pressure work done due to the compression or expansion of the gas. In the following analysis, it is important to note that the pressure $\bar{p}$, viscosity $\bar{\mu}$, thermal conductivity $\bar{K}$ and diffusion coefficient $\bar{D}$ in the base state vary only in the radial direction, owing to variations in the mole fraction. In addition, the viscosity, thermal conductivity and $\bar{D}' = \bar{D}\bar{n}$ are independent of the total number density, and they depend only on the temperature and mole fraction. Since the temperature is uniform in the base state, the variation in $\bar{\mu}$, $\bar{K}$ and $\bar{D}$ is due only to the variation in the mole fraction with the radial coordinate.

The perturbation to the equation of state is

$$\frac{\hat{\rho}_1}{m_1} + \frac{\hat{\rho}_2}{m_2} = \frac{\hat{p}}{k_B\bar{T}} - \left(\frac{\bar{\rho}_1}{m_1} + \frac{\bar{\rho}_2}{m_2}\right)\left(\frac{\hat{T}}{\bar{T}}\right). \tag{3.14}$$

Using an expansion in the small parameter $\epsilon = \Delta m/m_{av}$, we obtain

$$\begin{aligned}&\hat{\rho} + \frac{\epsilon(\hat{\rho}_2\bar{\rho}_{w1} - \hat{\rho}_1\bar{\rho}_{w2})}{\bar{\rho}_w} + \frac{\epsilon^2(\hat{\rho}_1\bar{\rho}_{w2}^2 + \hat{\rho}_2\bar{\rho}_{w1}^2)}{\bar{\rho}_w^2} \\ &\quad = \frac{\hat{p}m_{av}}{k_B\bar{T}} - \bar{\rho}\left(1 + \frac{\epsilon^2\bar{\rho}_{w1}\bar{\rho}_{w2}(\xi^2 + 2\xi + 2)}{2\bar{\rho}_w^2}\right)\frac{\hat{T}}{\bar{T}}.\end{aligned} \tag{3.15}$$

In (3.15), there is only one term that depends on the densities of the individual species $\hat{\rho}_1$ and $\hat{\rho}_2$. Since the species mass balance equations are written in terms of the mole

https://doi.org/10.1017/jfm.2014.365 Published online by Cambridge University Press

fraction $\hat{N}_1$ and the total density $\hat{\rho}$, it is necessary to convert the species densities $\hat{\rho}_1$ and $\hat{\rho}_2$ in terms of the total density perturbation $\hat{\rho}$ and the perturbation to the mole fraction $\hat{N}_1$. The perturbation $\hat{\rho}_1$ can be written as

$$\begin{aligned}\hat{\rho}_1 &= m_1(\bar{N}_1\hat{n} + \hat{N}_1\bar{n}) \\ &= m_1\left(\bar{N}_1\left(\frac{\hat{\rho}_1}{m_1} + \frac{\hat{\rho}_2}{m_2}\right) + \hat{N}_1\left(\frac{\bar{\rho}_1}{m_1} + \frac{\bar{\rho}_2}{m_2}\right)\right).\end{aligned} \tag{3.16}$$

The above implicit equation can be solved for $\hat{\rho}_1$. For the present purposes, it is sufficient to obtain an approximate solution up to first order in ϵ,

$$\hat{\rho}_1 = \bar{\rho}\hat{N}_1 + \hat{\rho}\bar{N}_1 + \epsilon(\hat{\rho}\bar{N}_1\bar{N}_2 + \hat{N}_1(\bar{\rho}_2\bar{N}_1 - \bar{\rho}_1\bar{N}_2)), \tag{3.17}$$

and a similar expression can be obtained for $\hat{\rho}_2$. These can be inserted into the term dependent on $\hat{\rho}_1$ and $\hat{\rho}_2$ in (3.15), to obtain, correct to $O(\epsilon^2)$,

$$\begin{aligned}&\frac{\epsilon(\hat{\rho}_2\bar{\rho}_{w1} - \hat{\rho}_1\bar{\rho}_{w2})}{\bar{\rho}_w} + \frac{\epsilon^2(\hat{\rho}_1\bar{\rho}_{w2}^2 + \hat{\rho}_2\bar{\rho}_{w1}^2)}{\bar{\rho}_w^2} \\ &= \epsilon\left(-\hat{N}_1\bar{\rho} + \hat{\rho}\left(\frac{\bar{N}_2\bar{\rho}_{w1} - \bar{N}_1\bar{\rho}_{w2}}{\bar{\rho}_w}\right)\right) \\ &\quad + \epsilon^2\left(\hat{\rho}\left(\frac{\bar{N}_1\bar{\rho}_{w2} - \bar{N}_2\bar{\rho}_{w1}}{\bar{\rho}_w}\right)^2 + \hat{N}_1\left(\bar{\rho}\bar{N}_1 + \bar{\rho}_1 - \frac{2\bar{\rho}\bar{\rho}_{w1}}{\bar{\rho}_w}\right)\right).\end{aligned} \tag{3.18}$$

An expansion in ϵ can be used for the mole fractions $\bar{N}_1$ and $\bar{N}_2$, as well as the mass densities $\bar{\rho}_1$ and $\bar{\rho}_2$, to obtain the following expressions for the terms in (3.18):

$$\frac{\bar{N}_1\bar{\rho}_{w2} - \bar{N}_2\bar{\rho}_{w1}}{\bar{\rho}_w} = -\frac{\epsilon\bar{\rho}_{w1}\bar{\rho}_{w2}}{\bar{\rho}_w} + O(\epsilon^2), \tag{3.19}$$

$$\bar{\rho}\bar{N}_1 + \bar{\rho}_1 - \frac{2\bar{\rho}\bar{\rho}_{w1}}{\bar{\rho}_w} = -\frac{\epsilon\bar{\rho}_{w1}\bar{\rho}_{w2}(1+2\xi)}{\mathrm{e}^{\xi}\bar{\rho}_w} + O(\epsilon^2). \tag{3.20}$$

Substituting these into (3.18), and retaining terms up to $O(\epsilon^2)$, we obtain

$$\frac{\epsilon(\hat{\rho}_2\bar{\rho}_{w1} - \hat{\rho}_1\bar{\rho}_{w2})}{\bar{\rho}_w} + \frac{\epsilon^2(\hat{\rho}_1\bar{\rho}_{w2}^2 + \hat{\rho}_2\bar{\rho}_{w1}^2)}{\bar{\rho}_w^2} = -\epsilon\hat{N}_1\bar{\rho} - \frac{\epsilon^2\hat{\rho}\bar{\rho}_{w1}\bar{\rho}_{w2}(1+\xi)}{\bar{\rho}_w^2} + O(\epsilon^3). \tag{3.21}$$

Substituting (3.21) into (3.15), we obtain

$$\hat{\rho}\left(1 - \frac{\epsilon^2\bar{\rho}_{w1}\bar{\rho}_{w2}(1+\xi)}{\bar{\rho}_w^2}\right) = \frac{\hat{p}m_{av}}{k_B\bar{T}} - \bar{\rho}\left(1 + \frac{\epsilon^2\bar{\rho}_{w1}\bar{\rho}_{w2}(\xi^2+2\xi+2)}{2\bar{\rho}_w^2}\right)\frac{\hat{T}}{\bar{T}} + \epsilon\bar{\rho}\hat{N}_1. \tag{3.22}$$

The above equation can be solved to obtain $\hat{\rho}$ in terms of $\hat{p}$, $\hat{T}$ and $\hat{N}_1$, and truncated at $O(\epsilon^2)$, to obtain

$$\hat{\rho} = \frac{\hat{p}m_{av}}{k_B\bar{T}}\left(1 + \frac{\epsilon^2\bar{\rho}_{w1}\bar{\rho}_{w2}(1+\xi)}{\bar{\rho}_w^2}\right) - \bar{\rho}\left(1 + \frac{\epsilon^2\bar{\rho}_{w1}\bar{\rho}_{w2}(2+\xi)^2}{2\bar{\rho}_w^2}\right)\frac{\hat{T}}{\bar{T}} + \epsilon\bar{\rho}\hat{N}_1. \tag{3.23}$$

https://doi.org/10.1017/jfm.2014.365 Published online by Cambridge University Press

First, we eliminate the density in the r momentum equation, (3.8), using the equation of state, (3.15), to obtain

$$-\frac{\Omega^2 r m_{av}\hat{p}}{k_B\bar{T}}\left(1+\frac{\epsilon^2\bar{\rho}_{w1}\bar{\rho}_{w2}(1+\xi)}{\bar{\rho}_w^2}\right)+\frac{\Omega^2 r\bar{\rho}\hat{T}}{\bar{T}}\left(1+\frac{\epsilon^2\bar{\rho}_{w1}\bar{\rho}_{w2}(2+\xi)^2}{2\bar{\rho}_w^2}\right)$$
$$-\epsilon\bar{\rho}\Omega^2 r\hat{N}_1-2\bar{\rho}\Omega\hat{v}_\theta+\frac{\partial\hat{p}}{\partial r}$$
$$=\bar{\mu}\left(\nabla^2\hat{v}_r-\frac{\hat{v}_r}{r^2}\right)+\frac{\bar{\mu}}{3}\left(\frac{\partial(\boldsymbol{\nabla}\cdot\hat{\boldsymbol{v}})}{\partial r}\right)-\frac{2}{3}(\boldsymbol{\nabla}\cdot\hat{\boldsymbol{v}})\frac{\partial\bar{\mu}}{\partial r}+2\frac{\partial\hat{v}_r}{\partial r}\frac{\partial\bar{\mu}}{\partial r}+f_r. \tag{3.24}$$

The identity

$$\bar{\rho}\frac{\partial}{\partial r}\left(\frac{\hat{p}}{\bar{\rho}}\right)=\frac{\partial\hat{p}}{\partial r}-\frac{\hat{p}}{\bar{\rho}}\frac{\partial\bar{\rho}}{\partial r}$$
$$=\frac{\partial\hat{p}}{\partial r}-\frac{\hat{p}m_{av}\Omega^2 r}{k_B\bar{T}}\left(1-\frac{\epsilon^2\bar{\rho}_{w1}\bar{\rho}_{w2}\xi}{\bar{\rho}_w^2}\right) \tag{3.25}$$

can be inserted into the momentum conservation equation, (3.24), and divided throughout by $r\bar{\rho}$, and the resulting equation is differentiated with respect to z, to obtain

$$\frac{1}{r}\frac{\partial}{\partial r}\left(\frac{1}{\bar{\rho}}\frac{\partial\hat{p}}{\partial z}\right)-\Omega\frac{\partial}{\partial z}\left(\frac{2\hat{v}_\theta}{r}-\frac{\Omega\hat{T}}{\bar{T}}\right)+\frac{\Omega^2}{\bar{T}}\frac{\partial\hat{T}}{\partial z}\left(\frac{\epsilon^2\bar{\rho}_{w1}\bar{\rho}_{w2}(2+\xi)^2}{2\bar{\rho}_w^2}\right)$$
$$-\frac{\epsilon^2 m_{av}\Omega^2\bar{\rho}_{w1}\bar{\rho}_{w2}(1+2\xi)}{k_B\bar{T}\bar{\rho}\bar{\rho}_w^2}\frac{\partial\hat{p}}{\partial z}-\epsilon\Omega^2\frac{\partial\hat{N}_1}{\partial z}$$
$$=\frac{\bar{\mu}}{r\bar{\rho}}\frac{\partial}{\partial z}\left(\nabla^2\hat{v}_r-\frac{\hat{v}_r}{r^2}\right)+\frac{\bar{\mu}}{3r\bar{\rho}}\left(\frac{\partial^2(\boldsymbol{\nabla}\cdot\hat{\boldsymbol{v}})}{\partial z\partial r}\right)-\frac{2}{3r\bar{\rho}}\frac{\partial(\boldsymbol{\nabla}\cdot\hat{\boldsymbol{v}})}{\partial z}\frac{\partial\bar{\mu}}{\partial r}$$
$$+\frac{2}{r\bar{\rho}}\frac{\partial^2\hat{v}_r}{\partial r\partial z}\frac{\partial\bar{\mu}}{\partial r}+\frac{\partial}{\partial z}\left(\frac{f_r}{r\bar{\rho}}\right). \tag{3.26}$$

Equation (3.10) is used to substitute for $\partial\hat{p}/\partial z$ in the above equation, and the equation is divided throughout by $\bar{\mu}$, to obtain

$$\frac{1}{r}\frac{\partial}{\partial r}\left(\frac{1}{\bar{\rho}}\nabla^2\hat{v}_z\right)-\frac{1}{\bar{\rho}r}\frac{\partial}{\partial z}\left(\nabla^2\hat{v}_r-\frac{\hat{v}_r}{r^2}\right)-\frac{1}{3r\bar{\rho}^3}\left(\frac{\partial\bar{\rho}}{\partial r}\right)\frac{\partial\mathscr{S}_m}{\partial z}+\frac{1}{3r\bar{\rho}^3}\left(\frac{\partial\bar{\rho}}{\partial r}\right)^2\frac{\partial\hat{v}_r}{\partial z}$$
$$+\frac{1}{\bar{\rho}\bar{\mu}r}\frac{\partial\bar{\mu}}{\partial r}\left(\nabla^2\hat{v}_z+\frac{\partial(\boldsymbol{\nabla}\cdot\hat{\boldsymbol{v}})}{\partial z}+\frac{\partial^2\hat{v}_z}{\partial r^2}-\frac{\partial^2\hat{v}_r}{\partial r\partial z}\right)+\frac{1}{\bar{\mu}r}\left(\frac{\partial\hat{v}_z}{\partial r}+\frac{\partial\hat{v}_r}{\partial z}\right)\frac{\partial}{\partial r}\left(\frac{1}{\bar{\rho}}\frac{\partial\bar{\mu}}{\partial r}\right)$$
$$+\frac{\Omega^2}{\bar{\mu}\bar{T}}\frac{\partial\hat{T}}{\partial z}\left(\frac{\epsilon^2\bar{\rho}_{w1}\bar{\rho}_{w2}(2+\xi)^2}{2\bar{\rho}_w^2}\right)-\frac{\epsilon^2 m_{av}\Omega^2\bar{\rho}_{w1}\bar{\rho}_{w2}(1+2\xi)}{k_B\bar{T}\bar{\mu}\bar{\rho}\bar{\rho}_w^2}\frac{\partial\hat{p}}{\partial z}-\frac{\epsilon\Omega^2}{\bar{\mu}}\hat{N}_1$$
$$-\frac{\Omega}{\bar{\mu}}\frac{\mathrm{d}}{\mathrm{d}z}\left(\frac{2\hat{v}_\theta}{r}-\frac{\Omega\hat{T}}{\bar{T}}\right)=\frac{1}{\bar{\mu}\bar{\rho}r}\left(\frac{\partial f_r}{\partial z}\right)-\frac{1}{\bar{\mu}r}\frac{\partial}{\partial r}\left(\frac{f_z}{\bar{\rho}}\right). \tag{3.27}$$

It should be noted that the form of equation (3.27) depends on the choice of b_1 and b_2 in (2.15) and (2.16). Owing to the choice $b_1=\bar{\rho}_{w1}/\bar{\rho}_w$ and $b_2=\bar{\rho}_{w2}/\bar{\rho}$, the only

https://doi.org/10.1017/jfm.2014.365 Published online by Cambridge University Press

$O(\epsilon)$ term is proportional to $\hat{N}_1$ in (3.27), while the coefficients of all other $O(\epsilon)$ terms reduce to zero. Other choices of b_1 and b_2 would have resulted in additional terms of $O(\epsilon)$, thereby making the algebraic manipulations more complicated.

The velocity components $\hat{v}_r$ and $\hat{v}_z$ can be expressed in terms of a stream function using the mass conservation (3.7),

$$r\bar{\rho}\hat{v}_r = -\frac{\partial\psi}{\partial z} + \int_0^r r'\,\mathrm{d}r'\,\mathscr{S}_m\,, \tag{3.28}$$

$$r\bar{\rho}\hat{v}_z = \frac{\partial\psi}{\partial r}. \tag{3.29}$$

The velocity is expressed in terms of the stream function, to obtain, from (3.27),

$$\begin{aligned}
&\frac{1}{r}\frac{\partial}{\partial r}\left(\frac{1}{\bar{\rho}r}\frac{\partial}{\partial r}\left(r\frac{\partial}{\partial r}\right)+\frac{1}{\bar{\rho}}\frac{\partial^2}{\partial z^2}\right)\left(\frac{1}{\bar{\rho}r}\frac{\partial\psi}{\partial r}\right)\\
&\quad+\left[\frac{1}{\bar{\rho}r}\frac{\partial}{\partial r}\left(\frac{1}{r}\frac{\partial}{\partial r}\left(r\frac{\partial}{\partial z}\right)\right)+\frac{1}{\bar{\rho}r}\frac{\partial^3}{\partial z^3}\right]\left(\frac{1}{\bar{\rho}r}\left(\frac{\partial\psi}{\partial z}\right)\right)-\frac{1}{3r^2\bar{\rho}^4}\left(\frac{\partial\bar{\rho}}{\partial r}\right)^2\frac{\partial^2\psi}{\partial z^2}\\
&\quad+\frac{1}{\bar{\rho}\bar{\mu}r}\frac{\partial\bar{\mu}}{\partial r}\left(\left(\nabla^2+\frac{\partial^2}{\partial r^2}\right)\left(\frac{1}{\bar{\rho}r}\frac{\partial\psi}{\partial r}\right)+\frac{\partial^2}{\partial r\partial z}\left(\frac{1}{\bar{\rho}r}\frac{\partial\psi}{\partial z}\right)\right)\\
&\quad+\frac{1}{\bar{\mu}r}\frac{\partial}{\partial r}\left(\frac{1}{\bar{\rho}}\frac{\partial\bar{\mu}}{\partial r}\right)\left(\frac{\partial}{\partial r}\left(\frac{1}{\bar{\rho}r}\frac{\partial\psi}{\partial r}\right)-\frac{1}{\bar{\rho}r}\frac{\partial^2\psi}{\partial z^2}\right)\\
&\quad-\left[\frac{1}{\bar{\rho}r}\frac{\partial}{\partial r}\left(\frac{1}{r}\frac{\partial}{\partial r}\left(r\frac{\partial}{\partial z}\right)\right)+\frac{1}{\bar{\rho}r}\frac{\partial^3}{\partial z^3}\right]\left(\frac{1}{\bar{\rho}r}\int_0^r r'\,\mathrm{d}r'\,\mathscr{S}_m\right)\\
&\quad+\frac{1}{3r^2\bar{\rho}^4}\left(\frac{\partial\bar{\rho}}{\partial r}\right)^2\left(\frac{\partial}{\partial z}\int_0^r r'\,\mathrm{d}r'\,\mathscr{S}_m\right)-\frac{1}{3r\bar{\rho}^3}\frac{\partial\bar{\rho}}{\partial r}\frac{\partial\mathscr{S}_m}{\partial z}\\
&\quad+\frac{1}{\bar{\rho}\bar{\mu}r}\frac{\partial\bar{\mu}}{\partial r}\left(\frac{\partial}{\partial z}\frac{\mathscr{S}_m}{\bar{\rho}}-\frac{\partial^2}{\partial r\partial z}\left(\frac{1}{\bar{\rho}r}\int_0^r r'\,\mathrm{d}r'\,\mathscr{S}_m\right)\right)\\
&\quad+\frac{1}{\bar{\mu}r}\frac{\partial}{\partial r}\left(\frac{1}{\bar{\rho}}\frac{\partial\bar{\mu}}{\partial r}\right)\left(\frac{1}{\bar{\rho}r}\frac{\partial}{\partial z}\int_0^r r'\,\mathrm{d}r'\,\mathscr{S}_m\right)+\frac{\Omega^2}{\bar{\mu}\bar{T}}\frac{\partial\hat{T}}{\partial z}\left(\frac{\epsilon^2\bar{\rho}_{w1}\bar{\rho}_{w2}(2+\xi)^2}{2\bar{\rho}_w^2}\right)\\
&\quad-\frac{\epsilon^2 m_{av}\Omega^2\bar{\rho}_{w1}\bar{\rho}_{w2}(1+2\xi)}{k_B\bar{T}\bar{\mu}\bar{\rho}\bar{\rho}_w^2}\frac{\partial\hat{p}}{\partial z}-\frac{\epsilon\Omega^2}{\bar{\mu}}\frac{\partial\hat{N}_1}{\partial z}\\
&\quad-\frac{\Omega}{\bar{\mu}}\frac{\partial}{\partial z}\left(\frac{2\hat{v}_\theta}{r}-\frac{\Omega\hat{T}}{\bar{T}}\right)-\frac{1}{\bar{\mu}\bar{\rho}r}\left(\frac{\partial f_r}{\partial z}\right)+\frac{1}{\bar{\mu}r}\frac{\partial}{\partial r}\left(\frac{f_z}{\bar{\rho}}\right)=0.
\end{aligned} \tag{3.30}$$

The stream function ψ is expressed in terms of the 'master potential' χ,

$$\psi = \frac{1}{r}\frac{\partial\chi}{\partial r}, \tag{3.31}$$

to obtain, from (3.30),

$$\begin{aligned}
&\frac{1}{r}\frac{\partial}{\partial r}\left(\frac{1}{\bar{\rho}r}\frac{\partial}{\partial r}\left(r\frac{\partial}{\partial r}\right)+\frac{1}{\bar{\rho}}\frac{\partial^2}{\partial z^2}\right)\left(\frac{1}{\bar{\rho}r}\frac{\partial}{\partial r}\left(\frac{1}{r}\frac{\partial\chi}{\partial r}\right)\right)-\frac{1}{3r^2\bar{\rho}^4}\left(\frac{\partial\bar{\rho}}{\partial r}\right)^2\frac{\partial^2}{\partial z^2}\left(\frac{1}{r}\frac{\partial\chi}{\partial r}\right)\\
&\quad+\left[\frac{1}{\bar{\rho}r}\frac{\partial}{\partial r}\left(\frac{1}{r}\frac{\partial}{\partial r}\left(r\frac{\partial}{\partial z}\right)\right)+\frac{1}{\bar{\rho}r}\frac{\partial^3}{\partial z^3}\right]\left[\frac{1}{\bar{\rho}r}\left(\frac{\partial}{\partial z}\left(\frac{1}{r}\frac{\partial\chi}{\partial r}\right)\right)\right]
\end{aligned}$$

https://doi.org/10.1017/jfm.2014.365 Published online by Cambridge University Press

$$+\frac{1}{\bar{\rho}\bar{\mu}r}\frac{\partial\bar{\mu}}{\partial r}\left[\left(\nabla^2+\frac{\partial^2}{\partial r^2}\right)\left(\frac{1}{\bar{\rho}r}\frac{\partial}{\partial r}\left(\frac{1}{r}\frac{\partial\chi}{\partial r}\right)\right)+\frac{\partial^2}{\partial r\partial z}\left(\frac{1}{\bar{\rho}r}\frac{\partial}{\partial z}\left(\frac{1}{r}\frac{\partial\chi}{\partial r}\right)\right)\right]$$
$$+\frac{1}{\bar{\mu}r}\frac{\partial}{\partial r}\left(\frac{1}{\bar{\rho}}\frac{\partial\bar{\mu}}{\partial r}\right)\left[\frac{\partial}{\partial r}\left(\frac{1}{\bar{\rho}r}\frac{\partial}{\partial r}\left(\frac{1}{r}\frac{\partial\chi}{\partial r}\right)\right)-\frac{1}{\bar{\rho}r}\frac{\partial^2}{\partial z^2}\left(\frac{1}{r}\frac{\partial\chi}{\partial r}\right)\right]$$
$$-\left[\frac{1}{\bar{\rho}r}\frac{\partial}{\partial r}\left(\frac{1}{r}\frac{\partial}{\partial r}\left(r\frac{\partial}{\partial z}\right)\right)+\frac{1}{\bar{\rho}r}\frac{\partial^3}{\partial z^3}\right]\left(\frac{1}{\bar{\rho}r}\int_0^r r'\,\mathrm{d}r'\,\mathscr{S}_m\right)$$
$$+\frac{1}{3r^2\bar{\rho}^4}\left(\frac{\partial\bar{\rho}}{\partial r}\right)^2\left(\frac{\partial}{\partial z}\int_0^r r'\,\mathrm{d}r'\,\mathscr{S}_m\right)-\frac{1}{3r\bar{\rho}^3}\frac{\partial\bar{\rho}}{\partial r}\frac{\partial\mathscr{S}_m}{\partial z}$$
$$+\frac{1}{\bar{\rho}\bar{\mu}r}\frac{\partial\bar{\mu}}{\partial r}\left(\frac{\partial}{\partial z}\frac{\mathscr{S}_m}{\bar{\rho}}-\frac{\partial^2}{\partial r\partial z}\left(\frac{1}{\bar{\rho}r}\int_0^r r'\,\mathrm{d}r'\,\mathscr{S}_m\right)\right)$$
$$+\frac{1}{\bar{\mu}r}\frac{\partial}{\partial r}\left(\frac{1}{\bar{\rho}}\frac{\partial\bar{\mu}}{\partial r}\right)\left(\frac{1}{\bar{\rho}r}\frac{\partial}{\partial z}\int_0^r r'\,\mathrm{d}r'\,\mathscr{S}_m\right)+\frac{\Omega^2}{\bar{\mu}\bar{T}}\frac{\partial\hat{T}}{\partial z}\left(\frac{\epsilon^2\bar{\rho}_{w1}\bar{\rho}_{w2}(2+\xi)^2}{2\bar{\rho}_w^2}\right)$$
$$-\frac{\epsilon^2 m_{av}\Omega^2\bar{\rho}_{w1}\bar{\rho}_{w2}(1+2\xi)}{k_B\bar{T}\bar{\mu}\bar{\rho}\bar{\rho}_w^2}\frac{\partial\hat{p}}{\partial z}-\frac{\epsilon\Omega^2}{\bar{\mu}}\frac{\partial\hat{N}_1}{\partial z}$$
$$-\frac{\Omega}{\bar{\mu}}\frac{\partial}{\partial z}\left(\frac{2\hat{v}_\theta}{r}-\frac{\Omega\hat{T}}{\bar{T}}\right)-\frac{1}{\bar{\mu}\bar{\rho}r}\left(\frac{\partial f_r}{\partial z}\right)+\frac{1}{\bar{\mu}r}\frac{\partial}{\partial r}\left(\frac{f_z}{\bar{\rho}}\right)=0. \tag{3.32}$$

4. Axial flow

First, we consider the axial flow along the cylinder surface, and assume that the radial extent of the boundary layer is small compared to the cylinder height. In this case, the axial derivatives of $\hat{v}_\theta$ and $\hat{T}$ on the right sides of (3.9) and (3.13) are small compared to the respective radial derivatives. The angular momentum conservation equation, (3.9), is rewritten as

$$2\bar{\rho}\Omega\hat{v}_r=\left(\frac{1}{r^2}\frac{\partial}{\partial r}\left(\bar{\mu}r^3\frac{\partial}{\partial r}\left(\frac{\hat{v}_\theta}{r}\right)\right)+\bar{\mu}\frac{\partial^2\hat{v}_\theta}{\partial z^2}\right)+f_\theta. \tag{4.1}$$

In this equation, the velocity $\hat{v}_r$ is expressed in terms of the master potential using (3.28) and (3.31),

$$-\frac{2\Omega}{r^2}\frac{\partial}{\partial r}\left(\frac{\partial\chi}{\partial z}\right)+\frac{2\Omega}{r}\int_0^r r'\,\mathrm{d}r'\,\mathscr{S}_m=\left(\frac{1}{r^2}\frac{\partial}{\partial r}\left(\bar{\mu}r^3\frac{\partial}{\partial r}\left(\frac{\hat{v}_\theta}{r}\right)\right)+\bar{\mu}\frac{\partial^2\hat{v}_\theta}{\partial z^2}\right)+f_\theta. \tag{4.2}$$

The previous equation is multiplied throughout by r^2, and integrated once with respect to the radial coordinate, with the condition $\partial\chi/\partial z=0$ and $r^2\,\partial(\hat{v}_\theta/r)/\partial r=0$ at the centre $r=0$, to obtain

$$-2\Omega\frac{\partial\chi}{\partial z}+2\Omega\int_0^r r'\,\mathrm{d}r'\left[\int_0^{r'} r''\,\mathrm{d}r''\,\mathscr{S}_m\right]$$
$$=\bar{\mu}\left(r^3\frac{\partial}{\partial r}\left(\frac{\hat{v}_\theta}{r}\right)\right)+\int_0^r r'^2\,\mathrm{d}r'\,\bar{\mu}\left(\frac{\partial^2\hat{v}_\theta}{\partial z^2}\right)+\int_0^r r'^2\,\mathrm{d}r'\,f_\theta. \tag{4.3}$$

https://doi.org/10.1017/jfm.2014.365 Published online by Cambridge University Press

The above equation is differentiated with respect to the z coordinate, and multiplied by $(2\Omega/\bar{\mu}^2 r^4)$, to obtain

$$\begin{aligned}\frac{1}{r}\frac{\partial}{\partial r}\left(\frac{2\Omega}{\bar{\mu}r}\frac{\partial \hat{v}_\theta}{\partial z}\right) &= -\frac{2\Omega}{\bar{\mu}^2 r^2}\frac{\partial \bar{\mu}}{\partial r}\frac{\partial \hat{v}_\theta}{\partial z} + \frac{2\Omega}{\bar{\mu}}\frac{\partial}{\partial z}\left(\frac{1}{r}\frac{\partial}{\partial r}\left(\frac{\hat{v}_\theta}{r}\right)\right) \\ &= -\frac{2\Omega}{\bar{\mu}^2 r^2}\frac{\partial \bar{\mu}}{\partial r}\frac{\partial \hat{v}_\theta}{\partial z} - \frac{4\Omega^2}{\bar{\mu}^2 r^4}\frac{\partial^2 \chi}{\partial z^2} + \frac{4\Omega^2}{\bar{\mu}^2 r^4}\int_0^r r'\,\mathrm{d}r'\left[\int_0^{r'} r''\,\mathrm{d}r''\,\frac{\partial \mathscr{S}_m}{\partial z}\right] \\ &\quad - \frac{2\Omega}{\bar{\mu}^2 r^4}\int_0^r r'^2\,\mathrm{d}r'\left(\bar{\mu}\frac{\partial^3 \hat{v}_\theta}{\partial z^3}\right) + \frac{2\Omega}{\bar{\mu}^2 r^4}\frac{\partial}{\partial z}\left(\int_0^r r'^2\,\mathrm{d}r' f_\theta\right). \end{aligned} \tag{4.4}$$

The temperature perturbation $\hat{T}$ in (3.32) can be expressed in terms of the master potential from the energy equation (3.13). In the temperature equation, the first term on the right is expressed in terms of the pressure gradient as follows. From (2.10) for the mean density of the two species, and the equation of state $\bar{p} = (\bar{\rho}_1/m_1 + \bar{\rho}_2/m_2)k_B\bar{T}$ for the base solid-body rotation, the coefficient of $\hat{v}_r$ in the first term on the right is

$$\frac{\bar{p}}{\bar{\rho}}\frac{\partial \bar{\rho}}{\partial r} = k_B \bar{T}\bar{\rho}_w \exp(-\xi)\left(1 + \frac{\epsilon^2 \rho_{w1}\rho_{w2}(2+\xi^2)}{2\rho_w^2}\right)\frac{\mathrm{d}\xi}{\mathrm{d}r}, \tag{4.5}$$

where ξ is the scaled radial coordinate in (2.22). The gradient of the mean pressure is

$$\begin{aligned}\frac{\partial \bar{p}}{\partial r} &= \bar{\rho}\Omega^2 r \\ &= k_B \bar{T}\rho_w \exp(-\xi)\left(1 + \frac{\epsilon^2 \rho_{w1}\rho_{w2}(2+\xi^2)}{2\rho_w^2}\right)\frac{\mathrm{d}\xi}{\mathrm{d}r}. \end{aligned} \tag{4.6}$$

Using (4.5) and (4.6), we can write the coefficient of $\hat{v}_r$ in the first term on the left, correct to $O(\epsilon^2)$, as

$$\begin{aligned}\frac{\bar{p}}{\bar{\rho}}\frac{\partial \bar{\rho}}{\partial r} &= \frac{\partial \bar{p}}{\partial r}\left(1 + \frac{\epsilon^2 \bar{\rho}_{w1}\bar{\rho}_{w2}}{\bar{\rho}_w^2}\right) \\ &= \bar{\rho}\Omega^2 r\left(1 + \frac{\epsilon^2 \bar{\rho}_{w1}\bar{\rho}_{w2}}{\bar{\rho}_w^2}\right). \end{aligned} \tag{4.7}$$

Expressing the radial velocity $\hat{v}_r$ in terms of the master potential using (3.28) and (3.26), we obtain

$$\frac{\Omega^2}{r}\frac{\partial}{\partial r}\left(\frac{\partial \chi}{\partial z}\right)\left(1 + \frac{\epsilon^2 \bar{\rho}_{w1}\bar{\rho}_{w2}}{\bar{\rho}_w^2}\right) - \Omega^2 \int_0^r r'\,\mathrm{d}r'\,\mathscr{S}_m = \left(\frac{1}{r}\frac{\partial}{\partial r}\left(\bar{K}r\frac{\partial \hat{T}}{\partial r}\right) + \bar{K}\frac{\partial^2 \hat{T}}{\partial z^2}\right) + \mathscr{S}_e'. \tag{4.8}$$

The previous equation can be multiplied by r, and integrated once with respect to the radial coordinate with lower limit zero and upper limit r, to obtain

$$\begin{aligned}\Omega^2\left(\frac{\partial \chi}{\partial z}\right)\left(1 + \frac{\epsilon^2 \bar{\rho}_{w1}\bar{\rho}_{w2}}{\bar{\rho}_w^2}\right) &= \bar{K}r\frac{\partial \hat{T}}{\partial r} + \int_0^r r'\,\mathrm{d}r'\,\bar{K}\left(\frac{\partial^2 \hat{T}}{\partial z^2}\right) + \int_0^r r'\,\mathrm{d}r'\,\mathscr{S}_e' \\ &\quad + \Omega^2 \int_0^r r'\,\mathrm{d}r'\left[\int_0^{r'} r''\,\mathrm{d}r''\,\mathscr{S}_m\right]. \end{aligned} \tag{4.9}$$

https://doi.org/10.1017/jfm.2014.365 Published online by Cambridge University Press

Here, we have used the symmetry condition that the radial derivative of the temperature perturbation is zero at the centre. The above equation is then multiplied by $\Omega^2/\bar{K}\bar{\mu}\bar{T}r^2$, and differentiated once with respect to z, to obtain

$$\begin{aligned}\frac{1}{r}\frac{\partial}{\partial r}\left(\frac{\Omega^2}{\bar{\mu}}\frac{\partial}{\partial z}\left(\frac{\hat{T}}{\bar{T}}\right)\right) &= -\frac{\Omega^2}{\bar{\mu}^2 r}\frac{\partial\bar{\mu}}{\partial r}\frac{\partial}{\partial z}\left(\frac{\hat{T}}{\bar{T}}\right)+\frac{\Omega^2}{\bar{\mu}}\frac{1}{r}\frac{\partial}{\partial r}\frac{\partial}{\partial z}\left(\frac{\hat{T}}{\bar{T}}\right)\\ &= -\frac{\Omega^2}{\bar{\mu}^2 r}\frac{\partial\bar{\mu}}{\partial r}\frac{\partial}{\partial z}\left(\frac{\hat{T}}{\bar{T}}\right)+\frac{\Omega^4}{\bar{K}\bar{\mu}\bar{T}r^2}\frac{\partial^2\chi}{\partial z^2}\left(1+\frac{\epsilon^2\bar{\rho}_{w1}\bar{\rho}_{w2}}{\bar{\rho}_w^2}\right)\\ &\quad -\frac{\Omega^2}{\bar{K}\bar{\mu}\bar{T}r^2}\int_0^r r'\,\mathrm{d}r'\left(\bar{K}\frac{\partial^3\hat{T}}{\partial z^3}\right)-\frac{\Omega^2}{\bar{K}\bar{\mu}\bar{T}r^2}\left(\frac{\partial}{\partial z}\int_0^r r'\,\mathrm{d}r'\,\mathscr{S}_e'\right)\\ &\quad -\frac{\Omega^4}{\bar{K}\bar{\mu}\bar{T}r^2}\int_0^r r'\,\mathrm{d}r'\left[\int_0^{r'} r''\,\mathrm{d}r''\,\frac{\partial\mathscr{S}_m}{\partial z}\right].\end{aligned}\tag{4.10}$$

We take the derivative $(1/r)\,\partial/\partial r$ of the equation for the master potential, (3.32), and then insert (4.4) and (4.10), to obtain

$$\begin{aligned}&\frac{1}{r}\frac{\partial}{\partial r}\left[\frac{1}{r}\frac{\partial}{\partial r}\left(\frac{1}{\bar{\rho}r}\frac{\partial}{\partial r}\left(r\frac{\partial}{\partial r}\right)+\frac{1}{\bar{\rho}}\frac{\partial^2}{\partial z^2}\right)\left(\frac{1}{\bar{\rho}r}\frac{\partial}{\partial r}\left(\frac{1}{r}\frac{\partial\chi}{\partial r}\right)\right)\right]\\ &+\frac{1}{r}\frac{\partial}{\partial r}\left[\frac{1}{\bar{\rho}r}\frac{\partial}{\partial r}\left(\frac{1}{r}\frac{\partial}{\partial r}\left(r\frac{\partial}{\partial z}\right)\right)+\frac{1}{\bar{\rho}r}\frac{\partial^3}{\partial z^3}\right]\left[\frac{1}{\bar{\rho}r}\left(\frac{\partial}{\partial z}\left(\frac{1}{r}\frac{\partial\chi}{\partial r}\right)\right)\right]\\ &-\frac{1}{r}\frac{\partial}{\partial r}\left(\frac{1}{3r^2\bar{\rho}^4}\left(\frac{\partial\bar{\rho}}{\partial r}\right)^2\frac{\partial^2}{\partial z^2}\left(\frac{1}{r}\frac{\partial\chi}{\partial r}\right)\right)\\ &+\left(\frac{4\Omega^2}{\bar{\mu}^2r^4}+\frac{\Omega^4}{\bar{K}\bar{\mu}\bar{T}r^2}\left(1+\frac{\epsilon^2\bar{\rho}_{w1}\bar{\rho}_{w2}}{\bar{\rho}_w^2}\right)\right)\frac{\partial^2\chi}{\partial z^2}\\ &+\frac{2\Omega}{\bar{\mu}^2r^4}\int_0^r r'^2\,\mathrm{d}r'\left(\bar{\mu}\frac{\partial^3\hat{v}_\theta}{\partial z^3}\right)-\frac{\Omega^2}{\bar{K}\bar{\mu}\bar{T}r^2}\int_0^r r'\,\mathrm{d}r'\left(\bar{K}\frac{\partial^3\hat{T}}{\partial z^3}\right)=\mathscr{S}+\mathscr{I},\end{aligned}\tag{4.11}$$

where the source term $\mathscr{S}$ and the inhomogeneous term $\mathscr{I}$ are

$$\begin{aligned}\mathscr{I} &= -\frac{1}{r}\frac{\partial}{\partial r}\left\{\frac{1}{\bar{\rho}\bar{\mu}r}\frac{\partial\bar{\mu}}{\partial r}\left[\left(\frac{1}{r}\frac{\partial}{\partial r}\left(r\frac{\partial}{\partial r}\right)+\frac{\partial^2}{\partial z^2}\right)\left(\frac{1}{\bar{\rho}r}\frac{\partial}{\partial r}\left(\frac{1}{r}\frac{\partial\chi}{\partial r}\right)\right)\right.\right.\\ &\quad\left.+\frac{1}{\bar{\rho}^2r}\frac{\partial\bar{\rho}}{\partial r}\left(\frac{1}{r}\frac{\partial}{\partial r}\frac{\partial^2\chi}{\partial z^2}\right)+\frac{\partial^2}{\partial r^2}\left(\frac{1}{\bar{\rho}r}\frac{\partial}{\partial r}\left(\frac{1}{r}\frac{\partial\chi}{\partial r}\right)\right)+\frac{\partial}{\partial r}\left(\frac{1}{\bar{\rho}r^2}\frac{\partial}{\partial r}\frac{\partial^2\chi}{\partial z^2}\right)\right]\\ &\quad+\frac{1}{\bar{\mu}r}\frac{\partial}{\partial r}\left(\frac{1}{\bar{\rho}}\frac{\partial\bar{\mu}}{\partial r}\right)\left[\frac{\partial}{\partial r}\left(\frac{1}{\bar{\rho}r}\frac{\partial}{\partial r}\left(\frac{1}{r}\frac{\partial\chi}{\partial r}\right)\right)-\frac{1}{\bar{\rho}r^2}\frac{\partial}{\partial r}\frac{\partial^2\chi}{\partial z^2}\right]\\ &\quad+\frac{\Omega^2}{\bar{\mu}}\frac{\partial}{\partial z}\left(\frac{\hat{T}}{\bar{T}}\right)\left(\frac{\epsilon^2\bar{\rho}_{w1}\bar{\rho}_{w2}(2+\xi)^2}{2\bar{\rho}_w^2}\right)-\frac{\epsilon^2\Omega^2\bar{\rho}_{w1}\bar{\rho}_{w2}(1+2\xi)}{\bar{\mu}\bar{\rho}\bar{\rho}_w}\frac{\partial}{\partial z}\left(\frac{\hat{p}m_{av}}{\bar{\rho}_w k_B\bar{T}}\right)\\ &\quad\left.-\frac{\epsilon\Omega^2}{\bar{\mu}}\frac{\partial\hat{N}_1}{\partial z}\right\}-\frac{2\Omega^2R}{\bar{\mu}^2r^2}\frac{\partial\bar{\mu}}{\partial r}\frac{\partial}{\partial z}\left(\frac{\hat{v}_\theta}{R\Omega}\right)+\frac{\Omega^2}{\bar{\mu}^2r}\frac{\partial\bar{\mu}}{\partial r}\frac{\partial}{\partial z}\left(\frac{\hat{T}}{\bar{T}}\right),\end{aligned}\tag{4.12}$$

https://doi.org/10.1017/jfm.2014.365 Published online by Cambridge University Press

$$\begin{aligned}\mathscr{S} = {} & \frac{1}{r}\frac{\partial}{\partial r}\left(\frac{1}{\bar{\mu}\bar{\rho}r}\left(\frac{\partial f_r}{\partial z}\right) - \frac{1}{\bar{\mu}r}\frac{\partial}{\partial r}\left(\frac{f_z}{\bar{\rho}}\right)\right) \\ & + \frac{1}{r}\frac{\partial}{\partial r}\left[\frac{1}{\bar{\rho}r}\frac{\partial}{\partial r}\left(\frac{1}{r}\frac{\partial}{\partial r}\left(r\frac{\partial}{\partial z}\right)\right) + \frac{1}{\bar{\rho}r}\frac{\partial^3}{\partial z^3}\right]\left(\frac{1}{\bar{\rho}r}\int_0^r r'\,\mathrm{d}r'\,\mathscr{S}_m\right) \\ & - \frac{1}{r}\frac{\partial}{\partial r}\left(\frac{1}{3r^2\bar{\rho}^4}\left(\frac{\partial\bar{\rho}}{\partial r}\right)^2\left(\frac{\partial}{\partial z}\int_0^r r'\,\mathrm{d}r'\,\mathscr{S}_m\right)\right) + \frac{1}{r}\frac{\partial}{\partial r}\left(\frac{1}{3r\bar{\rho}^3}\frac{\partial\bar{\rho}}{\partial r}\frac{\partial\mathscr{S}_m}{\partial z}\right) \\ & + \frac{4\Omega^2}{\bar{\mu}^2r^4}\int_0^r r'\,\mathrm{d}r'\left(\int_0^{r'} r''\,\mathrm{d}r''\,\frac{\partial\mathscr{S}_m}{\partial z}\right) + \frac{2\Omega}{\bar{\mu}^2r^4}\frac{\partial}{\partial z}\left(\int_0^r r'^2\,\mathrm{d}r'\,f_\theta\right) \\ & + \frac{\Omega^2}{\bar{K}\bar{\mu}\bar{T}r^2}\left(\frac{\partial}{\partial z}\int_0^r r'\,\mathrm{d}r'\,\mathscr{S}_e'\right) + \frac{\Omega^4}{\bar{K}\bar{\mu}\bar{T}r^2}\int_0^r r'\,\mathrm{d}r'\left[\int_0^{r'} r''\,\mathrm{d}r''\,\frac{\partial\mathscr{S}_m}{\partial z}\right]\mathrm{d}r \\ & - \frac{1}{r}\frac{\partial}{\partial r}\left\{\frac{1}{\bar{\rho}\bar{\mu}r}\frac{\partial\bar{\mu}}{\partial r}\left[\frac{1}{\bar{\rho}}\frac{\partial\mathscr{S}_m}{\partial z} - \frac{1}{\bar{\rho}^2r}\frac{\partial\bar{\rho}}{\partial r}\frac{\partial}{\partial z}\int_0^r r'\,\mathrm{d}r'\,\mathscr{S}_m\right.\right. \\ & \left.\left. - \frac{\partial^2}{\partial r\partial z}\left(\frac{1}{\bar{\rho}r}\int_0^r r'\,\mathrm{d}r'\,\mathscr{S}_m\right)\right] + \frac{1}{\bar{\mu}r}\frac{\partial}{\partial r}\left(\frac{1}{\bar{\rho}}\frac{\partial\bar{\mu}}{\partial r}\right)\left[\frac{1}{\bar{\rho}r}\frac{\partial}{\partial z}\int_0^r r'\,\mathrm{d}r'\,\mathscr{S}_m\right]\right\}. \quad (4.13)\end{aligned}$$

The radial coordinate is expressed in terms of the scaled radial coordinate ξ, defined in (2.22). With this transformation, it can easily be verified that

$$\frac{1}{r}\frac{\partial}{\partial r} = -\frac{2\mathscr{A}^2}{R^2}\frac{\partial}{\partial\xi}. \quad (4.14)$$

In addition, the z coordinate is expressed in terms of the scaled coordinate $\eta = z/Z$, where Z is the total cylinder height. The equation for the master potential (4.11) is expressed in terms of the scaled coordinates, and multiplied throughout by $(R^{10}\bar{\rho}_w^2/64\mathscr{A}^{12})(1/\bar{\mu}_wR^2Z)$ to obtain

$$\begin{aligned}& \frac{\partial^2}{\partial\xi^2}\left[\frac{1}{\bar{\rho}^*}\frac{\partial}{\partial\xi}\left(\left(1-\frac{\xi}{\mathscr{A}^2}\right)\frac{\partial}{\partial\xi}\left(\frac{1}{\bar{\rho}^*}\frac{\partial^2\chi^*}{\partial\xi^2}\right)\right)\right] + \frac{R^2}{4\mathscr{A}^4Z^2}\left[\frac{\partial}{\partial\xi^2}\left(\frac{1}{\bar{\rho}^{*2}}\frac{\partial}{\partial\xi^2}\frac{\partial^2\chi^*}{\partial\eta^2}\right)\right. \\ & \quad \left. + \frac{\partial}{\partial\xi}\left(\frac{1}{\bar{\rho}^*}\frac{\partial^2}{\partial\xi^2}\left(\frac{1}{\bar{\rho}^*}\frac{\partial}{\partial\xi}\frac{\partial^2\xi}{\partial\eta^2}\right)\right) - \frac{\partial}{\partial\xi}\left(\frac{1}{3\bar{\rho}^{*4}}\left(\frac{\partial\bar{\rho}^*}{\partial\xi}\right)^2\frac{\partial}{\partial\xi}\left(\frac{\partial^2\chi^*}{\partial\eta^2}\right)\right)\right] \\ & \quad + \frac{R^4}{16\mathscr{A}^8Z^4}\frac{\partial}{\partial\xi}\left(\frac{1}{\bar{\rho}^2(1-2\xi/\mathscr{A}^2)}\frac{\partial}{\partial\xi}\left(\frac{\partial^4\chi^*}{\partial\eta^4}\right)\right) \\ & \quad + \left(\frac{4Re^2}{\bar{\mu}^{*2}(1-\xi/\mathscr{A}^2)^2} + \frac{2\mathscr{A}^2Re^2Pr(1-\gamma^{-1})}{\bar{\mu}^*\bar{K}^*(1-\xi/\mathscr{A}^2)}\left(1+\frac{\epsilon^2\bar{\rho}_{w1}\bar{\rho}_{w2}}{\bar{\rho}_w^2}\right)\right)\frac{1}{64\mathscr{A}^{12}}\frac{R^2}{Z^2}\frac{\partial^2\chi^*}{\partial\eta^2} \\ & \quad - \frac{Re^2R^4}{16\mathscr{A}^{14}Z^4\bar{\mu}^*(1-\xi/\mathscr{A}^2)^2}\int_{\mathscr{A}^2}^{\xi}\mathrm{d}\xi'(1-\xi'/\mathscr{A}^2)^{1/2}\left(\frac{\partial^3}{\partial\eta^3}\left(\frac{\hat{v}_\theta}{R\Omega}\right)\right) \\ & \quad + \frac{Re^2R^4}{128\bar{\mu}^*\mathscr{A}^{14}Z^4(1-\xi/\mathscr{A}^2)}\int_{\mathscr{A}^2}^{\xi}\mathrm{d}\xi'\left(\frac{\partial^3}{\partial\eta^3}\left(\frac{\hat{T}}{\bar{T}}\right)\right) \\ & = \frac{(\mathscr{S}+\mathscr{I})R^8\bar{\rho}_w^2}{64\mathscr{A}^{12}\bar{\mu}_wZ}, \quad (4.15)\end{aligned}$$

https://doi.org/10.1017/jfm.2014.365 Published online by Cambridge University Press

where $\chi^* = \chi/(\bar{\mu}_w R^2 Z)$ is the scaled master potential, $\bar{\rho}^* = \bar{\rho}/\bar{\rho}_w$, $\bar{\mu}^* = \bar{\mu}/\bar{\mu}_w$, $\bar{K}^* = \bar{K}/\bar{K}_w$ and

$$\begin{aligned}
\frac{\mathscr{I} R^8 \bar{\rho}_w^2}{64\mathscr{A}^{12}\bar{\mu}_w Z} &= -\frac{\partial}{\partial\xi}\left\{\frac{1}{\bar{\rho}^*\bar{\mu}^*}\frac{\partial\bar{\mu}^*}{\partial\xi}\left[\left(\frac{\partial}{\partial\xi}\left(\left(1-\frac{\xi}{\mathscr{A}^2}\right)\frac{\partial}{\partial\xi}\right)+\frac{R^2}{4\mathscr{A}^4Z^2}\frac{\partial^2}{\partial\eta^2}\right)\right.\right.\\
&\quad\times\left(\frac{1}{\bar{\rho}^*}\frac{\partial^2\chi^*}{\partial\xi^2}\right)+\frac{R^2}{4\mathscr{A}^4Z^2}\frac{1}{\bar{\rho}^{*2}}\frac{\partial\bar{\rho}^*}{\partial\xi}\left(\frac{\partial}{\partial\xi}\frac{\partial^2\chi^*}{\partial\eta^2}\right)\\
&\quad+\left(1-\frac{\xi}{\mathscr{A}^2}\right)^{1/2}\frac{\partial}{\partial\xi}\left(\left(1-\frac{\xi}{\mathscr{A}^2}\right)^{1/2}\frac{\partial}{\partial\xi}\left(\frac{1}{\bar{\rho}^*}\frac{\partial^2\chi^*}{\partial\xi^2}\right)\right)\\
&\quad\left.+\frac{R^2}{4\mathscr{A}^4Z^2}\left(1-\frac{\xi}{\mathscr{A}^2}\right)^{1/2}\frac{\partial}{\partial\xi}\left(\frac{1}{\bar{\rho}^*(1-\xi/\mathscr{A}^2)^{1/2}}\frac{\partial}{\partial\xi}\frac{\partial^2\chi^*}{\partial\eta^2}\right)\right]\\
&\quad+\frac{1}{\bar{\mu}^*}\frac{\partial}{\partial\xi}\left(\frac{(1-\xi/\mathscr{A}^2)^{1/2}}{\bar{\rho}^*}\frac{\partial\bar{\mu}^*}{\partial\xi}\right)\left[\left(1-\frac{\xi}{\mathscr{A}^2}\right)^{1/2}\frac{\partial}{\partial\xi}\left(\frac{1}{\bar{\rho}^*}\left(\frac{\partial^2\chi^*}{\partial\xi^2}\right)\right)\right.\\
&\quad\left.-\frac{R^2}{4\mathscr{A}^4Z^2}\frac{1}{\bar{\rho}^*(1-\xi/\mathscr{A}^2)^{1/2}}\frac{\partial}{\partial\xi}\frac{\partial^2\chi^*}{\partial\eta^2}\right]\\
&\quad+\frac{Re^2R^2}{64\mathscr{A}^{12}Z^2\bar{\mu}^*}\frac{\partial}{\partial\eta}\left(\frac{\hat{T}}{\bar{T}}\right)(\epsilon^2\bar{\rho}^*_{w1}\bar{\rho}^*_{w2}(2+\xi)^2)-\frac{\epsilon Re^2R^2}{64\mathscr{A}^{12}Z^2\bar{\mu}^*}\frac{\partial\hat{N}_1}{\partial\eta}\\
&\quad-\frac{Re^2R^2}{64\mathscr{A}^{12}Z^2\bar{\mu}^*}\frac{\epsilon^2\bar{\rho}^*_{w1}\bar{\rho}^*_{w2}(1+2\xi)}{\bar{\rho}^*}\frac{\partial}{\partial\eta}\left(\frac{\hat{p}m_{av}}{\bar{\rho}_w k_B\bar{T}}\right)\Big\}\\
&\quad+\frac{Re^2R^2}{16\mathscr{A}^{10}Z^2\bar{\mu}^{*2}}\left(1+\frac{\xi}{\mathscr{A}^2}\right)^{-1/2}\frac{\partial\bar{\mu}^*}{\partial\xi}\frac{\partial}{\partial\eta}\left(\frac{\hat{v}_\theta}{R\Omega}\right)\\
&\quad-\frac{Re^2R^2}{32\mathscr{A}^{10}Z^2\bar{\mu}^{*2}}\frac{\partial\bar{\mu}^*}{\partial\xi}\frac{\partial}{\partial\eta}\left(\frac{\hat{T}}{\bar{T}}\right),
\end{aligned}\tag{4.16}$$

where $\bar{\rho}^*_{wi} = \bar{\rho}_{wi}/\bar{\rho}_w$. The source term, expressed in dimensionless form using the scaled sources $\mathscr{S}^*_m = \mathscr{S}_m R^2/\bar{\mu}_w$, $f^*_r = f_r\bar{\rho}_w R^3/\bar{\mu}^2_w$, $f^*_z = f_z\bar{\rho}_w R^4/\bar{\mu}^2_w Z$, $f^*_\theta = f_\theta R/\bar{\mu}_w\Omega$ and $\mathscr{S}^*_e = \mathscr{S}'_e R^2/\bar{K}_w\bar{T}$, is

$$\begin{aligned}
\frac{\mathscr{S} R^8\bar{\rho}_w^2}{64\mathscr{A}^{12}\bar{\mu}_w Z} &= -\frac{R^2}{32\mathscr{A}^{10}Z^2}\frac{\partial}{\partial\xi}\left(\frac{1}{\bar{\mu}^*\bar{\rho}^*(1-\xi/\mathscr{A}^2)}\left(\frac{\partial f^*_r}{\partial\eta}\right)+\frac{2\mathscr{A}^2}{\bar{\mu}^*}\frac{\partial}{\partial\xi}\left(\frac{f^*_z}{\bar{\rho}^*}\right)\right)\\
&\quad+\frac{R^2}{16\mathscr{A}^8Z^2}\frac{\partial}{\partial\xi}\left(\frac{1}{\bar{\rho}^*}\frac{\partial^2}{\partial\xi^2}\left(\frac{1}{\bar{\rho}^*}\frac{\partial}{\partial\eta}\int_{\mathscr{A}^2}^{\xi}\mathrm{d}\xi'\,\mathscr{S}^*_m\right)\right)\\
&\quad+\frac{R^4}{64\mathscr{A}^{12}Z^4}\frac{\partial}{\partial\xi}\left((1-\xi/\mathscr{A}^2)^{-2}\frac{\partial^3}{\partial\eta^3}\int_{\mathscr{A}^2}^{\xi}\mathrm{d}\xi'\,\mathscr{S}^*_m\right)\\
&\quad+\frac{R^2}{16\mathscr{A}^8Z^2}\left[-\frac{\partial}{\partial\xi}\left(\frac{1}{3\bar{\rho}^{*4}}\left(\frac{\partial\bar{\rho}^*}{\partial\xi}\right)^2\left(\frac{\partial}{\partial\eta}\int_{\mathscr{A}^2}^{\xi}\mathrm{d}\xi'\,\mathscr{S}^*_m\right)\right)\right.\\
&\quad\left.+\frac{\partial}{\partial\xi}\left(\frac{1}{3\bar{\rho}^{*3}}\frac{\partial\bar{\rho}}{\partial\xi}\frac{\partial\mathscr{S}^*_m}{\partial\eta}\right)\right]+\frac{Re^2R^2}{64\mathscr{A}^{16}Z^2\bar{\mu}^{*2}(1-\xi/\mathscr{A}^2)^4}\\
&\quad\times\left(\int_{\mathscr{A}^2}^{\xi}\mathrm{d}\xi'\int_{\mathscr{A}^2}^{\xi'}\mathrm{d}\xi''\frac{\partial\mathscr{S}^*_m}{\partial\eta}-\frac{\partial}{\partial\eta}\left(\int_{\mathscr{A}^2}^{\xi}\mathrm{d}\xi'(1-\xi'/\mathscr{A}^2)^{1/2}f^*_\theta\right)\right)
\end{aligned}$$

https://doi.org/10.1017/jfm.2014.365 Published online by Cambridge University Press

$$+\frac{Re^2R^2}{128\mathscr{A}^{14}Z^2}\frac{1}{\bar{K}^*\bar{\mu}^*(1-\xi/\mathscr{A}^2)^2}\left(-\left(\frac{\partial}{\partial\eta}\int_{\mathscr{A}^2}^{\xi}\mathrm{d}\xi'\mathscr{S}_e^{*\prime}\right)\right.$$
$$\left.+\int_{\mathscr{A}}^{\xi}\mathrm{d}\xi'\int_{\mathscr{A}}^{\xi'}\mathrm{d}\xi''\frac{\partial\mathscr{S}_m^*}{\partial\eta}\right)-\frac{R^2}{16\mathscr{A}^8Z^2}\frac{\partial}{\partial\xi}\left\{\frac{1}{\bar{\rho}^*\bar{\mu}^*}\frac{\partial\bar{\mu}^*}{\partial\xi}\left[\frac{1}{\bar{\rho}^*}\frac{\partial\mathscr{S}_m^*}{\partial\eta}\right.\right.$$
$$-\frac{1}{\bar{\rho}^{*2}}\frac{\partial\bar{\rho}^*}{\partial\xi}\frac{\partial}{\partial\eta}\int_{\mathscr{A}^2}^{\xi}\mathrm{d}\xi'\mathscr{S}_m^*-(1-\xi/\mathscr{A}^2)^{1/2}\frac{\partial^2}{\partial\xi\partial\eta}$$
$$\left.\times\left(\frac{1}{\bar{\rho}^*(1-\xi/\mathscr{A}^2)^{1/2}}\int_{\mathscr{A}^2}^{\xi}\mathrm{d}\xi'\mathscr{S}_m^*\right)\right]+\frac{1}{\bar{\mu}^*}\frac{\partial}{\partial\xi}\left(\frac{(1-\xi/\mathscr{A}^2)^{1/2}}{\bar{\rho}^*}\frac{\partial\bar{\mu}^*}{\partial\xi}\right)$$
$$\left.\times\left[\frac{1}{\bar{\rho}^*(1-\xi/\mathscr{A}^2)^{1/2}}\frac{\partial}{\partial\eta}\int_{\mathscr{A}^2}^{\xi}\mathrm{d}\xi'\mathscr{S}_m^*\right]\right\}. \tag{4.17}$$

The Onsager model is obtained in the limit of high aspect ratio $R/Z\ll 1$, where terms proportional to $Re^2R^2/\mathscr{A}^{12}Z^2$ are retained, but terms proportional to $R^n/\mathscr{A}^{2n}Z^n$ for $n\geqslant 2$ and $Re^2R^n/\mathscr{A}^{12}Z^n$ for $n\geqslant 4$ are neglected. In this case, the equation for the master potential reduces to

$$\frac{\partial^2}{\partial\xi^2}\left[\frac{1}{\bar{\rho}^*}\frac{\partial}{\partial\xi}\left(\left(1-\frac{\xi}{\mathscr{A}^2}\right)\frac{\partial}{\partial\xi}\left(\frac{1}{\bar{\rho}^*}\frac{\partial^2\chi^*}{\partial\xi^2}\right)\right)\right]+\left(\frac{4}{\bar{\mu}^{*2}(1-\xi/\mathscr{A}^2)^2}\right.$$
$$\left.+\frac{2\mathscr{A}^2Pr(1-\gamma^{-1})}{\bar{\mu}^*\bar{K}^*(1-\xi/\mathscr{A}^2)}\left(1+\frac{\epsilon^2\bar{\rho}_{w1}\bar{\rho}_{w2}}{\bar{\rho}_w^2}\right)\right)\frac{Re^2R^2}{64\mathscr{A}^{12}Z^2}\frac{\partial^2\chi^*}{\partial\eta^2}$$
$$=\frac{(\mathscr{S}+\mathscr{I})R^8\bar{\rho}_w^2}{64\mathscr{A}^{12}\bar{\mu}_wZ}, \tag{4.18}$$

where the approximation for the inhomogeneous term $\mathscr{I}$ is

$$\frac{\mathscr{I}R^8\bar{\rho}_w^2}{64\mathscr{A}^{12}\bar{\mu}_wZ}=-\frac{\partial}{\partial\xi}\left\{\frac{1}{\bar{\rho}^*\bar{\mu}^*}\frac{\partial\bar{\mu}^*}{\partial\xi}\left[\left(\frac{\partial}{\partial\xi}\left(\left(1-\frac{\xi}{\mathscr{A}^2}\right)\frac{\partial}{\partial\xi}\right)\right)\left(\frac{1}{\bar{\rho}^*}\frac{\partial^2\chi^*}{\partial\xi^2}\right)\right.\right.$$
$$\left.+\left(1-\frac{\xi}{\mathscr{A}^2}\right)^{1/2}\frac{\partial}{\partial\xi}\left(\left(1-\frac{\xi}{\mathscr{A}^2}\right)^{1/2}\frac{\partial}{\partial\xi}\left(\frac{1}{\bar{\rho}^*}\frac{\partial^2\chi^*}{\partial\xi^2}\right)\right)\right]$$
$$-\frac{1}{\bar{\mu}^*}\frac{\partial}{\partial\xi}\left(\frac{(1-\xi/\mathscr{A}^2)^{1/2}}{\bar{\rho}^*}\frac{\partial\bar{\mu}^*}{\partial\xi}\right)\left[\left(1-\frac{\xi}{\mathscr{A}^2}\right)^{1/2}\frac{\partial}{\partial\xi}\left(\frac{1}{\bar{\rho}^*}\left(\frac{\partial^2\chi^*}{\partial\xi^2}\right)\right)\right]$$
$$+\frac{Re^2R^2}{64\mathscr{A}^{12}Z^2\bar{\mu}^*}\frac{\partial}{\partial\eta}\left(\frac{\hat{T}}{\bar{T}}\right)\left(\frac{\epsilon^2\bar{\rho}_{w1}^*\bar{\rho}_{w2}^*(2+\xi)^2}{2}\right)-\frac{\epsilon Re^2R^2}{64\mathscr{A}^{12}Z^2\bar{\mu}^*}\frac{\partial\hat{N}_1}{\partial\eta}$$
$$\left.-\frac{Re^2R^2}{64\mathscr{A}^{12}Z^2\bar{\mu}^*}\frac{\epsilon^2\bar{\rho}_{w1}^*\bar{\rho}_{w2}^*(1+2\xi)}{\bar{\rho}^*}\frac{\partial}{\partial\eta}\left(\frac{\hat{p}m_{av}}{\bar{\rho}_wk_B\bar{T}}\right)\right\}$$
$$+\frac{Re^2R^2}{16\mathscr{A}^{10}Z^2\bar{\mu}^{*2}}\left(1+\frac{\xi}{\mathscr{A}^2}\right)^{-1/2}\frac{\partial\bar{\mu}^*}{\partial\xi}\frac{\partial}{\partial\eta}\left(\frac{\hat{v}_\theta}{R\Omega}\right)$$
$$-\frac{Re^2R^2}{32\mathscr{A}^{10}Z^2\bar{\mu}^{*2}}\frac{\partial\bar{\mu}^*}{\partial\xi}\frac{\partial}{\partial\eta}\left(\frac{\hat{T}}{\bar{T}}\right), \tag{4.19}$$

https://doi.org/10.1017/jfm.2014.365 Published online by Cambridge University Press

while the approximation for the source term is

$$\frac{\mathscr{S}R^8\bar{\rho}_w^2}{64\mathscr{A}^{12}\bar{\mu}_w Z} = \frac{Re^2R^2}{64\mathscr{A}^{16}Z^2\bar{\mu}^{*2}(1-\xi/\mathscr{A}^2)^4}\left(\int_{\mathscr{A}^2}^{\xi}\mathrm{d}\xi'\int_{\mathscr{A}^2}^{\xi'}\mathrm{d}\xi''\,\frac{\partial\mathscr{S}_m^*}{\partial\eta} - \frac{\partial}{\partial\eta}\left(\int_{\mathscr{A}^2}^{\xi}\mathrm{d}\xi'(1-\xi'/\mathscr{A}^2)^{1/2}f_\theta^*\right)\right) + \frac{Re^2R^2}{128\mathscr{A}^{14}Z^2}\frac{1}{\bar{K}^*\bar{\mu}^*(1-\xi/\mathscr{A}^2)^2}\left(-\left(\frac{\partial}{\partial\eta}\int_{\mathscr{A}^2}^{\xi}\mathrm{d}\xi'\mathscr{S}_e^{*\prime}\right) + \int_{\mathscr{A}}^{\xi}\mathrm{d}\xi'\int_{\mathscr{A}}^{\xi'}\mathrm{d}\xi''\frac{\partial\mathscr{S}_m^*}{\partial\eta}\right). \tag{4.20}$$

Equation (4.18) can be rewritten as

$$\mathscr{L}_6\chi^* + \frac{Re^2R^2}{64\mathscr{A}^{12}Z^2}\frac{\partial^2\chi^*}{\partial\eta^2} = \mathscr{S}^* + \mathscr{I}^*, \tag{4.21}$$

where the operator $\mathscr{L}_6$ is a sixth-order differential operator that is a function only of ξ,

$$\mathscr{L}_6 = \mathscr{F}^{-1}\frac{\partial^2}{\partial\xi^2}\left[\frac{1}{\bar{\rho}^*}\frac{\partial}{\partial\xi}\left(\left(1-\frac{\xi}{\mathscr{A}^2}\right)\frac{\partial}{\partial\xi}\left(\frac{1}{\bar{\rho}^*}\frac{\partial^2}{\partial\xi^2}\right)\right)\right], \tag{4.22}$$

$$\mathscr{I}^* = \mathscr{F}^{-1}\frac{\mathscr{I}R^8\bar{\rho}_w^2}{64\mathscr{A}^2\bar{\mu}_w Z} \tag{4.23}$$

and

$$\mathscr{S}^* = \mathscr{F}^{-1}\frac{\mathscr{S}R^8\bar{\rho}_w^2}{64\mathscr{A}^2\bar{\mu}_w Z}, \tag{4.24}$$

where

$$\mathscr{F} = \left(\frac{4}{\bar{\mu}^{*2}(1-\xi/\mathscr{A}^2)^2} + \frac{2\mathscr{A}^2Pr(1-\gamma^{-1})}{\bar{\mu}^*\bar{K}^*(1-\xi/\mathscr{A}^2)}\left(1+\frac{\epsilon^2\bar{\rho}_{w1}\bar{\rho}_{w2}}{\bar{\rho}_w^2}\right)\right). \tag{4.25}$$

Here, we choose to incorporate the term $\epsilon^2\bar{\rho}_{w1}\bar{\rho}_{w2}/\bar{\rho}_w^2$ into the function $\mathscr{F}$, rather than using an expansion in the parameter ϵ, since this term is just a constant.

The sixth-order differential equation (4.21) requires six boundary conditions in the ξ coordinate. Of these, the symmetry conditions $\hat{v}_r = 0$ and $\partial\hat{v}_z/\partial r = 0$ at the centre $r = 0$ reduce to

$$\frac{\partial}{\partial\eta}\frac{\partial\chi^*}{\partial\xi} = 0 \quad \text{at } \xi = \mathscr{A}^2, \tag{4.26}$$

$$\frac{\partial}{\partial\xi}\left(\frac{1}{\bar{\rho}^*}\frac{\partial^2\chi^*}{\partial\xi^2}\right) = 0 \quad \text{at } \xi = \mathscr{A}^2, \tag{4.27}$$

$$\chi^* = 0 \quad \text{at } \xi = \mathscr{A}^2. \tag{4.28}$$

The third boundary condition (4.28) arises because we can set χ^* equal to zero at any location in the flow, since the velocity and temperature fields are related to derivatives of χ^* and it is convenient to choose $\chi^* = 0$ along the axis. For a long-cylinder approximation with $Z \gg R$, the boundary condition (4.26) reduces to $\partial\chi^*/\partial\xi = 0$ if we assume that there is no variation in χ^* along the axis. The

https://doi.org/10.1017/jfm.2014.365 Published online by Cambridge University Press

boundary conditions at the wall of the cylinder are the no-penetration condition $\hat{v}_r = 0$, the no-slip/slip condition $\hat{v}_z = V_z$ and the temperature boundary condition. The no-penetration condition is

$$\frac{\partial}{\partial \eta}\frac{\partial \chi^*}{\partial \xi} = 0 \quad \text{at } \xi = 0. \tag{4.29}$$

The velocity slip condition in the axial direction can be written as

$$\frac{1}{\bar{\rho}^*}\frac{\partial^2 \chi^*}{\partial \xi^2} = V_z \quad \text{at } \xi = 0, \tag{4.30}$$

where V_z is the slip velocity. The temperature boundary condition can be obtained from (3.32), assuming that $\hat{v}_\theta = 0$ at the wall. If we neglect terms of $O(R^2/Z^2)$ or $O(ReR^4/Z^4)$ or smaller, equation (3.32) can be written as

$$\begin{aligned}
&\mathscr{L}_5\chi^* + \left\{\frac{1}{\bar{\rho}^*\bar{\mu}^*}\frac{\partial \bar{\mu}^*}{\partial \xi}\left[\left(\frac{\partial}{\partial \xi}\left(\left(1-\frac{\xi}{\mathscr{A}^2}\right)\frac{\partial}{\partial \xi}\right)\right) + \left(\frac{1}{\bar{\rho}^*}\frac{\partial^2 \chi^*}{\partial \xi^2}\right)\right.\right. \\
&\quad \left.\left. + \left(1-\frac{\xi}{\mathscr{A}^2}\right)^{1/2}\frac{\partial}{\partial \xi}\left(\left(1-\frac{\xi}{\mathscr{A}^2}\right)^{1/2}\frac{\partial}{\partial \xi}\left(\frac{1}{\bar{\rho}^*}\frac{\partial^2 \chi^*}{\partial \xi^2}\right)\right)\right]\right. \\
&\quad - \frac{1}{\bar{\mu}^*}\frac{\partial}{\partial \xi}\left(\frac{(1-\xi/\mathscr{A}^2)^{1/2}}{\bar{\rho}^*}\frac{\partial \bar{\mu}^*}{\partial \xi}\right)\left[\left(1-\frac{\xi}{\mathscr{A}^2}\right)^{1/2}\frac{\partial}{\partial \xi}\left(\frac{1}{\bar{\rho}^*}\left(\frac{\partial^2 \chi^*}{\partial \xi^2}\right)\right)\right] \\
&\quad - \frac{Re^2R^2}{64\mathscr{A}^{12}Z^2\bar{\mu}^*}\frac{\partial}{\partial \eta}\left(\frac{\hat{T}}{\bar{T}}\right)\left(\frac{\epsilon^2\bar{\rho}^*_{w1}\bar{\rho}^*_{w2}(2+\xi)^2}{2}\right) + \frac{\epsilon ReR^2}{64\mathscr{A}^{12}Z^2\bar{\mu}^*}\frac{\partial \hat{N}_1}{\partial \eta} \\
&\quad \left. + \frac{Re^2R^2}{64\mathscr{A}^{12}Z^2\bar{\mu}^*}\frac{\epsilon^2\bar{\rho}^*_{w1}\bar{\rho}^*_{w2}(1+2\xi)}{\bar{\rho}^*}\frac{\partial}{\partial \eta}\left(\frac{\hat{p}m_{av}}{\bar{\rho}_w k_B \bar{T}}\right)\right\} \\
&= \frac{Re^2R^2}{64\mathscr{A}^{12}Z^2\bar{\mu}^*}\frac{\partial}{\partial \eta}\left(\frac{\hat{T}}{\bar{T}}\right).
\end{aligned} \tag{4.31}$$

Equation (4.31) can be simplified at $\xi = 0$, considering that $\bar{\mu}^* = 1$ and $\bar{\rho}^* = 1$, since the viscosity and density are scaled by their values at the wall,

$$\begin{aligned}
&\mathscr{L}_5\chi^* + \left\{\frac{1}{\bar{\rho}^*\bar{\mu}^*}\frac{\partial \bar{\mu}^*}{\partial \xi}\left[\left(\frac{\partial}{\partial \xi}\left(\left(1-\frac{\xi}{\mathscr{A}^2}\right)\frac{\partial}{\partial \xi}\right)\right) + \left(\frac{1}{\bar{\rho}^*}\frac{\partial^2 \chi^*}{\partial \xi^2}\right)\right.\right. \\
&\quad \left.\left. + \left(1-\frac{\xi}{\mathscr{A}^2}\right)^{1/2}\frac{\partial}{\partial \xi}\left(\left(1-\frac{\xi}{\mathscr{A}^2}\right)^{1/2}\frac{\partial}{\partial \xi}\left(\frac{1}{\bar{\rho}^*}\frac{\partial^2 \chi^*}{\partial \xi^2}\right)\right)\right]\right. \\
&\quad - \frac{1}{\bar{\mu}^*}\frac{\partial}{\partial \xi}\left(\frac{(1-\xi/\mathscr{A}^2)^{1/2}}{\bar{\rho}^*}\frac{\partial \bar{\mu}^*}{\partial \xi}\right)\left[\left(1-\frac{\xi}{\mathscr{A}^2}\right)^{1/2}\frac{\partial}{\partial \xi}\left(\frac{1}{\bar{\rho}^*}\left(\frac{\partial^2 \chi^*}{\partial \xi^2}\right)\right)\right] \\
&\quad \left. - \frac{Re^2R^2}{64\mathscr{A}^{12}Z^2\bar{\mu}^*}\frac{\partial \hat{N}_1}{\partial \eta} - \frac{Re^2R^2}{64\mathscr{A}^{12}Z^2\bar{\mu}^*}\frac{\epsilon^2\bar{\rho}^*_{w1}\bar{\rho}^*_{w2}}{\bar{\rho}^*}\frac{\partial}{\partial \eta}\left(\frac{\hat{p}m_{av}}{\bar{\rho}_w k_B \bar{T}}\right)\right\} \\
&= \frac{Re^2R^2}{64\mathscr{A}^{12}Z^2\bar{\mu}^*}\frac{\partial}{\partial \eta}\left(\frac{\hat{T}}{\bar{T}}\right)\left(1+\left(\frac{2\epsilon^2\bar{\rho}^*_{w1}\bar{\rho}^*_{w2}}{\bar{\rho}^2_w}\right)\right),
\end{aligned} \tag{4.32}$$

https://doi.org/10.1017/jfm.2014.365 Published online by Cambridge University Press

where the fifth-order operator $\mathscr{L}_5$ is

$$\mathscr{L}_5 = \frac{\partial}{\partial\xi}\left(\frac{1}{\bar{\rho}^*}\frac{\partial}{\partial\xi}\left(\left(1-\frac{\xi}{\mathscr{A}^2}\right)\frac{\partial}{\partial\xi}\left(\frac{1}{\bar{\rho}^*}\frac{\partial^2}{\partial\xi^2}\right)\right)\right). \tag{4.33}$$

The solution of (4.21) is obtained using an expansion in the small parameter ϵ for the master potential, the velocities and temperature of the form

$$\chi^* = \chi^{(0)} + \epsilon\chi^{(1)} + \epsilon^2\chi^{(2)}. \tag{4.34}$$

In the inhomogeneous term (4.19), it is clear that the largest contribution is $O(\epsilon)$. This is because the viscosity of the base flow, $\bar{\mu}$, is independent of position when the mass difference in the two species is neglected, and so $\mathrm{d}\bar{\mu}^*/\mathrm{d}\xi$ is $O(\epsilon)$. Using this, the inhomogeneous term can be written as

$$\mathscr{I}^* = \epsilon\mathscr{I}^{(1)} + \epsilon^2\mathscr{I}^{(2)}, \tag{4.35}$$

where

$$\begin{aligned}\mathscr{I}^{(1)} = &-\frac{\partial}{\partial\xi}\left\{\frac{1}{\epsilon\bar{\rho}^*\bar{\mu}^*}\frac{\partial\bar{\mu}^*}{\partial\xi}\left[\left(\frac{\partial}{\partial\xi}\left(\left(1-\frac{\xi}{\mathscr{A}^2}\right)\frac{\partial}{\partial\xi}\right)\right)\left(\frac{1}{\bar{\rho}^*}\frac{\partial^2\chi^{(0)}}{\partial\xi^2}\right)\right.\right.\\
&\left.+\left(1-\frac{\xi}{\mathscr{A}^2}\right)^{1/2}\frac{\partial}{\partial\xi}\left(\left(1-\frac{\xi}{\mathscr{A}^2}\right)^{1/2}\frac{\partial}{\partial\xi}\left(\frac{1}{\bar{\rho}^*}\frac{\partial^2\chi^{(0)}}{\partial\xi^2}\right)\right)\right]\\
&-\frac{1}{\epsilon\bar{\mu}^*}\frac{\partial}{\partial\xi}\left(\frac{(1-\xi/\mathscr{A}^2)^{1/2}}{\bar{\rho}^*}\frac{\partial\bar{\mu}^*}{\partial\xi}\right)\left[\left(1-\frac{\xi}{\mathscr{A}^2}\right)^{1/2}\frac{\partial}{\partial\xi}\left(\frac{1}{\bar{\rho}^*}\left(\frac{\partial^2\chi^{(0)}}{\partial\xi^2}\right)\right)\right]\\
&\left.-\frac{Re^2R^2}{64\mathscr{A}^{12}Z^2\bar{\mu}^*}\frac{\partial\hat{N}_1^{(0)}}{\partial\eta}\right\}+\frac{Re^2R^2}{16\mathscr{A}^{10}Z^2\bar{\mu}^{*2}\epsilon}\left(1+\frac{\xi}{\mathscr{A}^2}\right)^{-1/2}\frac{\partial\bar{\mu}^*}{\partial\xi}\frac{\partial}{\partial\eta}\left(\frac{\hat{v}_\theta^{(0)}}{R\Omega}\right)\\
&-\frac{Re^2R^2}{32\mathscr{A}^{10}Z^2\bar{\mu}^{*2}\epsilon}\frac{\partial\bar{\mu}^*}{\partial\xi}\frac{\partial}{\partial\eta}\left(\frac{\hat{T}^{(0)}}{\bar{T}}\right),\end{aligned} \tag{4.36}$$

$$\begin{aligned}\mathscr{I}^{(2)} = &-\frac{\partial}{\partial\xi}\left\{\frac{1}{\epsilon\bar{\rho}^*\bar{\mu}^*}\frac{\partial\bar{\mu}^*}{\partial\xi}\left[\left(\frac{\partial}{\partial\xi}\left(\left(1-\frac{\xi}{\mathscr{A}^2}\right)\frac{\partial}{\partial\xi}\right)\right)\left(\frac{1}{\bar{\rho}^*}\frac{\partial^2\chi^{(1)}}{\partial\xi^2}\right)\right.\right.\\
&\left.+\left(1-\frac{\xi}{\mathscr{A}^2}\right)^{1/2}\frac{\partial}{\partial\xi}\left(\left(1-\frac{\xi}{\mathscr{A}^2}\right)^{1/2}\frac{\partial}{\partial\xi}\left(\frac{1}{\bar{\rho}^*}\frac{\partial^2\chi^{(1)}}{\partial\xi^2}\right)\right)\right]\\
&-\frac{1}{\epsilon\bar{\mu}^*}\frac{\partial}{\partial\xi}\left(\frac{(1-\xi/\mathscr{A}^2)^{1/2}}{\bar{\rho}^*}\frac{\partial\bar{\mu}^*}{\partial\xi}\right)\left[\left(1-\frac{\xi}{\mathscr{A}^2}\right)^{1/2}\frac{\partial}{\partial\xi}\left(\frac{1}{\bar{\rho}^*}\left(\frac{\partial^2\chi^{(1)}}{\partial\xi^2}\right)\right)\right]\\
&+\frac{Re^2R^2}{64\mathscr{A}^{12}Z^2\bar{\mu}^*}\frac{\partial}{\partial\eta}\left(\frac{\hat{T}^{(0)}}{\bar{T}}\right)\left(\frac{\bar{\rho}_{w1}^*\bar{\rho}_{w2}^*(2+\xi)^2}{2}\right)\\
&\left.-\frac{Re^2R^2}{64\mathscr{A}^{12}Z^2\bar{\mu}^*}\frac{\partial\hat{N}_1^{(1)}}{\partial\eta}-\frac{Re^2R^2}{64\mathscr{A}^{12}Z^2\bar{\mu}^*}\frac{\bar{\rho}_{w1}^*\bar{\rho}_{w2}^*(1+2\xi)}{\bar{\rho}^*}\frac{\partial}{\partial\eta}\left(\frac{\hat{p}^{(0)}m_{av}}{\bar{\rho}_w k_B\bar{T}}\right)\right\}\end{aligned}$$

https://doi.org/10.1017/jfm.2014.365 Published online by Cambridge University Press

$$+\frac{Re^2R^2}{16\mathscr{A}^{10}Z^2\bar{\mu}^{*2}\epsilon}\left(1+\frac{\xi}{\mathscr{A}^2}\right)^{-1/2}\frac{\partial\bar{\mu}^*}{\partial\xi}\frac{\partial}{\partial\eta}\left(\frac{\hat{v}_\theta^{(1)}}{R\Omega}\right)$$

$$-\frac{Re^2R^2}{32\mathscr{A}^{10}Z^2\bar{\mu}^{*2}\epsilon}\frac{\partial\bar{\mu}^*}{\partial\xi}\frac{\partial}{\partial\eta}\left(\frac{\hat{T}^{(1)}}{\bar{T}}\right). \tag{4.37}$$

The hierarchy of equations for $\chi^{(0)}$, $\chi^{(1)}$ and $\chi^{(2)}$ can be written as

$$\mathscr{L}_6\chi^{(0)}+\frac{Re^2R^2}{64\mathscr{A}^{12}Z^2}\frac{\partial^2\chi^{(0)}}{\partial\eta^2}=\mathscr{S}^{(0)}, \tag{4.38}$$

$$\mathscr{L}_6\chi^{(1)}+\frac{Re^2R^2}{64\mathscr{A}^{12}Z^2}\frac{\partial^2\chi^{(1)}}{\partial\eta^2}=\mathscr{I}^{(1)}, \tag{4.39}$$

$$\mathscr{L}_6\chi^{(2)}+\frac{Re^2R^2}{64\mathscr{A}^{12}Z^2}\frac{\partial^2\chi^{(2)}}{\partial\eta^2}=\mathscr{I}^{(2)}. \tag{4.40}$$

The boundary conditions at the centre of the cylinder, (4.26)–(4.28), and the boundary conditions (4.29) at the wall are applied for $\chi^{(i)*}$ for $i=0$, 1 and 2. The slip boundary condition for the axial velocity (4.30) can be expanded as

$$\frac{1}{\bar{\rho}^*}\frac{\partial^2\chi^{(0)}}{\partial\xi^2}=V_z, \tag{4.41}$$

$$\frac{1}{\bar{\rho}^*}\frac{\partial^2\chi^{(1)}}{\partial\xi^2}=0, \tag{4.42}$$

$$\frac{1}{\bar{\rho}^*}\frac{\partial^2\chi^{(2)}}{\partial\xi^2}=0, \tag{4.43}$$

where V_z is the slip velocity at the wall. The temperature condition (4.32) can be expanded as

$$\mathscr{L}_5\chi^{(0)}=\frac{Re^2R^2}{32\mathscr{A}^{12}Z^2\bar{\mu}^*}\frac{\partial}{\partial\eta}\left(\frac{\hat{T}}{\bar{T}}\right), \tag{4.44}$$

$$\begin{aligned}\mathscr{L}_5\chi^{(1)}+\Bigg\{&\frac{1}{\epsilon\bar{\rho}^*\bar{\mu}^*}\frac{\partial\bar{\mu}^*}{\partial\xi}\left[\left(\frac{\partial}{\partial\xi}\left(\left(1-\frac{\xi}{\mathscr{A}^2}\right)\frac{\partial}{\partial\xi}\right)\right)+\left(\frac{1}{\bar{\rho}^*}\frac{\partial^2\chi^{(0)}}{\partial\xi^2}\right)\right.\\&\left.+\left(1-\frac{\xi}{\mathscr{A}^2}\right)^{1/2}\frac{\partial}{\partial\xi}\left(\left(1-\frac{\xi}{\mathscr{A}^2}\right)^{1/2}\frac{\partial}{\partial\xi}\left(\frac{1}{\bar{\rho}^*}\frac{\partial^2\chi^{(0)}}{\partial\xi^2}\right)\right)\right]\\&-\frac{1}{\epsilon\bar{\mu}^*}\frac{\partial}{\partial\xi}\left(\frac{(1-\xi/\mathscr{A}^2)^{1/2}}{\bar{\rho}^*}\frac{\partial\bar{\mu}^*}{\partial\xi}\right)\left[\left(1-\frac{\xi}{\mathscr{A}^2}\right)^{1/2}\frac{\partial}{\partial\xi}\left(\frac{1}{\bar{\rho}^*}\left(\frac{\partial^2\chi^{(0)}}{\partial\xi^2}\right)\right)\right]\\&-\frac{Re^2R^2}{32\mathscr{A}^{12}Z^2\bar{\mu}^*}\frac{\partial\hat{N}_1^{(0)}}{\partial\eta}\Bigg\}=0,\end{aligned} \tag{4.45}$$

$$\begin{aligned}\mathscr{L}_5\chi^{(2)}+\Bigg\{&\frac{1}{\epsilon\bar{\rho}^*\bar{\mu}^*}\frac{\partial\bar{\mu}^*}{\partial\xi}\left[\left(\frac{\partial}{\partial\xi}\left(\left(1-\frac{\xi}{\mathscr{A}^2}\right)\frac{\partial}{\partial\xi}\right)\right)+\left(\frac{1}{\bar{\rho}^*}\frac{\partial^2\chi^{(1)}}{\partial\xi^2}\right)\right.\\&\left.+\left(1-\frac{\xi}{\mathscr{A}^2}\right)^{1/2}\frac{\partial}{\partial\xi}\left(\left(1-\frac{\xi}{\mathscr{A}^2}\right)^{1/2}\frac{\partial}{\partial\xi}\left(\frac{1}{\bar{\rho}^*}\frac{\partial^2\chi^{(1)}}{\partial\xi^2}\right)\right)\right]\end{aligned}$$

https://doi.org/10.1017/jfm.2014.365 Published online by Cambridge University Press

$$-\frac{1}{\epsilon\bar{\mu}^*}\frac{\partial}{\partial\xi}\left(\frac{(1-\xi/\mathscr{A}^2)^{1/2}}{\bar{\rho}^*}\frac{\partial\bar{\mu}^*}{\partial\xi}\right)\left[\left(1-\frac{\xi}{\mathscr{A}^2}\right)^{1/2}\frac{\partial}{\partial\xi}\left(\frac{1}{\bar{\rho}^*}\left(\frac{\partial^2\chi^{(1)}}{\partial\xi^2}\right)\right)\right]$$
$$-\frac{Re^2R^2}{64\mathscr{A}^{12}Z^2\bar{\mu}^*}\frac{\partial\hat{N}_1^{(1)}}{\partial\eta}-\frac{Re^2R^2}{64\mathscr{A}^{12}Z^2\bar{\mu}^*}\frac{\epsilon^2\bar{\rho}^*_{w1}\bar{\rho}^*_{w2}}{\bar{\rho}^*}\frac{\partial}{\partial\eta}\left(\frac{\hat{p}^{(0)}m_{av}}{\bar{\rho}_w k_B\bar{T}}\right)\Bigg\}$$
$$=\frac{Re^2R^2}{32\mathscr{A}^{12}Z^2\bar{\mu}^*}\frac{\partial}{\partial\eta}\left(\frac{\hat{T}}{\bar{T}}\right)\left(\frac{2\bar{\rho}^*_{w1}\bar{\rho}^*_{w2}}{\bar{\rho}_w^2}\right). \tag{4.46}$$

Once the solutions for $\chi^{(i)}$ are obtained, the fluid velocity components $\hat{v}_r^{(i)}$ and $\hat{v}_z^{(i)}$ are obtained using (3.28), (3.29) and (3.31). The velocity $\hat{v}_\theta^{(i)}$ is calculated from (3.9), where the axial derivatives are neglected consistent with the approximation in the Onsager model,

$$2\bar{\rho}\Omega\hat{v}_r^{(i)}=\frac{4\mathscr{A}^4}{R^2(1-\xi/\mathscr{A}^2)^{1/2}}\frac{\partial}{\partial\xi}\left((1-\xi/\mathscr{A}^2)^2\bar{\mu}\frac{\partial}{\partial\xi}\left(\frac{\hat{v}_\theta^{(i)}}{(1-\xi/\mathscr{A}^2)^{1/2}}\right)\right)+f_\theta^{(i)}, \tag{4.47}$$

where the leading-order force density is assumed to be the applied force density, $f_\theta^{(0)}=f_\theta$, and $f_\theta^{(1)}=f_\theta^{(2)}=0$. The above second-order differential equation is solved with two boundary conditions, $\hat{v}_\theta^{(i)}=0$ at the wall $\xi=0$ ($r=R$), and $\partial\hat{v}_\theta^{(i)}/\partial\xi=0$ at the centre $\xi=\mathscr{A}^2$ ($r=0$), to obtain velocity $\hat{v}_\theta$. The temperature field is determined from (3.13), where the axial derivatives are neglected,

$$0=\frac{\bar{p}\hat{v}_r^{(i)}}{\bar{\rho}}\frac{\partial\bar{\rho}}{\partial r}+\frac{4\mathscr{A}^4}{R^2}\frac{\partial}{\partial\xi}\left(\bar{K}(1-\xi/\mathscr{A}^2)\frac{\partial\hat{T}^{(i)}}{\partial\xi}\right)+\mathscr{S}_{\mathrm{e}}^{(i)'}, \tag{4.48}$$

where the leading-order contribution to the energy source is equal to the total energy source, $S_e^{(0)\prime}=S_e'$, and $S_e^{(1)\prime}=S_e^{(2)\prime}=0$. The above second-order differential equation is solved with boundary conditions $\hat{T}^{(0)}=\hat{T}_w$, $\hat{T}^{(1)}=0$, $\hat{T}^{(2)}=0$ at the wall $\xi=0$ (where $\hat{T}_w$ is the wall temperature), and $\partial\hat{T}^{(i)}/\partial\xi=0$ at the centre $\xi=\mathscr{A}^2$, to obtain the temperature field. The axial pressure gradient is calculated using (3.10), with the axial velocity derivatives neglected for the radial boundary layer. The mole fraction $\hat{N}_1^{(i)}$ is calculated from the diffusion equation (2.25). In this, the divergence of the velocity times the mass density can first be simplified as follows:

$$\begin{aligned}\frac{1}{r}\frac{\partial(\hat{v}_r\bar{\rho}_1)}{\partial r}+\frac{\partial(\hat{v}_z\bar{\rho}_1)}{\partial z}&=\frac{1}{r}\frac{\partial}{\partial r}\left(-\frac{\bar{\rho}_1}{\bar{\rho}}\left(\frac{\partial\psi}{\partial z}+\int_0^r r'dr'\mathscr{S}_m\right)\right)+\frac{\partial}{\partial z}\left(\frac{\bar{\rho}_1}{\bar{\rho}r}\frac{\partial\psi}{\partial r}\right)\\&=-\frac{\partial\psi}{\partial z}\left(\frac{1}{r}\frac{\partial}{\partial r}\left(\frac{\bar{\rho}_1}{\bar{\rho}}\right)\right)-\frac{1}{r}\frac{\partial}{\partial r}\left(\frac{\bar{\rho}_1}{\bar{\rho}}\int_0^r r'dr'\mathscr{S}_m\right)\\&=-\left(\frac{1}{r}\frac{\partial}{\partial r}\left(\frac{\bar{\rho}_1}{\bar{\rho}}\right)\right)\frac{1}{r}\frac{\partial^2\chi}{\partial r\partial z}-\frac{1}{r}\frac{\partial}{\partial r}\left(\frac{\bar{\rho}_1}{\bar{\rho}}\int_0^r r'dr'\mathscr{S}_m\right).\end{aligned} \tag{4.49}$$

This is inserted into the diffusion equation (2.25), and the spatial coordinates are expressed in terms of ξ and η, to obtain

https://doi.org/10.1017/jfm.2014.365 Published online by Cambridge University Press

$$\frac{\partial}{\partial\xi}\left[\frac{\bar{D}'_{12}m_{av}m_1^*m_2^*(1-\xi/\mathscr{A}^2)}{m_1^*\bar{N}_1+m_2^*\bar{N}_2}\left(\frac{4\mathscr{A}^4}{R^2}\left(\frac{\partial\hat{N}_1}{\partial\xi}+\frac{\epsilon m_{av}\bar{N}_1\bar{N}_2}{\bar{\rho}k_B\bar{T}}\frac{\partial\hat{p}}{\partial\xi}-\frac{k_T}{\bar{T}}\frac{\partial\hat{T}}{\partial\xi}\right)\right.\right.$$
$$\left.\left.-\frac{2\mathscr{A}^2\epsilon m_{av}\Omega^2}{k_B\bar{T}}\left(-(\bar{N}_2-\bar{N}_1)\hat{N}_1+\frac{\hat{T}}{\bar{T}}+\frac{\hat{\rho}}{\bar{\rho}}\right)\right)\right]$$
$$+\frac{\bar{D}'_{12}m_{av}}{Z^2}\frac{m_1^*m_2^*}{\bar{N}_1m_1^*+\bar{N}_2m_2^*}\left(\frac{\partial^2\hat{N}_1}{\partial\eta^2}+\frac{\epsilon m_{av}\bar{N}_1\bar{N}_2}{\bar{\rho}k_B\bar{T}}\frac{\partial^2\hat{p}}{\partial\eta^2}-k_T\frac{\partial^2\hat{T}}{\partial\eta^2}\right)$$
$$+\frac{1}{r}\frac{\partial^2\chi}{\partial r\partial z}\left(\frac{1}{r}\frac{\partial}{\partial r}\left(\frac{\bar{\rho}_1}{\bar{\rho}}\right)\right)+\frac{1}{r}\frac{\partial}{\partial r}\left(\frac{\bar{\rho}_1}{\bar{\rho}}\int_0^r r'dr'\mathscr{S}_m\right)=0. \tag{4.50}$$

The axial derivatives are neglected in comparison to the radial derivatives in the limit $R^2/Z^2\ll 1$, and the master potential is defined in terms of the scaled master potential $\chi=\bar{\mu}_wR^2Z\chi^*$, to obtain the equation

$$\frac{4\mathscr{A}^4m_{av}}{R^2}\frac{\partial}{\partial\xi}\left[\frac{\bar{D}'_{12}m_1^*m_2^*(1-\xi/\mathscr{A}^2)}{m_1^*\bar{N}_1+m_2^*\bar{N}_2}\left(\frac{\partial\hat{N}_1}{\partial\xi}+\frac{\epsilon m_{av}\bar{N}_1\bar{N}_2}{\bar{\rho}k_B\bar{T}}\frac{\partial\hat{p}}{\partial\xi}-\frac{k_T}{\bar{T}}\frac{\partial\hat{T}}{\partial\xi}\right.\right.$$
$$\left.\left.-\frac{\epsilon m_{av}\Omega^2R^2}{2\mathscr{A}^2k_B\bar{T}}\left(-(\bar{N}_2-\bar{N}_1)\hat{N}_1+\frac{\hat{T}}{\bar{T}}+\frac{\hat{\rho}}{\bar{\rho}}\right)\right)\right]$$
$$+\frac{\bar{\mu}_w}{R^2}\frac{\partial^2\chi^*}{\partial\xi\partial\eta}\left(\frac{\partial}{\partial\xi}\left(\frac{\bar{\rho}_1^*}{\bar{\rho}^*}\right)\right)+\frac{\bar{\mu}_w}{R^2}\frac{\partial}{\partial\xi}\left(\frac{\bar{\rho}_1^*}{\bar{\rho}^*}\int_{\mathscr{A}^2}^{\xi}\mathrm{d}\xi'\mathscr{S}_m^*\right)=0. \tag{4.51}$$

Substituting for $\hat{\rho}$ from (3.23), the above equation becomes

$$\frac{4\mathscr{A}^4m_{av}\bar{D}'_{12}}{R^2}\frac{\partial}{\partial\xi}\left[\frac{\bar{D}_{12}^*m_1^*m_2^*(1-\xi/\mathscr{A}^2)}{m_1^*\bar{N}_1+m_2^*\bar{N}_2}\left(\frac{\partial\hat{N}_1}{\partial\xi}+\frac{\epsilon m_{av}\bar{N}_1\bar{N}_2}{\bar{\rho}k_B\bar{T}}\frac{\partial\hat{p}}{\partial\xi}-\frac{k_T}{\bar{T}}\frac{\partial\hat{T}}{\partial\xi}\right.\right.$$
$$-\frac{\epsilon m_{av}\Omega^2R^2}{2\mathscr{A}^2k_B\bar{T}}\left(-(\bar{N}_2-\bar{N}_1)\hat{N}_1+\frac{\hat{p}m_{av}}{\bar{\rho}k_B\bar{T}}\left(1+\frac{\epsilon^2(1+\xi)\bar{\rho}_{w1}\bar{\rho}_{w2}}{\bar{\rho}_w^2}\right)\right.$$
$$\left.\left.\left.-\frac{\epsilon^2(2+\xi)^2\bar{\rho}_{w1}\bar{\rho}_{w2}}{\bar{\rho}_w^2}\frac{\hat{T}}{\bar{T}}\right)\right)\right]+\frac{\bar{\mu}_w}{R^2}\frac{\partial^2\chi^*}{\partial\xi\partial\eta}\left(\frac{\partial}{\partial\xi}\left(\frac{\bar{\rho}_1}{\bar{\rho}}\right)\right)$$
$$+\frac{\bar{\mu}_w}{R^2}\frac{\partial}{\partial\xi}\left(\frac{\bar{\rho}_1^*}{\bar{\rho}^*}\int_{\mathscr{A}^2}^{\xi}\mathrm{d}\xi'\mathscr{S}_m^*\right)=0. \tag{4.52}$$

Scaling the above equation, we obtain

$$\frac{\partial}{\partial\xi}\left[\frac{\bar{D}_{12}^*m_1^*m_2^*(1-\xi/\mathscr{A}^2)}{m_1^*\bar{N}_1+m_2^*\bar{N}_2}\left(\frac{\partial\hat{N}_1}{\partial\xi}+\frac{\epsilon m_{av}\bar{N}_1\bar{N}_2}{\bar{\rho}k_B\bar{T}}\frac{\partial\hat{p}}{\partial\xi}-\frac{k_T}{\bar{T}}\frac{\partial\hat{T}}{\partial\xi}\right.\right.$$
$$\left.\left.-\frac{\epsilon m_{av}\Omega^2R^2}{2\mathscr{A}^2k_B\bar{T}}\left(-(\bar{N}_2-\bar{N}_1)\hat{N}_1+\frac{\hat{p}m_{av}}{\bar{\rho}k_B\bar{T}}\left(1+\frac{\epsilon^2(1+\xi)\bar{\rho}_{w1}\bar{\rho}_{w2}}{\bar{\rho}_w^2}\right)\right.\right.\right.$$

https://doi.org/10.1017/jfm.2014.365 Published online by Cambridge University Press

$$-\frac{\epsilon^2(2+\xi)^2\bar{\rho}_{w1}\bar{\rho}_{w2}}{\bar{\rho}_w^2}\frac{\hat{T}}{\bar{T}}\Bigg)\Bigg)\Bigg]$$
$$+Sc\left(\frac{\partial^2\chi^*}{\partial\xi\,\partial\eta}\left(\frac{\partial}{\partial\xi}\left(\frac{\bar{\rho}_1}{\bar{\rho}}\right)\right)+\frac{\partial}{\partial\xi}\left(\frac{\bar{\rho}_1^*}{\bar{\rho}^*}\int_{\mathscr{A}^2}^{\xi}\mathrm{d}\xi'\mathscr{S}_m^*\right)\right)=0, \tag{4.53}$$

where $Sc = (\bar{\mu}_w/m_{av}\bar{D}'_w)$, equation (2.20), is the Schmidt number based on the viscosity, diffusivity and number density at the wall in the base state, $m_1^* = m_1/m_{av}$ and $m_2^* = m_2/m_{av}$.

Equation (4.53) can be expanded in a series in ϵ and solved at each order to determine $\hat{N}_1$:

$$\frac{\partial}{\partial\xi}\left[\frac{\bar{D}_{12}^*m_1^*m_2^*(1-\xi/\mathscr{A}^2)}{m_1^*\bar{N}_1+m_2^*\bar{N}_2}\left(\frac{\partial\hat{N}_1^{(0)}}{\partial\xi}-\frac{k_T}{\bar{T}}\frac{\partial\hat{T}^{(0)}}{\partial\xi}\right)\right]$$
$$+Sc\left[\frac{\partial^2\chi^{(0)}}{\partial\xi\,\partial\eta}\left(\frac{\partial}{\partial\xi}\left(\frac{\bar{\rho}_1}{\bar{\rho}}\right)\right)+\frac{\partial}{\partial\xi}\left(\frac{\bar{\rho}_1^*}{\bar{\rho}^*}\int_{\mathscr{A}^2}^{\xi}\mathrm{d}\xi'\mathscr{S}_m^*\right)\right]=0, \tag{4.54}$$

$$\frac{\partial}{\partial\xi}\left[\frac{\bar{D}_{12}^*m_1^*m_2^*(1-\xi/\mathscr{A}^2)}{m_1^*\bar{N}_1+m_2^*\bar{N}_2}\left(\frac{\partial\hat{N}_1^{(1)}}{\partial\xi}+\frac{m_{av}\bar{N}_1\bar{N}_2}{\bar{\rho}k_B\bar{T}}\frac{\partial\hat{p}^{(0)}}{\partial\xi}-\frac{k_T}{\bar{T}}\frac{\partial\hat{T}^{(1)}}{\partial\xi}\right.\right.$$
$$\left.\left.-\frac{m_{av}\Omega^2R^2}{2\mathscr{A}^2k_B\bar{T}}\left(-(\bar{N}_2-\bar{N}_1)\hat{N}_1^{(0)}+\frac{\hat{p}^{(0)}m_{av}}{\bar{\rho}k_B\bar{T}}\right)\right)\right]+Sc\frac{\partial^2\chi^{(1)}}{\partial\xi\,\partial\eta}\left(\frac{\partial}{\partial\xi}\left(\frac{\bar{\rho}_1}{\bar{\rho}}\right)\right)=0, \tag{4.55}$$

$$\frac{\partial}{\partial\xi}\left[\frac{\bar{D}_{12}^*m_1^*m_2^*(1-\xi/\mathscr{A}^2)}{m_1^*\bar{N}_1+m_2^*\bar{N}_2}\left(\frac{\partial\hat{N}_1^{(2)}}{\partial\xi}+\frac{m_{av}\bar{N}_1\bar{N}_2}{\bar{\rho}k_B\bar{T}}\frac{\partial\hat{p}^{(1)}}{\partial\xi}-\frac{k_T}{\bar{T}}\frac{\partial\hat{T}^{(2)}}{\partial\xi}\right.\right.$$
$$\left.\left.-\frac{m_{av}\Omega^2R^2}{2\mathscr{A}^2k_B\bar{T}}\left(-(\bar{N}_2-\bar{N}_1)\hat{N}_1^{(1)}+\frac{\hat{p}^{(1)}m_{av}}{\bar{\rho}k_B\bar{T}}\right)\right)\right]+Sc\frac{\partial^2\chi^{(2)}}{\partial\xi\,\partial\eta}\left(\frac{\partial}{\partial\xi}\left(\frac{\bar{\rho}_1}{\bar{\rho}}\right)\right)=0. \tag{4.56}$$

Equations (4.38)–(4.46) are inhomogeneous linear differential equations with inhomogeneous boundary conditions. These are solved as follows. The solution is first separated into two parts,

$$\chi=\chi_h+\chi_b, \tag{4.57}$$

where χ_h is the solution for the inhomogeneous equation with homogeneous boundary conditions, and χ_b is the solution of the homogeneous differential equation with the inhomogeneous boundary conditions.

The solution for χ_h is of the form

$$\mathscr{L}_6\chi_h+\frac{Re^2R^2}{64\mathscr{A}^{12}Z^2}\frac{\partial^2\chi_h}{\partial\eta^2}=\mathscr{I}^{(i)}, \tag{4.58}$$

with boundary conditions

$$\frac{\partial\chi_h}{\partial\xi}=0 \quad \text{at } \xi=0, \tag{4.59}$$
$$\frac{\partial^2\chi_h}{\partial\xi^2}=0 \quad \text{at } \xi=0, \tag{4.60}$$
$$\mathscr{L}_5\chi_h=0 \quad \text{at } \xi=0, \tag{4.61}$$
$$\chi_h=0 \quad \text{at } \xi=\mathscr{A}^2, \tag{4.62}$$

https://doi.org/10.1017/jfm.2014.365 Published online by Cambridge University Press

$$\frac{\partial \chi_h}{\partial \xi} = 0 \quad \text{at } \xi = \mathscr{A}^2, \tag{4.63}$$

$$\mathscr{L}_3 \chi_h = 0 \quad \text{at } \xi = \mathscr{A}^2, \tag{4.64}$$

which is calculated using separation of variables,

$$\chi_h = G(\xi)H(\eta). \tag{4.65}$$

It can be shown that the operator $\mathscr{L}_6$ is self-adjoint when the inner product of two functions of ξ in the domain $0 \leqslant \xi \leqslant \mathscr{A}^2$ is defined with the weighting function $\mathscr{F}$ (4.25),

$$(A, B) = \int_0^{\mathscr{A}^2} \mathrm{d}\xi \; \mathscr{F}(\xi)A(\xi)B(\xi). \tag{4.66}$$

With this definition, the inner adjoint operator for $\mathscr{L}_6$ is evaluated as

$$\begin{aligned}(A, \mathscr{L}_6 B) &= \int_0^{\mathscr{A}^2} \mathrm{d}\xi \, A(\xi)\mathscr{L}_6 B(\xi) \\ &= A(\xi)\mathscr{L}_5 B(\xi)|_{\xi=0}^{\mathscr{A}^2} - \frac{\mathrm{d}A(\xi)}{\mathrm{d}\xi}\mathscr{L}_4 B(\xi)\bigg|_{\xi=0}^{\mathscr{A}^2} + \frac{\mathrm{d}^2 A(\xi)}{\mathrm{d}\xi^2}\mathscr{L}_3 B(\xi)\bigg|_{\xi=0}^{\mathscr{A}^2} \\ &\quad - \frac{\mathrm{d}^2 B(\xi)}{\mathrm{d}\xi^2}\mathscr{L}_3 A(\xi)\bigg|_{\xi=0}^{\mathscr{A}^2} + \frac{\mathrm{d}B(\xi)}{\mathrm{d}\xi}\mathscr{L}_5 A(\xi)\bigg|_{\xi=0}^{\mathscr{A}^2} - B(\xi)\mathscr{L}_5 A(\xi)|_{\xi=0}^{\mathscr{A}^2} \\ &\quad + \int_0^{\mathscr{A}^2} \mathrm{d}\xi B(\xi)\mathscr{L}_6 A(\xi).\end{aligned} \tag{4.67}$$

It is evident that the operator $\mathscr{L}_6$ in (4.67) is self-adjoint if the inner product is defined in (4.66) and if the functions $A(\xi)$ and $B(\xi)$ satisfy the boundary conditions (4.59)–(4.64). The eigenvalue problem is expressed as

$$\mathscr{L}_6 \mathscr{G}_m = -\alpha_m \mathscr{G}_m, \tag{4.68}$$

where the eigenvalues α_m are real and the eigenfunctions are defined to be orthonormal,

$$(\mathscr{G}_m, \mathscr{G}_{m'}) = \delta_{mm'}. \tag{4.69}$$

The solution for χ_h, with zero normal velocity conditions at the end-plates in the z direction, can then be written as

$$\chi_h = \sum_{m,n} A_{mn}\mathscr{G}_m(\xi)(\sqrt{2}\sin(n\pi\eta)), \tag{4.70}$$

where the coefficients A_{mn} are

$$A_{mn} = -\frac{1}{\alpha_m + (n\pi ReR/8\mathscr{A}^6 Z)^2}\int_0^{\mathscr{A}^2} \mathrm{d}\xi \int_0^1 \mathrm{d}\eta \, \mathscr{F}(\xi)\mathscr{I}^{(i)}(\xi, \eta)\mathscr{G}_m(\xi)(\sqrt{2}\sin(n\pi\eta)). \tag{4.71}$$

For the homogeneous equation with inhomogeneous boundary conditions, the differential equation is of the form

$$\mathscr{L}_6 \chi_b + \frac{Re^2 R^2}{64\mathscr{A}^{12} Z^2}\frac{\partial^2 \chi_b}{\partial \eta^2} = 0. \tag{4.72}$$

https://doi.org/10.1017/jfm.2014.365 Published online by Cambridge University Press

For a linear temperature gradient at the wall, χ_b is also a linear function of η. The solution is of the form

$$\chi_b = \mathscr{H}(\xi), \tag{4.73}$$

where T_0 is the wall temperature at $\eta = 0$, T' is the wall temperature gradient and $\mathscr{H}$ is the solution of the equation

$$\mathscr{L}_6\mathscr{H}(\xi) = 0, \tag{4.74}$$

with boundary conditions

$$\frac{\partial \mathscr{H}}{\partial \xi} = 0 \quad \text{at } \xi = 0, \tag{4.75}$$

$$\frac{1}{\bar{\rho}^*}\frac{\partial^2 \mathscr{H}}{\partial \xi^2} = V_z \quad \text{at } \xi = 0, \tag{4.76}$$

$$\mathscr{L}_5\mathscr{H} = -\frac{Re^2}{32\mathscr{A}^{10}}\frac{R^2}{Z^2}\frac{1}{\bar{T}}\left.\frac{\mathrm{d}T}{\mathrm{d}\eta}\right|_w \quad \text{at } \xi = 0, \tag{4.77}$$

$$\mathscr{H} = 0 \quad \text{at } \xi = \mathscr{A}^2, \tag{4.78}$$

$$\frac{\partial \mathscr{H}}{\partial \xi} = 0 \quad \text{at } \xi = \mathscr{A}^2, \tag{4.79}$$

$$\mathscr{L}_3\mathscr{H} = 0 \quad \text{at } \xi = \mathscr{A}^2, \tag{4.80}$$

with $(\mathrm{d}T/\mathrm{d}\eta)|_w$ the temperature gradient at the wall, and T_0 the average temperature. The form of the inhomogeneous boundary condition, (4.78), is derived from the boundary conditions (4.46) at the wall.

5. Radial flow at end-caps

For the radial flow, the axial distance from the end-caps is small compared to the radius of the cylinder. The starting point is (3.30) for the stream function, where the velocity $\hat{v}_\theta$ and temperature $\hat{T}$ are substituted from the right sides of (3.9) and (3.13) as follows. The calculation is carried out without considering internal sources and sinks, because these are not usually relevant for the axial flow at the end-caps. The momentum equation in the θ direction, (3.9), is written in terms of the stream function as

$$-\frac{2\Omega}{r}\frac{\partial \psi}{\partial z} = \frac{1}{r^2}\frac{\partial}{\partial r}\left(r^3\bar{\mu}\frac{\partial}{\partial r}\left(\frac{\hat{v}_\theta}{r}\right)\right) + \bar{\mu}\frac{\partial^2 \hat{v}_\theta}{\partial z^2}. \tag{5.1}$$

This is multiplied by $-2\Omega/\bar{\mu}^2 r$ and integrated with respect to the z coordinate with the boundary condition $\psi = 0$ at the end-cap $z = z_0$ to obtain

$$-\frac{2\Omega}{\bar{\mu}r}\frac{\partial \hat{v}_\theta}{\partial z} = \frac{4\Omega^2}{\bar{\mu}^2 r^2}\psi + \int_{z_0}^{z}\mathrm{d}z\,\frac{2\Omega}{\bar{\mu}r^3}\frac{\partial}{\partial r}\left(r^3\frac{\partial}{\partial r}\left(\frac{\hat{v}_\theta}{r}\right)\right). \tag{5.2}$$

The temperature equation (3.13) is expressed in terms of the stream function to obtain

$$-\frac{\bar{p}}{\bar{\rho}^2 r}\frac{\partial \bar{\rho}}{\partial r}\frac{\partial \psi}{\partial z} + \frac{1}{r}\frac{\partial}{\partial r}\left(r\bar{K}\frac{\partial \hat{T}}{\partial r}\right) + \bar{K}\frac{\partial^2 \hat{T}}{\partial z^2} = 0. \tag{5.3}$$

https://doi.org/10.1017/jfm.2014.365 Published online by Cambridge University Press

This equation is integrated once with respect to z, and multiplied by $\Omega^2/\bar{K}\bar{\mu}\bar{T}$, to obtain

$$\frac{\Omega^2}{\bar{\mu}\bar{T}}\frac{\partial\hat{T}}{\partial z}=\frac{\Omega^2\bar{p}}{\bar{K}\bar{\mu}\bar{T}\bar{\rho}^2 r}\frac{\partial\bar{\rho}}{\partial r}\psi-\frac{\Omega^2}{\bar{K}\bar{\mu}\bar{T}}\int_{z_0}^{z}\mathrm{d}z\,\frac{1}{r}\frac{\partial}{\partial r}\left(r\bar{K}\frac{\partial\hat{T}}{\partial r}\right). \tag{5.4}$$

The expansion

$$\begin{aligned}\frac{\bar{p}}{\bar{\rho}^2 r}\frac{\partial\bar{\rho}}{\partial r} &= \frac{1}{\bar{\rho}r}\frac{\partial\bar{p}}{\partial r}\left(1+\frac{\epsilon^2\bar{\rho}_{w1}\bar{\rho}_{w2}}{\bar{\rho}_w^2}\right)\\ &= \Omega^2\left(1+\frac{\epsilon^2\bar{\rho}_{w1}\bar{\rho}_{w2}}{\bar{\rho}_w^2}\right)\end{aligned} \tag{5.5}$$

is used in the above expression to obtain

$$\begin{aligned}&\left(1+\frac{\epsilon^2\bar{\rho}_{w1}\bar{\rho}_{w2}(2+\xi)^2}{2\bar{\rho}_w^2}\right)\frac{\Omega^2}{\bar{\mu}\bar{T}}\frac{\partial\hat{T}}{\partial z}\\ &\quad=\frac{\Omega^4}{\bar{K}\bar{\mu}\bar{T}}\left(1+\frac{\epsilon^2\bar{\rho}_{w1}\bar{\rho}_{w2}((2+\xi)^2+2)}{2\bar{\rho}_w^2}\right)\psi\\ &\qquad-\left(1+\frac{\epsilon^2\bar{\rho}_{w1}\bar{\rho}_{w2}(2+\xi)^2}{2\bar{\rho}_w^2}\right)\frac{\Omega^2}{\bar{K}\bar{\mu}\bar{T}}\int_{z_0}^{z}\mathrm{d}z\left(\frac{1}{r}\frac{\partial}{\partial r}\left(r\bar{K}\frac{\partial\hat{T}}{\partial r}\right)\right).\end{aligned} \tag{5.6}$$

Equations (5.2) and (5.6) are inserted into the equation for the stream function, (3.30), to give

$$\begin{aligned}&\frac{1}{r}\frac{\partial}{\partial r}\left(\frac{1}{\bar{\rho}r}\frac{\partial}{\partial r}\left(r\frac{\partial}{\partial r}\right)+\frac{1}{\bar{\rho}}\frac{\partial^2}{\partial z^2}\right)\left(\frac{1}{\bar{\rho}r}\frac{\partial\psi}{\partial r}\right)\\ &\quad+\left[\frac{1}{\bar{\rho}r}\frac{\partial}{\partial r}\left(\frac{1}{r}\frac{\partial}{\partial r}\left(r\frac{\partial}{\partial z}\right)\right)+\frac{1}{\bar{\rho}r}\frac{\partial^3}{\partial z^3}\right]\left(\frac{1}{\bar{\rho}r}\left(\frac{\partial\psi}{\partial z}\right)\right)-\frac{1}{3r^2\bar{\rho}^4}\left(\frac{\partial\bar{\rho}}{\partial r}\right)^2\frac{\partial^2\psi}{\partial z^2}\\ &\quad+\frac{1}{\bar{\rho}\bar{\mu}r}\frac{\partial\bar{\mu}}{\partial r}\left(\left(\nabla^2+\frac{\partial^2}{\partial r^2}\right)\left(\frac{1}{\bar{\rho}r}\frac{\partial\psi}{\partial r}\right)+\frac{\partial^2}{\partial r\partial z}\left(\frac{1}{\bar{\rho}r}\frac{\partial\psi}{\partial z}\right)\right)\\ &\quad+\frac{1}{\bar{\mu}r}\frac{\partial}{\partial r}\left(\frac{1}{\bar{\rho}}\frac{\partial\bar{\mu}}{\partial r}\right)\left(\frac{\partial}{\partial r}\left(\frac{1}{\bar{\rho}r}\frac{\partial\psi}{\partial r}\right)-\frac{1}{\bar{\rho}r}\frac{\partial^2\psi}{\partial z^2}\right)\\ &\quad+\psi\left(\frac{4\Omega^2}{\bar{\mu}^2r^2}+\frac{\Omega^4}{\bar{K}\bar{\mu}\bar{T}}\left(1+\frac{\epsilon^2((2+\xi)^2+2)\bar{\rho}_{w1}\bar{\rho}_{w2}}{2\bar{\rho}_w^2}\right)\right)\\ &\quad-\frac{\Omega^2}{\bar{\mu}}\frac{\partial\hat{N}_1}{\partial z}-\frac{\epsilon^2 m_{av}\Omega^2\bar{\rho}_{w1}\bar{\rho}_{w2}(1+2\xi)}{k_B\bar{T}\bar{\mu}\bar{\rho}\bar{\rho}_w^2}\frac{\partial\hat{p}}{\partial z}+\int_{z_0}^{z}\mathrm{d}z\frac{2\Omega}{\bar{\mu}r^3}\frac{\partial}{\partial r}\left(r^3\frac{\partial}{\partial r}\left(\frac{\hat{v}_\theta}{r}\right)\right)\\ &\quad-\frac{\Omega^2}{\bar{K}\bar{\mu}\bar{T}}\left(1+\frac{\epsilon^2\bar{\rho}_{w1}\bar{\rho}_{w2}(2+\xi)^2}{2\bar{\rho}_w^2}\right)\left(\int_{z_0}^{z}\mathrm{d}z\frac{1}{r}\frac{\partial}{\partial r}\left(r\bar{K}\frac{\partial\hat{T}}{\partial r}\right)\right)=0.\end{aligned} \tag{5.7}$$

Equation (5.7) can be simplified by including only the highest derivative of ψ with respect to z in the limit where the boundary layer thickness δ_Z is small compared to the radial extent R. The resulting equation is scaled using $r^*=r/R$, $z^*=z/\delta_Z$ and $\psi^*=\psi/\bar{\mu}_w\delta_Z$, and multiplied by $\bar{\rho}_w^2\delta_Z^3R^2/\bar{\mu}_w$ to give

https://doi.org/10.1017/jfm.2014.365 Published online by Cambridge University Press

$$\frac{1}{\bar{\rho}^{*2}r^{*2}}\frac{\partial^4\psi^*}{\partial z^{*4}}+\psi^*\left(\frac{4Re^2\delta_Z^4}{\bar{\mu}^{*2}r^{*2}R^4}+\frac{2\mathscr{A}^2Re^2Pr(1-\gamma^{-1})\delta_Z^4}{R^4\bar{K}^*\bar{\mu}^*}\left(1+\frac{\epsilon^2((2+\xi)^2+2)\bar{\rho}_{w1}\bar{\rho}_{w2}}{2\bar{\rho}_w^2}\right)\right)$$
$$-\frac{\epsilon Re^2\delta_Z^2}{R^2\bar{\mu}^*}\frac{\partial\hat{N}_1}{\partial z}-\frac{\epsilon^2Re^2\delta_Z^2}{R^2}\frac{\bar{\rho}^*_{w1}\bar{\rho}^*_{w2}(1+2\xi)}{\bar{\mu}^*\bar{\rho}^*\bar{\rho}^{*2}_w}\frac{\partial}{\partial z^*}\left(\frac{\hat{p}m_{av}}{\bar{\rho}_wk_B\bar{T}}\right)=0. \tag{5.8}$$

Equation (5.8) cannot be solved autonomously, but it is necessary to couple this with the diffusion equation in order to obtain the stream function. We return to the solution of (2.25) for the species mole fractions, where (4.49) is used for the velocities. If (2.25) is scaled in a manner similar to (4.50), we obtain

$$\frac{\bar{D}'_{12}m_{av}}{R^2}\frac{1}{r^*}\frac{\partial}{\partial r^*}\left[\frac{m_1^*m_2^*r^*}{m_1^*\bar{N}_1+m_2^*\bar{N}_2}\left(\frac{\partial\hat{N}_1}{\partial r^*}+2\epsilon\mathscr{A}^2r^*\left(-(\bar{N}_2-\bar{N}_1)\hat{N}_1+\hat{T}^*+\frac{\hat{\rho}^*}{\bar{\rho}^*}\right)\right.\right.$$
$$\left.\left.+\frac{2\epsilon\mathscr{A}^2\bar{N}_1\bar{N}_2}{Re^2\bar{\rho}^*}\frac{\partial\hat{p}^*}{\partial r^*}-\frac{k_T}{\bar{T}}\frac{\partial\hat{T}}{\partial r^*}\right)\right]+\frac{\bar{D}'_{12}m_{av}}{\delta_Z^2}\frac{m_1^*m_2^*}{\bar{N}_1m_1^*+\bar{N}_2m_2^*}$$
$$\times\left(\frac{\partial^2\hat{N}_1}{\partial z^{*2}}+\frac{2\epsilon\mathscr{A}^2\bar{N}_1\bar{N}_2}{Re^2\bar{\rho}^*}\frac{\partial^2\hat{p}^*}{\partial z^{*2}}-\frac{k_T}{\bar{T}}\frac{\partial^2\hat{T}^*}{\partial z^{*2}}\right)-\frac{2\mathscr{A}^2\bar{\mu}_w}{R^2}\frac{\partial\psi^*}{\partial z^*}\left(\frac{\partial}{\partial\xi}\left(\frac{\bar{\rho}_1^*}{\bar{\rho}^*}\right)\right)=0. \tag{5.9}$$

In the leading approximation in the limit $\delta_Z/R\ll1$, the above equation can be reduced to

$$\frac{\partial}{\partial z^*}\left[\frac{\bar{D}^*_{12}m_1^*m_2^*}{\bar{N}_1m_1^*+\bar{N}_2m_2^*}\left(\frac{\partial\hat{N}_1}{\partial z^*}+\frac{\epsilon\bar{N}_1\bar{N}_2}{\bar{\rho}^*}\frac{\partial}{\partial z^*}\left(\frac{\hat{p}m_{av}}{\bar{\rho}_wk_B\bar{T}}\right)-\frac{k_T}{\bar{T}}\frac{\partial\hat{T}}{\partial z^*}\right)\right.$$
$$\left.-\frac{2\mathscr{A}^2Sc\delta_Z^2}{R^2}\left(\frac{\partial}{\partial\xi}\left(\frac{\bar{\rho}_1^*}{\bar{\rho}^*}\right)\right)\psi^*\right]=0, \tag{5.10}$$

where $Sc=\bar{\mu}_w/(m_{av}\bar{D}'_w)$ is the Schmidt number (2.20). Equation (5.10) can be solved, subject to the zero-flux conditions at $z^*=z_0^*$, to obtain

$$\frac{\partial\hat{N}_1}{\partial z^*}=-\frac{\epsilon\bar{N}_1\bar{N}_2}{\bar{\rho}^*}\frac{\partial}{\partial z^*}\left(\frac{\hat{p}m_{av}}{\bar{\rho}_wk_B\bar{T}}\right)+\frac{k_T}{\bar{T}}\frac{\partial\hat{T}}{\partial z^*}+\frac{2\mathscr{A}^2Sc\delta_Z^2}{R^2}\frac{m_1^*\bar{N}_1+m_2^*\bar{N}_2}{m_1^*m_2^*\bar{D}^*_{12}}\left(\frac{\partial}{\partial\xi}\frac{\bar{\rho}_1^*}{\bar{\rho}^*}\right)\psi^*. \tag{5.11}$$

Equation (5.11) is substituted into (5.8) to obtain

$$\frac{1}{\bar{\rho}^{*2}r^{*2}}\frac{\partial^4\psi^*}{\partial z^{*4}}+\psi^*\left(\frac{4Re^2\delta_Z^4}{\bar{\mu}^{*2}r^{*2}R^4}+\frac{2\mathscr{A}^2Re^2Pr(1-\gamma^{-1})\delta_Z^4}{R^4\bar{K}^*\bar{\mu}^*}\left(1+\frac{\epsilon^2((2+\xi)^2+2)\bar{\rho}_{w1}\bar{\rho}_{w2}}{2\bar{\rho}_w^2}\right)\right)$$
$$+\frac{\epsilon^2Re^2}{\bar{\mu}^*\bar{\rho}^*}\frac{\delta_Z^2}{R^2}\frac{\partial}{\partial z^*}\left(\frac{\hat{p}m_{av}}{\bar{\rho}_wk_B\bar{T}}\right)\left(\bar{N}_1\bar{N}_2-\frac{\bar{\rho}_{w1}\bar{\rho}_{w2}(1+2\xi)}{\bar{\rho}_w^2}\right)$$
$$-\frac{\epsilon Re^2\delta_Z^2}{\bar{\mu}^*R^2}\frac{k_T}{\bar{T}}\frac{\partial\hat{T}}{\partial z^*}-\frac{2\epsilon\mathscr{A}^2Re^2Sc}{\bar{\mu}^*}\frac{\delta_Z^4}{R^4}\left(\frac{m_1^*\bar{N}_1+m_2^*\bar{N}_2}{\bar{D}^*_{12}m_1^*m_2^*}\right)\left(\frac{\partial}{\partial\xi}\left(\frac{\bar{\rho}_1^*}{\bar{\rho}^*}\right)\right)\psi^*$$
$$=0. \tag{5.12}$$

We can use the following approximation correct to leading order in ϵ to simplify the prefactor of the pressure gradient term in (5.12),

https://doi.org/10.1017/jfm.2014.365 Published online by Cambridge University Press

$$\left(\bar{N}_1\bar{N}_2 - \frac{\bar{\rho}_{w1}\bar{\rho}_{w2}(1+2\xi)}{\bar{\rho}_w^2}\right) = -\frac{2\bar{\rho}_{w1}\bar{\rho}_{w2}\xi}{\bar{\rho}_w^2}. \tag{5.13}$$

Equation (5.6) can be used to substitute for the temperature field,

$$\frac{1}{\bar{T}}\frac{\partial \hat{T}}{\partial z^*} = 2\mathscr{A}^2 Pr(1-\gamma^{-1})\frac{\delta_Z^2}{R^2}\frac{1}{\bar{K}^*}\left(1+\frac{\epsilon^2\bar{\rho}_{w1}^*\bar{\rho}_{w2}^*}{\bar{\rho}_w^{*2}}\right)\psi^*. \tag{5.14}$$

The above equation is substituted into (5.12) to obtain

$$\begin{aligned}&\frac{1}{\bar{\rho}^{*2}r^{*2}}\frac{\partial^4\psi^*}{\partial z^{*4}} + \frac{\psi^* Re^2\delta_Z^4}{R^4}\left[\frac{4}{\bar{\mu}^{*2}r^{*2}} + \frac{2\mathscr{A}^2 Pr(1-\gamma^{-1})}{\bar{K}^*\bar{\mu}^*}\right.\\ &\times\left(1-2\epsilon k_T + \frac{\epsilon^2((2+\xi)^2+2)\bar{\rho}_{w1}\bar{\rho}_{w2}}{2\bar{\rho}_w^2}\right) - \frac{2\epsilon\mathscr{A}^2 Sc}{\bar{\mu}^*}\left(\frac{m_1^*\bar{N}_1 + m_2^*\bar{N}_2}{\bar{D}_{12}^* m_1^* m_2^*}\right)\\ &\left.\times\left(\frac{\partial}{\partial\xi}\left(\frac{\bar{\rho}_1^*}{\bar{\rho}^*}\right)\right)\right] - \frac{\epsilon^2 Re^2}{\bar{\mu}^*\bar{\rho}^*}\frac{\delta_Z^2}{R^2}\frac{\partial}{\partial z^*}\left(\frac{\hat{p}m_{av}}{\bar{\rho}_w k_B\bar{T}}\right)\left(\frac{2\bar{\rho}_{w1}\bar{\rho}_{w2}\xi}{\bar{\rho}_w^2}\right) = 0.\end{aligned} \tag{5.15}$$

The pressure in the above equation can be substituted from the z momentum conservation equation,

$$\begin{aligned}\frac{\partial\hat{p}}{\partial z} &= \bar{\mu}\nabla^2\hat{v}_z - \frac{\bar{\mu}}{3}\frac{\hat{v}_r}{\bar{\rho}}\frac{\partial\bar{\rho}}{\partial r} + \frac{\partial\bar{\mu}}{\partial r}\left(\frac{\partial\hat{v}_r}{\partial z} + \frac{\partial\hat{v}_z}{\partial r}\right)\\ &= \bar{\mu}\nabla^2\left(\frac{1}{\bar{\rho}r}\frac{\partial\psi}{\partial r}\right) + \frac{\bar{\mu}}{3}\frac{1}{\bar{\rho}^2 r}\frac{\partial\bar{\rho}}{\partial r}\frac{\partial^2\psi}{\partial z^2} + \frac{\partial\bar{\mu}}{\partial r}\left(\frac{\partial}{\partial r}\left(\frac{1}{\bar{\rho}r}\frac{\partial\psi}{\partial r}\right) - \frac{1}{\bar{\rho}r}\frac{\partial^2\psi}{\partial z^2}\right).\end{aligned} \tag{5.16}$$

Retaining only the highest z derivatives on the right side of the above equation, and suitably scaling all the terms, we obtain

$$\frac{\partial}{\partial z^*}\left(\frac{\hat{p}m_{av}}{\bar{\rho}_w k_B\bar{T}}\right) = -\frac{4\mathscr{A}^4}{Re^2}\left(\frac{\bar{\mu}^*}{\bar{\rho}^*}\frac{\partial}{\partial\xi} + \frac{\bar{\mu}^*}{3\bar{\rho}^{*2}}\frac{\partial\bar{\rho}^*}{\partial\xi} - \frac{1}{\bar{\rho}^*}\frac{\partial\bar{\mu}^*}{\partial\xi}\right)\frac{\partial^2\psi^*}{\partial z^{*2}}. \tag{5.17}$$

Equation (5.17) is inserted into (5.15) to obtain

$$\begin{aligned}&\frac{1}{\bar{\rho}^{*2}r^{*2}}\frac{\partial^4\psi^*}{\partial z^{*4}} + \frac{\psi^* Re^2\delta_Z^4}{R^4}\left[\frac{4}{\bar{\mu}^{*2}r^{*2}}\right.\\ &+\frac{2\mathscr{A}^2 Pr(1-\gamma^{-1})}{\bar{K}^*\bar{\mu}^*}\left(1-2\epsilon k_T + \frac{\epsilon^2((2+\xi)^2+2)\bar{\rho}_{w1}\bar{\rho}_{w2}}{2\bar{\rho}_w^2}\right)\\ &\left.-\frac{2\epsilon\mathscr{A}^2 Sc}{\bar{\mu}^*}\left(\frac{m_1^*\bar{N}_1 + m_2^*\bar{N}_2}{\bar{D}_{12}^* m_1^* m_2^*}\right)\left(\frac{\partial}{\partial\xi}\left(\frac{\bar{\rho}_1^*}{\bar{\rho}^*}\right)\right)\right]\\ &+\frac{4\epsilon^2\mathscr{A}^4}{\bar{\rho}^{*2}}\frac{\delta_Z^2}{R^2}\left(\frac{2\bar{\rho}_{w1}\bar{\rho}_{w2}\xi}{\bar{\rho}_w^2}\right)\left(\frac{\bar{\mu}^*}{\bar{\rho}^*}\frac{\partial}{\partial\xi} + \frac{\bar{\mu}^*}{3\bar{\rho}^{*2}}\frac{\partial\bar{\rho}^*}{\partial\xi} - \frac{1}{\bar{\rho}^*}\frac{\partial\bar{\mu}^*}{\partial\xi}\right)\frac{\partial^2\psi^*}{\partial z^{*2}} = 0.\end{aligned} \tag{5.18}$$

The boundary layer thickness is defined as $\delta_z/R = Re^{-1/2}$, to obtain the final scaled equation:

https://doi.org/10.1017/jfm.2014.365 Published online by Cambridge University Press

$$\frac{1}{\bar{\rho}^{*2}r^{*2}}\frac{\partial^4\psi^*}{\partial z^{*4}}+\psi^*\left[\frac{4}{\bar{\mu}^{*2}r^{*2}}+\frac{2\mathscr{A}^2Pr(1-\gamma^{-1})}{\bar{K}^*\bar{\mu}^*}\left(1-2\epsilon k_T+\frac{\epsilon^2((2+\xi)^2+2)\bar{\rho}_{w1}\bar{\rho}_{w2}}{2\bar{\rho}_w^2}\right)\right.$$
$$\left.-\frac{2\epsilon\mathscr{A}^2Sc}{\bar{\mu}^*}\left(\frac{m_1^*\bar{N}_1+m_2^*\bar{N}_2}{\bar{D}_{12}^*m_1^*m_2^*}\right)\left(\frac{\partial}{\partial\xi}\left(\frac{\bar{\rho}_1^*}{\bar{\rho}^*}\right)\right)\right]$$
$$+\frac{4\epsilon^2\mathscr{A}^4}{Re\bar{\rho}^{*2}}\left(\frac{2\bar{\rho}_{w1}\bar{\rho}_{w2}\xi}{\bar{\rho}_w^2}\right)\left(\frac{\bar{\mu}^*}{\bar{\rho}^*}\frac{\partial}{\partial\xi}+\frac{\bar{\mu}^*}{3\bar{\rho}^{*2}}\frac{\partial\bar{\rho}^*}{\partial\xi}-\frac{1}{\bar{\rho}^*}\frac{\partial\bar{\mu}^*}{\partial\xi}\right)\frac{\partial^2\psi^*}{\partial z^{*2}}=0. \tag{5.19}$$

Equation (5.19) is solved using an expansion of the form

$$\psi^*=\psi^{(0)}+\epsilon^2\psi^{(2)}. \tag{5.20}$$

The equations for $\psi^{(0)}$ and $\psi^{(2)}$ are

$$\frac{1}{\bar{\rho}^{*2}r^{*2}}\frac{\partial^4\psi^{(0)}}{\partial z^{*4}}+\psi^{(0)}\left[\frac{4}{\bar{\mu}^{*2}r^{*2}}\right.$$
$$+\frac{2\mathscr{A}^2Pr(1-\gamma^{-1})}{\bar{K}^*\bar{\mu}^*}\left(1-2\epsilon k_T+\frac{\epsilon^2((2+\xi)^2+2)\bar{\rho}_{w1}\bar{\rho}_{w2}}{2\bar{\rho}_w^2}\right)$$
$$\left.-\frac{2\epsilon\mathscr{A}^2Sc}{\bar{\mu}^*}\left(\frac{m_1^*\bar{N}_1+m_2^*\bar{N}_2}{\bar{D}_{12}^*m_1^*m_2^*}\right)\left(\frac{\partial}{\partial\xi}\left(\frac{\bar{\rho}_1^*}{\bar{\rho}^*}\right)\right)\right]=0, \tag{5.21}$$
$$\frac{1}{\bar{\rho}^{*2}r^{*2}}\frac{\partial^4\psi^{(2)}}{\partial z^{*4}}+\psi^{(2)}\left[\frac{4}{\bar{\mu}^{*2}r^{*2}}\right.$$
$$+\frac{2\mathscr{A}^2Pr(1-\gamma^{-1})}{\bar{K}^*\bar{\mu}^*}\left(1-2\epsilon k_T+\frac{\epsilon^2((2+\xi)^2+2)\bar{\rho}_{w1}\bar{\rho}_{w2}}{2\bar{\rho}_w^2}\right)$$
$$\left.-\frac{2\mathscr{A}^2Sc}{\bar{\mu}^*}\left(\frac{m_1^*\bar{N}_1+m_2^*\bar{N}_2}{\bar{D}_{12}^*m_1^*m_2^*}\right)\left(\frac{\partial}{\partial\xi}\left(\frac{\bar{\rho}_1^*}{\bar{\rho}^*}\right)\right)\right]$$
$$+\frac{4\mathscr{A}^4}{Re\bar{\rho}^{*2}}\left(\frac{2\bar{\rho}_{w1}\bar{\rho}_{w2}\xi}{\bar{\rho}_w^2}\right)\left(\frac{\bar{\mu}^*}{\bar{\rho}^*}\frac{\partial}{\partial\xi}+\frac{\bar{\mu}^*}{3\bar{\rho}^{*2}}\frac{\partial\bar{\rho}^*}{\partial\xi}-\frac{1}{\bar{\rho}^*}\frac{\partial\bar{\mu}^*}{\partial\xi}\right)\frac{\partial^2\psi^{(0)}}{\partial z^{*2}}=0. \tag{5.22}$$

We have chosen to include the $O(\epsilon)$ term in the $O(1)$ equation (5.21), since this is a z^*-independent term that can be directly integrated to obtain $\psi^{(0)}$.

The leading-order solution $\psi^{(0)}$ is similar to that for the Carrier–Maslen solution. With this definition, we obtain the generalization of the Carrier–Maslen equation,

$$\psi^*=C\left(\frac{1-\iota}{2}\mathrm{e}^{-(1+\iota)z^\dagger/\sqrt{2}}-\frac{1+\iota}{2}\mathrm{e}^{-(1-\iota)z^\dagger/\sqrt{2}}\right), \tag{5.23}$$

where the scaled coordinate $z^\dagger$ is a function of the radial coordinate,

$$z^\dagger = z^*\left[\frac{4}{\bar{\mu}^{*2}r^{*2}}+\frac{2\mathscr{A}^2Pr(1-\gamma^{-1})}{\bar{K}^*\bar{\mu}^*}\left(1-2\epsilon k_T+\frac{\epsilon^2((2+\xi)^2+2)\bar{\rho}_{w1}\bar{\rho}_{w2}}{2\bar{\rho}_w^2}\right)\right.$$
$$\left.-\frac{2\epsilon\mathscr{A}^2Sc}{\bar{\mu}^*}\left(\frac{m_1^*\bar{N}_1+m_2^*\bar{N}_2}{\bar{D}_{12}^*m_1^*m_2^*}\right)\left(\frac{\partial}{\partial\xi}\left(\frac{\bar{\rho}_1^*}{\bar{\rho}^*}\right)\right)\right]^{1/4}. \tag{5.24}$$

In the solution (5.24), we have neglected the exponentially growing solutions, since we require that $\psi^{(0)}\to 0$ for $z^\dagger\to\infty$. The boundary conditions at the end-cap $z^*=0$ are the no-slip conditions, $\hat{v}_r=0$ and $\hat{v}_z=0$. Both components of the velocity are

https://doi.org/10.1017/jfm.2014.365 Published online by Cambridge University Press

proportional to $\partial\psi^{(0)}/\partial z^{\dagger}$ (through the dependence of $z^{\dagger}$ on r and z). Therefore, one of the constants in the solution has been fixed from the condition $\partial\psi^{(0)}/\partial z^{\dagger}=0$ at $z^{\dagger}=0$. The fourth constant is determined from the total mass flow rate condition,

$$\begin{aligned}\psi(r,z=\infty)-\psi(r,z=0) &= -\int_0^{\infty} r\,\mathrm{d}z\,\bar{\rho}v_r \\ &= \frac{F}{2\pi},\end{aligned} \tag{5.25}$$

where F is the total mass flow rate. This can be expressed in terms of the dimensionless variables as

$$\psi^{(0)}(r,z=0)=C=\frac{F}{2\pi\bar{\mu}^{(0)}\delta_Z}, \tag{5.26}$$

where C is the constant of integration in (5.23). Here, we have assumed, without loss of generality, that $\psi^{*}(r,z\to\infty)=0$.

Equation (5.22) for $\psi^{(2)}$ is evaluated numerically with two boundary conditions, the normal velocity condition $\partial\psi^{(2)}/\partial z^{\dagger}=0$ at $z^{\dagger}=0$, and the condition on the flow rate,

$$\psi^{(2)}(r,z=0)=0, \tag{5.27}$$

since we have assumed that the flow leading-order solution accounts for the total flow rate in the boundary layer.

6. Results

The DSMC method is used to simulate the two-dimensional axisymmetric gas flow in the r–z plane. The details of the DSMC simulation and validation are provided in appendix C. The initial gas mixture contains 50 % mole fraction of each component for two different values of $\epsilon_a=2\Delta m/(m_1+m_2)=0.2$ and 0.5. The diffuse reflection boundary condition with thermal accommodation coefficient 1 is used in all the simulations. The simulation time step is selected to be small compared to the inverse of the collision frequency (time between collisions). The mean collision time, calculated from the mean free path and the molecular velocity at the wall, is approximately 2.752×10^{-9} s. The time step used in the simulations is 1.0×10^{-10} s, which is less than the mean collision time. The simulation procedure is not provided here, since it has been discussed extensively earlier (Bird 1994). The number of intervals along the radial direction is 400, with clustering towards the rotating sidewall, while there are 1600, 3200 and 6400 intervals along the axial direction, with clustering towards the top and bottom end-caps for aspect ratio $Z/D=2$, 4 and 8, respectively. Results are shown here only for $Z/D=2$, since this shows the poorest agreement between theory and simulations. There are 100 molecules per cell on average.

The stratification parameter $\mathscr{A}$ is varied in the range 0.707–3.535, and Reynolds number in the range 10^2–10^6. There is better agreement between simulations and theory as the aspect ratio and Reynolds number increase, and so results are reported only for the smallest aspect ratio $Z/D=2$ and $Re=10^2$ and 10^4. There are four types of forcing for the secondary flow: a wall thermal gradient, inflow/outflow of gas along the axis, momentum source inside the flow domain, and mass source/sink inside the flow domain. The flow geometry and coordinate system for the four types of forcing for the secondary flow are shown in figure 1 here and in figures 10 and 13 of Pradhan & Kumaran (2011).

https://doi.org/10.1017/jfm.2014.365 Published online by Cambridge University Press

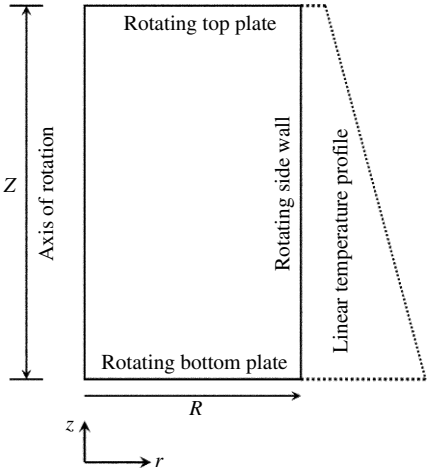


FIGURE 1. Computational domain and coordinate system for forcing due to wall thermal gradient.

(*a*) In the case of a wall thermal drive, a linear temperature gradient is imposed at the rotating wall, as shown in figure 1. The wall temperature influences the gas temperature through the diffuse reflection boundary condition, where the velocity of the reflected molecules is chosen from a Maxwell–Boltzmann distribution with mean velocity and temperature equal to those of the wall. The non-dimensional parameter $F_T = (Z/\bar{T})\,\mathrm{d}T/\mathrm{d}z$ is used to quantify the temperature gradient, where $\bar{T}$ is the wall temperature averaged over the height.

(*b*) In the case of mass input/output along the axis, there is an inflow of gas at the cylinder axis at $\eta = 0.5$, as shown in figure 10 of Pradhan & Kumaran (2011). There is a radial expansion of the gas due to the centrifugal acceleration, and then a separation into two streams upwards and downwards at the wall of the cylinder. The streams flow radially inwards at the end-caps, and there is an exit of gas at two locations on the axis, one near the bottom end-cover ($\eta = z/Z = 0.15$) and the other near the top end-cover ($\eta = z/Z = 0.85$). Here, Z is the total cylinder height and z is the axial distance from the bottom end-cap. A dimensionless feed rate F^* is defined by scaling the feed rate F by the gas holdup H and the angular velocity Ω,

$$F^* = F/(H\Omega). \tag{6.1}$$

The dimensionless feed rate provides the magnitude of the perturbation to the base flow due to external feed. Simulations have been carried out for $F^* = 0.1$ and 0.2.

(*c*) The DSMC simulation procedure outlined in Pradhan & Kumaran (2011) is used to model the internal sources of mass, momentum and energy for the configurations previously studied in Wood & Sanders (1983); the configurations are shown in figure 13 of Pradhan & Kumaran (2011). These are added in a region of radius 10^{-3} times the cylinder radius R, in order to approximate a delta function. The input/output of mass is accomplished by randomly adding/removing molecules at a predetermined time interval determined on the basis of the mass input/output desired. In the case of addition of molecules, the molecular velocity is randomly chosen from a Gaussian distribution with the same mean velocity

https://doi.org/10.1017/jfm.2014.365 Published online by Cambridge University Press

and temperature as the gas. To ensure no change in momentum and energy, the mean velocity and the fluctuating velocity of all other molecules in the domain are scaled by a suitable factor. The earlier results of Wood & Sanders (1983) are used to first validate the simulations using a mass source and sink placed symmetrically at $(\eta = 0.25, \xi = 8)$ and $(\eta = 0.75, \xi = 8)$. After this, calculations are carried out for two configurations, one with source/sink outside the radial boundary layer at $(\eta = 0.25, \xi^* = 0.25)$ and $(\eta = 0.75, \xi^* = 0.25)$, and the second inside the radial boundary layer at $(\eta = 0.25, \xi^* = 0.01)$ and $(\eta = 0.75, \xi^* = 0.01)$, respectively. Here, $\xi^* = \xi/\mathscr{A}^2$.

(*d*) A momentum source is also simulated for the configuration studied earlier in Wood & Sanders (1983), where a source is placed at $(\eta = 0.5, \xi = 8)$, as shown in figure 13 of Pradhan & Kumaran (2011). In order to exert a force on the flow at a point, a constant acceleration is imposed on all the molecules at each collision step in the desired direction, and the acceleration magnitude is chosen so that the sum of the rates of change of momentum of all molecules is equal to the applied force. In order to add energy, the fluctuating velocity of all molecules in the domain is scaled by a constant factor. The factor is determined such that the desired energy input/output rate is equal to the increase/decrease in energy divided by the time between collisions.

First, the simulation results are validated against the analytical results for the mole fraction profiles in the absence of forcing, and then the results for the secondary flow due to forcing are provided. We have verified that the temperature is a constant, and the angular velocity increases linearly with radius. The comparison of number density results obtained from DSMC simulations with those of analytical solution for stratification parameter $\mathscr{A}$ in the range 0.707–3.535 are shown in figure 2(*a–d*). There is excellent agreement between analytical and numerical results for lower values of the stratification parameter, and near the wall. The maximum difference is less than 5 % near the centre, where the number density is orders of magnitude smaller than the wall number density for higher values of the stratification parameter. We have also carried out simulations for different holdups, and found similar agreement between analytical and numerical results. The variation of the local Knudsen number, which is the ratio of the local mean free path, $(\sqrt{2}\pi(n_1 + n_2)d^2)^{-1}$, and the cylinder radius R with the radial coordinate is shown in figure 3. This figure shows that the Knudsen number could be greater than 100 at the centre of the channel for the highest stratification parameter used here, but could be smaller than 10^{-2} for the smallest stratification parameter. For comparison, the global Knudsen number based on the average number density (total number of molecules divided by the cylinder volume) is 7.6622×10^{-2} for $\mathscr{A} = 0.707$, 1.5323×10^{-1} for $\mathscr{A} = 1.414$, 2.2985×10^{-1} for $\mathscr{A} = 2.121$ and 3.8309×10^{-1} for $\mathscr{A} = 3.535$.

6.1. *Wall temperature gradient*

The results for the secondary flow are determined as a function of the parameter $F_T = (Z/\bar{T})\,\mathrm{d}T/\mathrm{d}z$, where $\bar{T}$ is the average temperature. A relatively large value of $F_T = 0.2$ is used in the simulations. In the presence of secondary flow, there is an axial velocity slip and a temperature slip at the wall. This axial velocity slip is shown in figure 4(*a*), where the axial velocity at the rotating sidewall, non-dimensionalized by $R\Omega$ and scaled by F_T, is plotted as a function of stratification parameter at the axial location $\eta = 0.5$. The slip velocity for a two-component gas mixture is observed to be larger than that for a single component with the same mean velocity, and it is

https://doi.org/10.1017/jfm.2014.365 Published online by Cambridge University Press

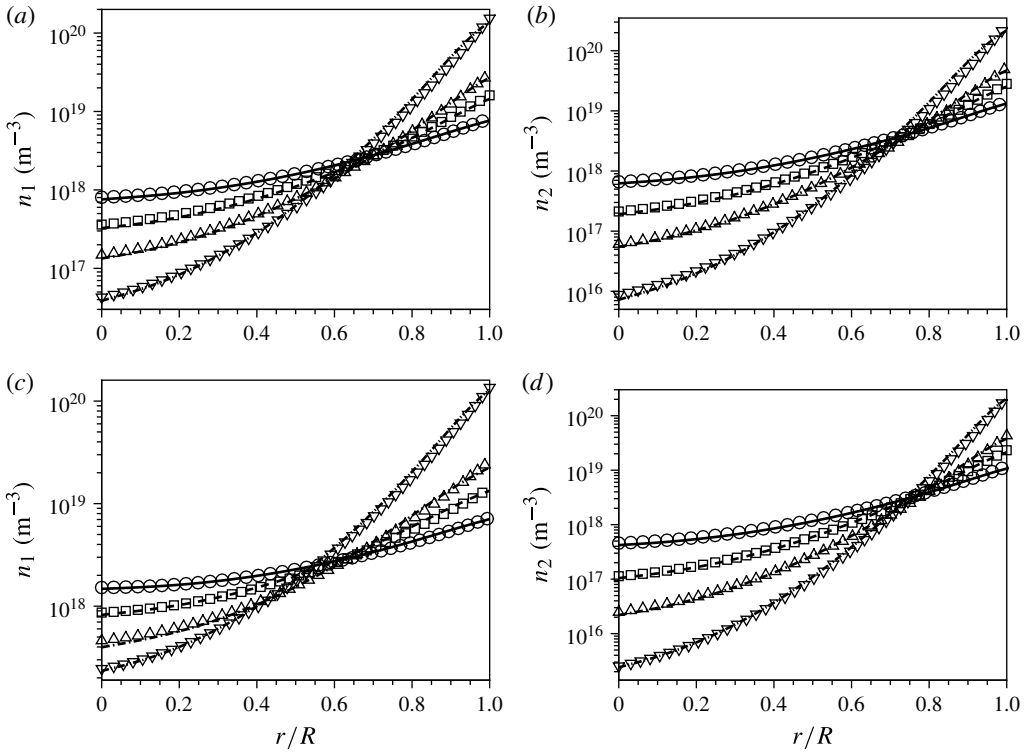


FIGURE 2. Variation of number density of (*a*,*c*) component 1 (n_1) and (*b*,*d*) component 2 (n_2), expressed in molecules per m^3 along the radial coordinate (r/R) at $\eta = 0.5$, aspect ratio $Z/D = 2$ and $Re = 10^4$, and for (*a*,*b*) $\epsilon_a = 0.2$ and (*c*,*d*) $\epsilon_a = 0.5$. The symbols show the DSMC results for $\mathscr{A} = 0.707$ (◯), $\mathscr{A} = 1.414$ (□), $\mathscr{A} = 2.121$ (△) and $\mathscr{A} = 3.535$ (▽). The lines show the analytical solution for $\mathscr{A} = 0.707$ (——), $\mathscr{A} = 1.414$ (– – –), $\mathscr{A} = 2.121$ (– · –·) and $\mathscr{A} = 3.535$ (– ··– ··).

found that the slip velocity increases as the difference in molecular mass increases. In agreement with the previous study (Pradhan & Kumaran 2011), it is found that the slip velocity shows very little dependence on the Reynolds number, but increases proportional to F_T. In figure 4(*b*), the axial slip velocity at the wall is shown at $\eta = 0.675$ for inflow/outflow of gas along the axis. The qualitative features are similar to those for a secondary flow driven by an axial temperature gradient. It is important to incorporate the axial velocity and temperature slip in order to obtain quantitative agreement between the analytical results and simulations.

It is a rather counter-intuitive result that the slip velocity is decreasing as the parameter $\mathscr{A}$ decreases. There are two reasons for this. Firstly, the magnitude of the secondary flow velocity is increasing as the parameter A decreases, as can be seen from plots of the mass fluxes in figures 6 and 7 below. In fact, these figures plot the ratio $(\rho v_z/\rho_w \Omega R)(Re/4\mathscr{A}^4)$, which increases by a factor of approximately 3 when A increases from 0.707 to 1.414. So the actual secondary flow velocity is increasing by approximately $3 \times \Omega \times \mathscr{A}^4$ when Re and the wall density are a constant. Secondly, what is plotted in figure 4 is the ratio of the slip velocity and the angular velocity Ω. The angular velocity is also increasing linearly with A. The ratio of the slip velocity and the maximum secondary flow velocity actually decreases as $\mathscr{A}$ is increased.

https://doi.org/10.1017/jfm.2014.365 Published online by Cambridge University Press

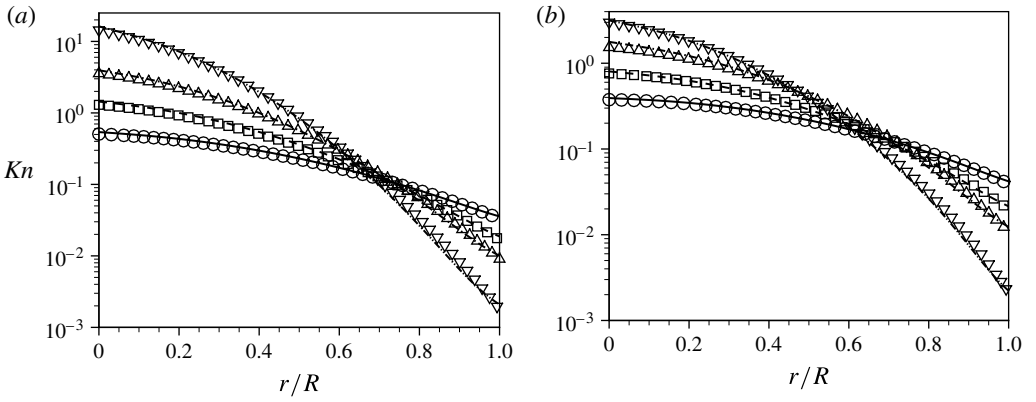


FIGURE 3. Variation of Knudsen number along the radial coordinate (r/R) at $\eta = 0.5$, aspect ratio $Z/D = 2$, $Re = 10^4$ for (a) $\epsilon_a = 0.2$ and (b) $\epsilon_a = 0.5$. The symbols show the DSMC results for $\mathscr{A} = 0.707$ (◯), $\mathscr{A} = 1.414$ (□), $\mathscr{A} = 2.121$ (△) and $\mathscr{A} = 3.535$ (▽). The lines show the analytical solution for $\mathscr{A} = 0.707$ (——), $\mathscr{A} = 1.414$ (– – –), $\mathscr{A} = 2.121$ (– · – ·) and $\mathscr{A} = 3.535$ (– · · – · ·). The average Knudsen number, based on the average number density (total number of molecules divided by the cylinder volume), is 7.6622×10^{-2} for $\mathscr{A} = 0.707$, 1.5323×10^{-1} for $\mathscr{A} = 1.414$, 2.2985×10^{-1} for $\mathscr{A} = 2.121$ and 3.8309×10^{-1} for $\mathscr{A} = 3.535$.

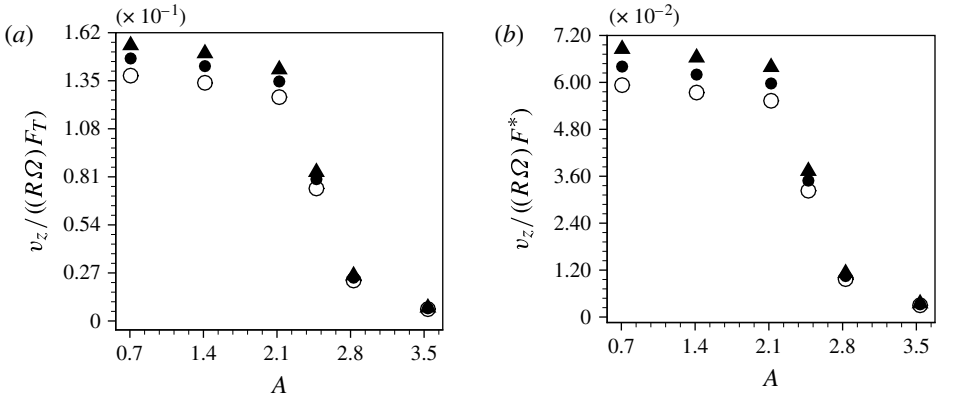


FIGURE 4. Axial slip velocity at the curved surface, scaled by $R\Omega F_T$ and $R\Omega F^*$, respectively, for (a) wall thermal forcing at $\eta = 0.5$, and (b) inflow/outflow of gas along the axis at $\eta = 0.675$. The symbols show the DSMC results at $Re = 10^2$, F_T or $F^* = 0.2$, for a single component (◯) and a binary gas mixture with $\epsilon_a = 0.2$ (●) and 0.5 (▲).

The master potential and axial mass flux profiles correct to $O(1)$, $O(\epsilon)$ and $O(\epsilon^2)$ are shown in figures 5 and 6 for $\epsilon_a = 2\Delta m/(m_1 + m_2) = 0.2$ and 0.5. The results are shown for $\mathscr{A} = 1.414$ and $\mathscr{A} = 0.707$, and better convergence is obtained for $\mathscr{A} = 3.535$ and 2.121 (for which results are not shown here). Figure 5 shows that the first correction to the master potential could be quite large, nearly equal in magnitude to the leading-order solution for the lowest Reynolds number and stratification parameter considered here. However, the second correction is always significantly

https://doi.org/10.1017/jfm.2014.365 Published online by Cambridge University Press

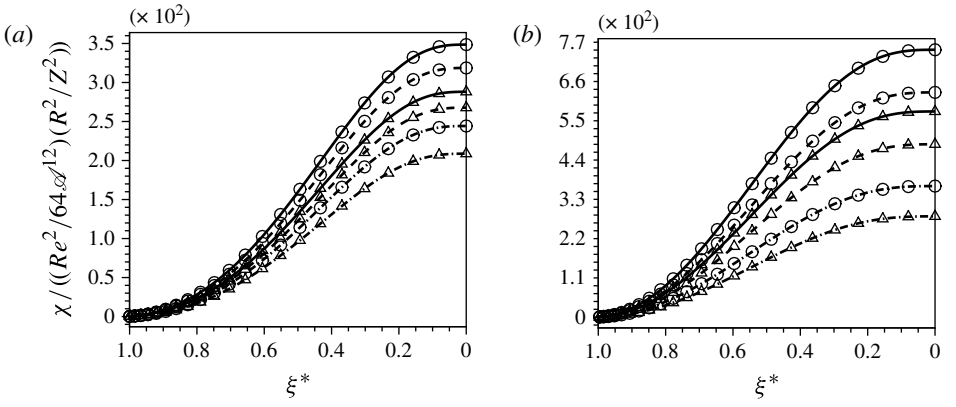


FIGURE 5. Master potential scaled by $(Re^2/64\mathscr{A}^{12})(R^2/Z^2)$ as a function of ξ^* at $\eta = 0.5$, for a linear wall temperature gradient with $F_T = 0.2$, and (*a*) $\mathscr{A} = 1.414$ and (*b*) $\mathscr{A} = 0.707$. The lines show the analytical solutions with wall slip correct to $O(1)$ (– · – · –), $O(\epsilon)$ (– – –), and $O(\epsilon^2)$ (——), and the symbols show the results for $\epsilon_a = 0.2$ (△) and $\epsilon_a = 0.5$ (◯).

smaller than the first correction, indicating the possibility that the expansion in ϵ is convergent even for ϵ_a as large as 0.5. The analytical solutions are compared with the DSMC results for the axial mass flux in figure 6. The results correct to $O(\epsilon^2)$ are in significantly better agreement with simulations in comparison to the leading-order results, and the trends indicate that the effect of including the mass difference is to increase the axial mass flux in the secondary flow in comparison to the generalized Onsager model, which does not include the mass difference. For the lowest Reynolds number of 100 and the lowest stratification parameter of 0.707, there is a difference of approximately 15–20 % between the $O(\epsilon^2)$ analytical results and the DSMC simulations. For higher Reynolds number and stratification parameter, the agreement is much better. The secondary flow mass flux in simulations is always higher than that predicted theoretically up to $O(\epsilon^2)$, indicating that higher-order corrections may further increase the magnitude of the secondary flow.

6.2. *Inflow/outflow along the axis*

The axial mass flux profiles for the $O(1)$, $O(\epsilon)$ and $O(\epsilon^2)$ solutions are shown in figure 7 for $\epsilon_a = 2\Delta m/(m_1 + m_2) = 0.2$ and 0.5 for the mass inflow/outflow along the axis. As in the case of the wall thermal drive, the $O(\epsilon)$ correction to the master potential is comparable to the leading-order solution for the lowest Reynolds number and stratification parameter for $\epsilon_a = 0.5$. However, the second correction is significantly smaller than the first correction, implying convergence of the series. The $O(\epsilon)$ and $O(\epsilon^2)$ solutions for the mass flux do consistently converge towards to the DSMC results in all the cases we have analysed. There is a difference of 15–20 % between the $O(\epsilon^2)$ solution and the DSMC result for the lowest values of the stratification parameter considered here, but the difference is negligible for higher values of the stratification parameter. In all cases, it is consistently observed that the solution correct to $O(\epsilon^2)$ is in much better agreement with DSMC results in comparison to the Onsager model with no mass difference.

https://doi.org/10.1017/jfm.2014.365 Published online by Cambridge University Press

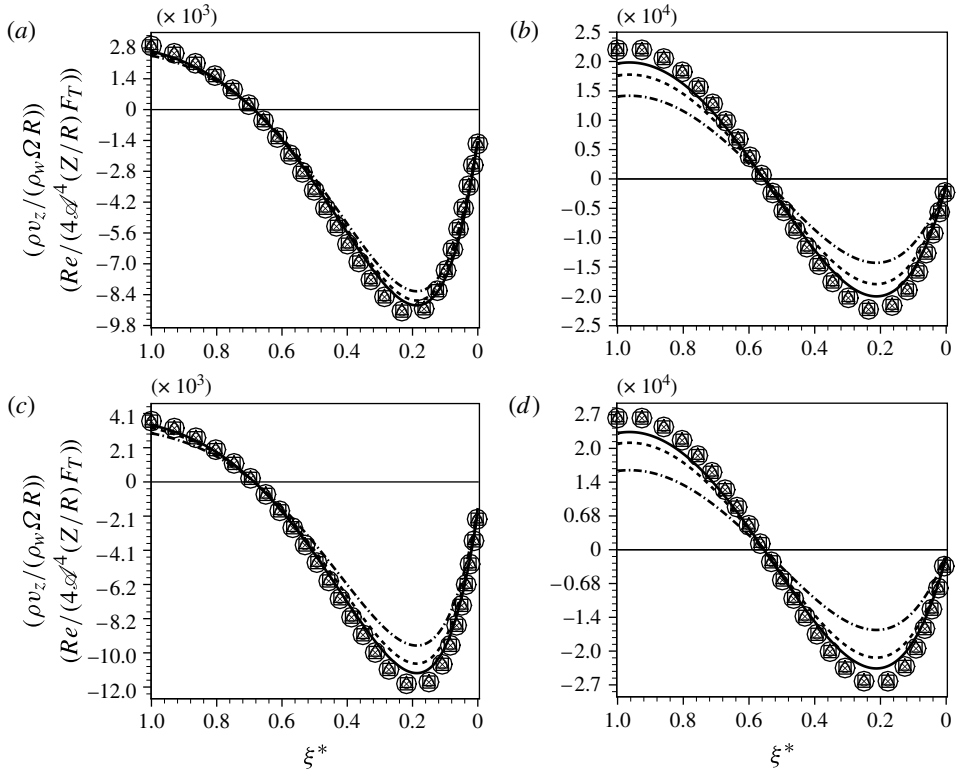


FIGURE 6. Axial mass flux, scaled by $\rho_w \Omega R$, $4\mathscr{A}^4(Z/R)F_T/Re$, as a function of ξ^* at $\eta = 0.5$ for (a,c) $\mathscr{A} = 1.414$ and (b,d) $\mathscr{A} = 0.707$ for (a,b) $\epsilon_a = 0.2$ and (c,d) $\epsilon_a = 0.5$. The symbols show the DSMC results for $Re = 10^4$, $F_T = 0.1$ ($\otimes$), $Re = 10^4$, $F_T = 0.2$ ($\triangle$), $Re = 10^2$, $F_T = 0.1$ ($\square$) and $Re = 10^2$, $F_T = 0.2$ ($\bigcirc$). The lines show the analytical solutions correct to $O(1)$ ($- \cdot - \cdot$), $O(\epsilon)$ ($- - -$) and $O(\epsilon^2)$ (——).

6.3. *Radial flow at end-caps*

The Carrier–Maslen solutions, incorporating the $O(\epsilon^2)$ correction due to the mass difference, are compared with the results of DSMC simulations for the radial flow at the end-caps. It is necessary to specify the total mass flow rate at a fixed radial location in order to specify the boundary condition in (5.26). The mass flux is specified as one-half of the rate of inflow along the axis, since the inflow at the axis separates symmetrically at the cylindrical wall and one-half of the inflow goes upwards/downwards and inwards along the end-caps. The flow at the end-caps could not be modelled for a linear temperature gradient, because there is circulation with upward flow along the cylindrical surface and downward flow closer to the axis, resulting in a varying flux along the radial end-caps. This results in a variation in the radial mass with position, and consequently the mass flux in the generalized Carrier–Maslen equation cannot be set equal to a constant. Therefore, we compute the end-cap solutions only for the secondary flow due to an axial mass source. The wall slip for the radial flow at the wall is found to be much smaller than that for the axial flow. The radial velocity at the end-caps, non-dimensionalized by $R\Omega$, is plotted as a function of scaled axial coordinate η^* at $\xi^* = 0.1$, 0.2 and 0.5 in figures

https://doi.org/10.1017/jfm.2014.365 Published online by Cambridge University Press

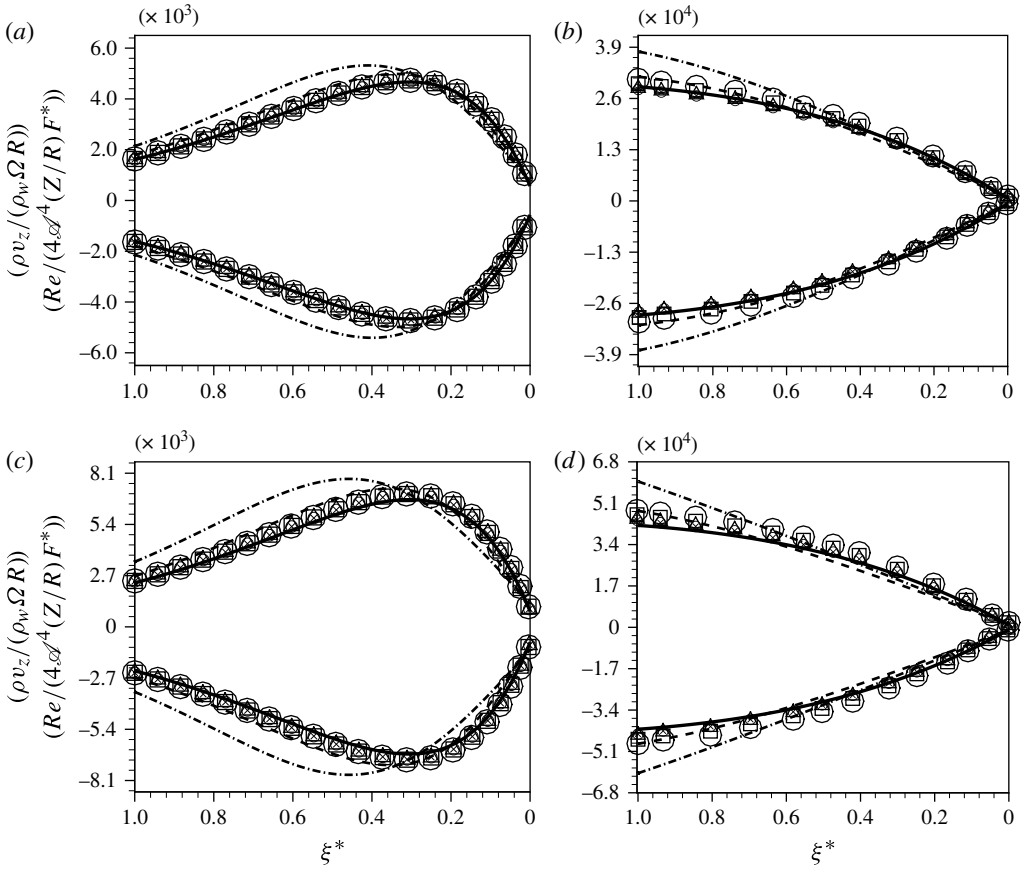


FIGURE 7. Axial mass flux, scaled by $(\rho_w \Omega R)(4\mathscr{A}^4(Z/R)F^*/Re)$, as a function of ξ^* at $\eta = 0.325$ and 0.675 for (a,c) $\mathscr{A} = 1.414$ and (b,d) $\mathscr{A} = 0.707$, for (a,b) $\epsilon_a = 0.2$ and (c,d) $\epsilon_a = 0.5$. The symbols show the DSMC results for $Re = 10^4$, $F^* = 0.1$ ($\otimes$), $Re = 10^4$, $F^* = 0.2$ ($\triangle$), $Re = 10^2$, $F^* = 0.1$ ($\square$), $Re = 10^2$, $F^* = 0.2$ ($\bigcirc$). The lines show the analytical solutions correct to $O(1)$ ($- \cdot - \cdot$), $O(\epsilon)$ ($- - -$) and $O(\epsilon^2)$ (——).

8 and 9. Progressing inwards from the wall of the cylinder, it is observed that there is an expansion of the boundary layer by a factor of 5 when the distance from the cylinder wall is increased from $\xi^* = 0.1$ to $\xi^* = 0.5$, while the mass flux remains a constant. The prediction for the radial velocity correct to $O(\epsilon^2)$ is in quantitative agreement with the DSMC solutions. The leading-order result (neglecting the mass difference between the two species) does capture the trends, but the magnitude is somewhat lower than the DSMC results.

An interesting feature is that the relative difference between the solutions correct to $O(1)$ and $O(\epsilon^2)$ for the Carrier–Maslen solutions is much smaller than that for the generalized Onsager model. There are two reasons for this. Firstly, the $O(\epsilon)$ corrections to the Carrier–Maslen equations could be incorporated within (5.21) for $\psi^{(0)}$, since these were known functions of the number and mass density in the base flow. Secondly, the inhomogeneous term in (5.22) for $\psi^{(2)}$ contains a factor of $1/Re$, which is small in the high-Reynolds-number limit. For these two reasons, the leading

https://doi.org/10.1017/jfm.2014.365 Published online by Cambridge University Press

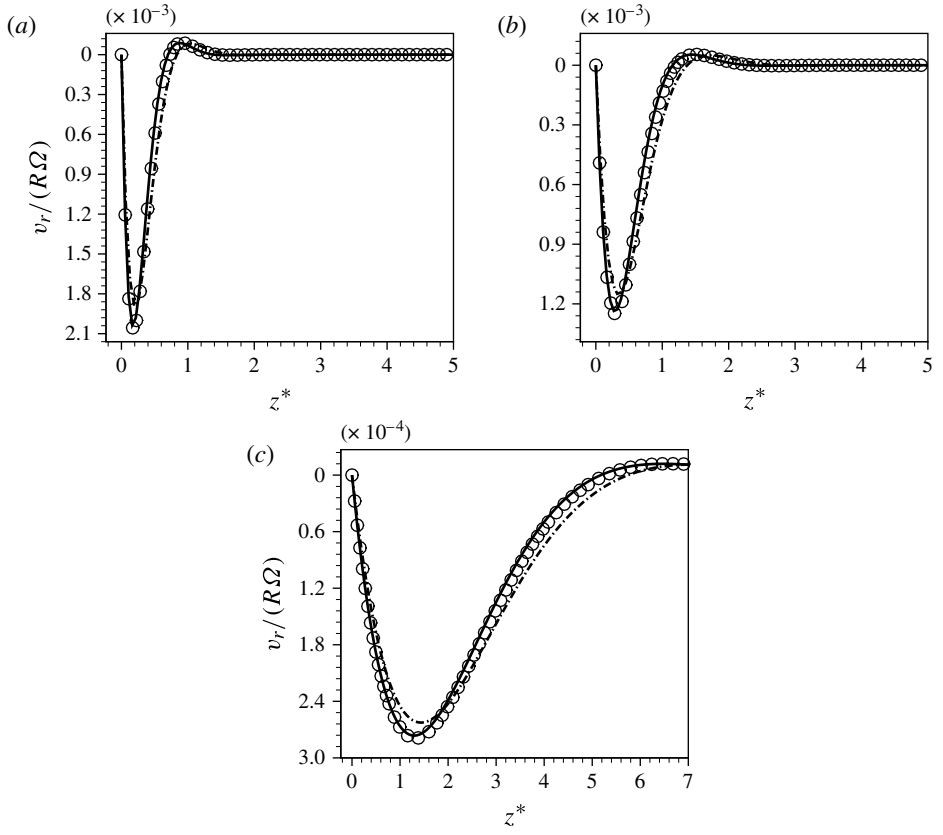


FIGURE 8. The radial velocity, scaled by $R\Omega$, as a function of scaled axial coordinate z^*, at (*a*) $\xi^* = 0.1$, (*b*) 0.2 and (*c*) 0.5, for $\mathscr{A} = 3.535$, $Re = 100$, $F^* = 0.2$ and $\epsilon_a = 0.5$. The DSMC results are shown by symbols (◯), and the lines show the analytical solutions correct to $O(1)$ (– · – ·), and $O(\epsilon^2)$ (——).

approximation for the generalized Carrier–Maslen equations gives a significantly more accurate solution in comparison to that for the generalized Onsager equation.

6.4. *Internal sources*

Next, we consider the axial flow generated by a momentum source in the θ direction. The analytical solution is independent of the Reynolds number and aspect ratio if the axial mass flux is scaled by $(\rho_w \Omega R,\ 4\mathscr{A}^4(Z/R)/Re)$. This scaled axial mass flux is plotted as a function of normalized radial scale height (ξ^*) for different stratification parameters and Reynolds numbers for an isothermal sidewall in figure 10. In the simulations, there is an increase in the frequency of collision of molecules when the wall is close to the momentum source, resulting in heating (close to the source there is an increase of 90 % in the temperature of the wall). In order to maintain a constant temperature, additional energy is removed from the wall at the location close to the source. It was earlier observed (Pradhan & Kumaran 2011) that there is much better agreement between simulations and theory when the constant-temperature boundary condition is enforced by energy removal from the wall. It should be noted that energy removal is necessary because the energy dissipation term (double dot

https://doi.org/10.1017/jfm.2014.365 Published online by Cambridge University Press

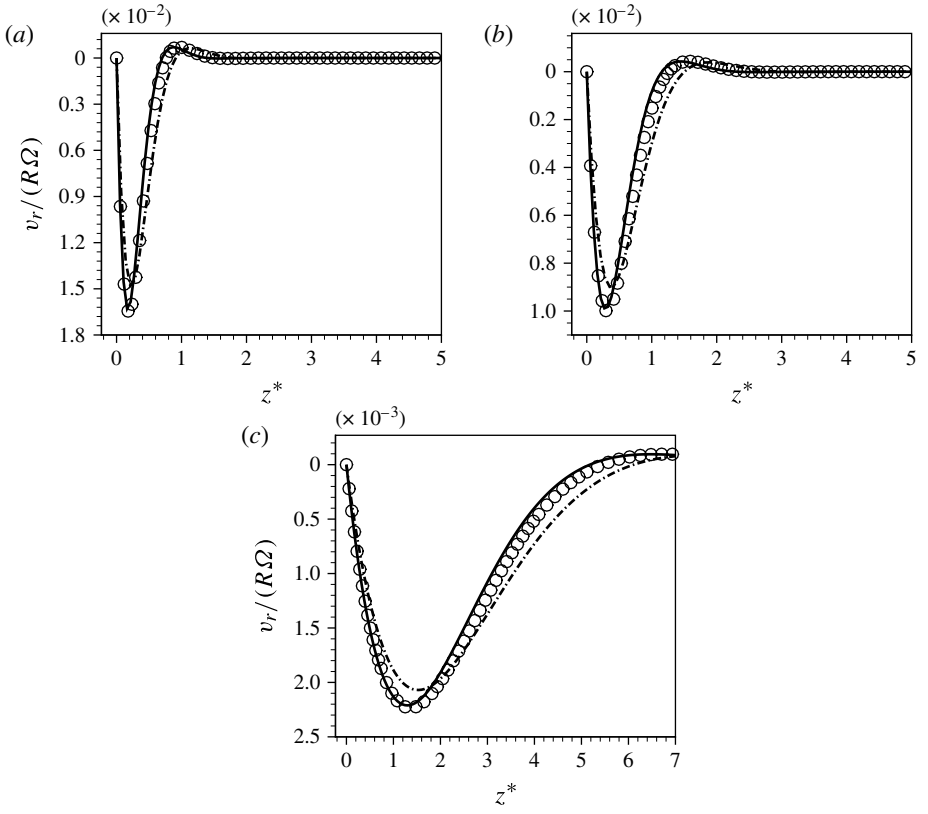


FIGURE 9. The radial velocity, scaled by $R\Omega$, as a function of scaled axial coordinate z^*, at (*a*) $\xi^* = 0.1$, (*b*) 0.2 and (*c*) 0.5, for $\mathscr{A} = 0.707$, $Re = 100$, $F^* = 0.2$ and $\epsilon_a = 0.5$. The DSMC results are shown by symbols (◯). The lines show the analytical solutions correct to $O(1)$ (– · – ·) and $O(\epsilon^2)$ (——).

product of the viscous stress and rate of deformation tensors) is second-order in the velocity perturbation. This is not included in the linearization approximation that we have used, as can be seen from the energy equation (3.11). Therefore, the viscous heating is not captured by the Onsager model, and it is necessary to explicitly remove energy to maintain a constant temperature at the wall.

The results with wall energy removal are shown at the axial location $\eta = 0.45$, which is close to the source, and where the axial slip velocity is a maximum. The mass flux is significantly higher when the source is placed inside the radial boundary layer, owing to the larger number density and the higher frequency of molecular collisions. In all cases, the solutions correct to $O(\epsilon^2)$ are in much better agreement with DSMC results than the $O(1)$ solutions, which do not incorporate the mass difference. There is a maximum difference of approximately 25 % between the analytical and DSMC results for the lowest stratification parameter 0.707 and Reynolds number 100 within the axial boundary layer, but there is quantitative agreement between analytical and DSMC results for higher values of the stratification parameter.

The scaled axial mass flux, non-dimensionalized by $(\rho_w \Omega R)(4\mathscr{A}^4(Z/R)/ReF^*)$, for a mass source and sink within the flow are plotted as a function of ξ for different stratification parameters and Reynolds numbers in figure 11. The results are plotted

https://doi.org/10.1017/jfm.2014.365 Published online by Cambridge University Press

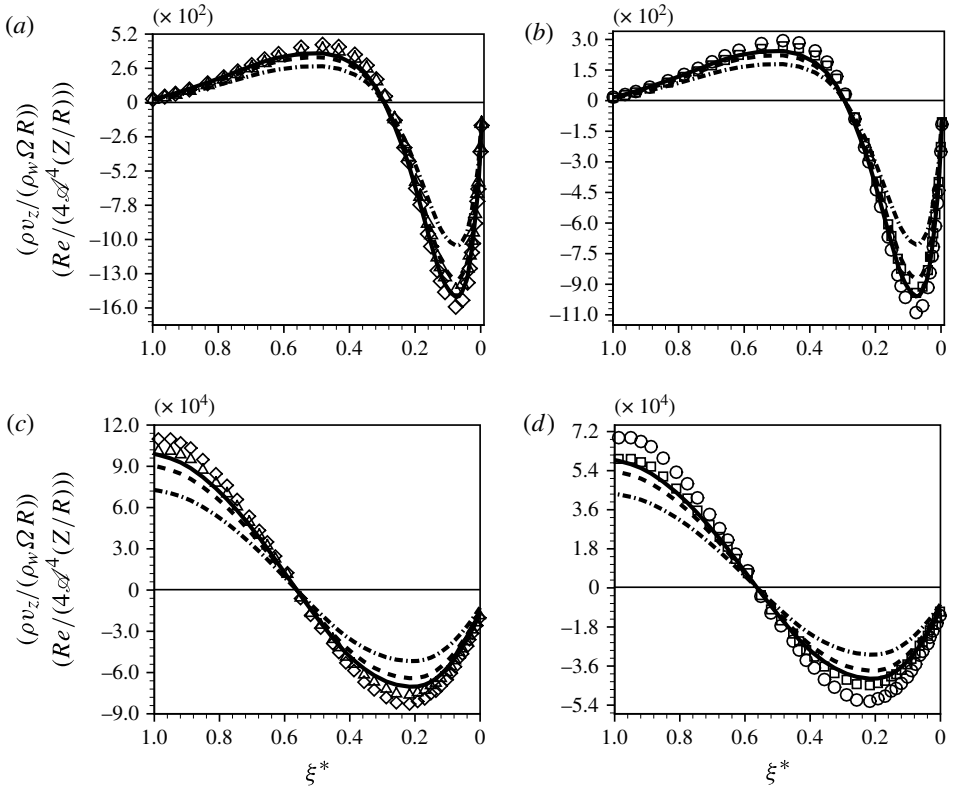


FIGURE 10. Axial mass flux, scaled by $\rho_w \Omega R$, $4\mathscr{A}^4(Z/R)/Re$, as a function of ξ^* at the axial location $\eta = 0.45$, scaled source strength = 0.2, for $\epsilon_a = 0.5$ and for (*a*,*b*) $\mathscr{A} = 2.121$ and (*c*,*d*) $\mathscr{A} = 0.707$, when the source is at $\eta = 0.5$ and is (*a*,*c*) within the radial boundary layer at $\xi_s^* = 0.01$ and (*b*,*d*) outside the radial boundary layer at $\xi_s^* = 0.25$. The symbols show the DSMC results for $Re = 10^2$, $\xi_s^* = 0.01$ ($\diamond$), $Re = 10^4$, $\xi_s^* = 0.01$ ($\triangle$), $Re = 10^2$, $\xi_s^* = 0.25$ ($\bigcirc$), $Re = 10^4$, $\xi_s^* = 0.25$ ($\square$). The lines show the analytical solutions correct to $O(1)$ (– · – ·), $O(\epsilon)$ (– – –) and $O(\epsilon^2)$ (——).

only at the axial location $\eta = 0.18$, where the axial velocity slip was found to be a maximum, and the difference between analytical and numerical results is a maximum. The qualitative trends in the mass flux are well captured by the leading-order solution, but the results are not in quantitative agreement with simulations. The $O(\epsilon^2)$ solutions are higher, by a factor of approximately 3/2, than the $O(1)$ solutions when the parameter ϵ_a is 0.5. However, the difference between the $O(\epsilon)$ and $O(\epsilon^2)$ solutions is much smaller, suggesting that the ϵ expansion is convergent even for $\epsilon_a = 0.5$. There is good quantitative agreement between the $O(\epsilon^2)$ solutions and the DSMC simulations, to within approximately 20 % for the lowest stratification parameter of 0.7071, aspect ratio 2 and at $Re = 100$. The results for higher aspect ratios, not shown here, are in even better agreement with the simulation results.

7. Conclusions

In this study, we examined how the species mass difference can be incorporated into the Onsager model to make it applicable to systems where the difference in

https://doi.org/10.1017/jfm.2014.365 Published online by Cambridge University Press

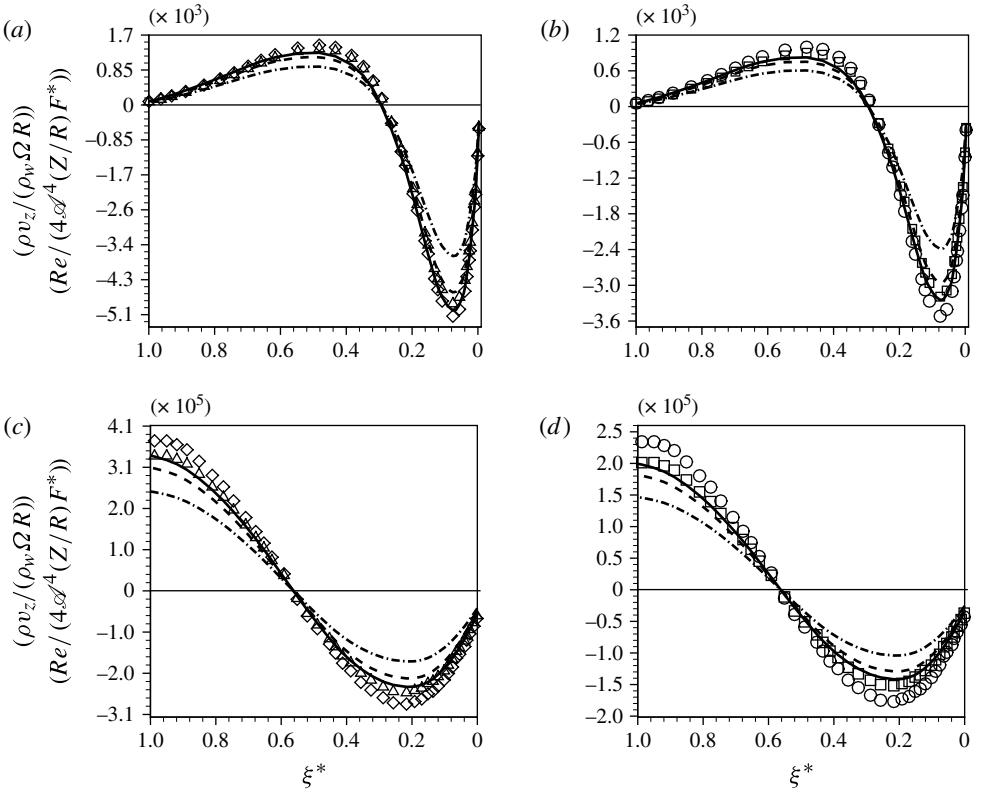


FIGURE 11. Axial mass flux, scaled by $(\rho_w\,\Omega R)(4\mathscr{A}^4(Z/R)/ReF^*)$, as a function of ξ^* for $F^* = 0.2$ and $\epsilon_a = 0.5$ at the axial location $\eta = 0.18$ for (a,b) $\mathscr{A} = 2.121$ and (c,d) $\mathscr{A} = 0.707$ when the source is (a,c) within the radial boundary layer at $\xi_s^* = 0.01$ and (b,d) outside the radial boundary layer at $\xi_s^* = 0.25$. The symbols show the DSMC results for $Re = 10^2$, $\xi_s^* = 0.01$ ($\diamond$), $Re = 10^4$, $\xi_s^* = 0.01$ ($\triangle$), $Re = 10^2$, $\xi_s^* = 0.25$ ($\circ$), $Re = 10^4$, $\xi_s^* = 0.25$ ($\square$). The lines show the analytical solutions correct to $O(1)$ (– · – ·), $O(\epsilon)$ (– – –) and $O(\epsilon^2)$ (——).

molecular masses is not much smaller than the average molecular mass. In the base state, the flow is considered to be a solid-body rotation with constant temperature, but the variation in the mole fraction is taken into account. Owing to this, there is a variation in the viscosity and thermal conductivity in the radial direction. In addition, the total pressure is written as the sum of partial pressures of the two species, and is not approximated as an exponential function of the distance from the wall. The dilute gas equation of state is used for the pressure, while the Chapman–Enskog theory (Chapman & Cowling 1970) for hard-sphere gases is used for the thermal conductivity and viscosity. It is important to note that all of the analysis has been carried out only for the simplest hard-sphere molecular model, in order to enable quantitative comparisons between the simulations and analytical solutions. For simulating real systems, it is necessary to use more realistic collision models, such as the variable hard-sphere model, which provide more realistic molecule–molecule and molecule–wall interactions.

In the analysis of the secondary flow, the equation for the master potential is expanded in an asymptotic series in the parameter $\epsilon = \Delta m/m_{av}$, where Δm is the

https://doi.org/10.1017/jfm.2014.365 Published online by Cambridge University Press

difference in the molecular masses of the two species, and m_{av} is a suitably defined average molecular mass based on the wall mass densities of the two species in the base state in order to simplify the algebra.

An important point to note is that this is not a regular perturbation expansion, where all quantities are expanded in a series in ϵ. Rather, we have attempted to use numerically accurate representations where possible. For example, a regular perturbation expansion would involve using ϵ expansions for (2.10) and (2.12) for the number and mass densities, and consequently expansions for the mean viscosity, thermal conductivity and pressure in (3.8)–(3.12). Here, we have chosen to use the actual functional forms for the mean quantities, and use an ϵ expansion only where it is absolutely necessary to reduce the equations to the generalized Onsager form. Owing to this, our solutions contain terms that would normally be higher-order in a regular ϵ expansion. For this reason, the solutions are expected to be more accurate than those obtained for a regular perturbation expansion.

The leading-order equation and boundary conditions for the master potential are nearly identical to the sixth-order differential equation of the generalized Onsager model (Pradhan & Kumaran 2011). The important difference is that the density and mole fraction are not assumed to decrease exponentially from the wall, but the actual species densities and mole fraction are used. The mean velocity and temperature obtained by solving the leading-order equations are used in the species balance equations for the mole fractions of the two species, and the corrections for the number density and mass density of the two species due to the secondary flow are obtained. These appear as inhomogeneous terms in the equation for the $O(\epsilon)$ correction for the master potential. This equation is solved with appropriate boundary conditions to obtain the $O(\epsilon)$ correction to the master potential and flow velocity. This is then used in the $O(\epsilon)$ contribution to the species balance equation, and the hierarchical procedure is repeated until the $O(\epsilon^2)$ correction to the secondary flow velocity and mole fraction are calculated. A similar hierarchical procedure is used for the Carrier–Maslen model for the end-cap boundary layers.

The results of the Onsager hierarchy, up to $O(\epsilon^2)$, are compared with the results of DSMC simulations for the axisymmetric flow of a two-species hard-sphere molecular gas. The constitutive relations for mass diffusion, viscosity and heat conduction predicted by the DSMC simulations are compared with the Chapman–Enskog theory (Chapman & Cowling 1970) in order to validate the constitutive relations used in the analysis. After this, the results of the $O(\epsilon^2)$ Onsager hierarchy for the secondary flow are compared with DSMC simulations for three types of forcing: a wall temperature gradient, inflow/outflow of gas along the axis, and mass/momentum input due to inserts within the flow.

In all cases, the comparison with DSMC simulations reveals that the analytical solution correct to $O(\epsilon^2)$ is in quantitative agreement with the DSMC results in all cases. There is agreement to within 15–20 % even at the lowest Reynolds number of 100, the lowest stratification parameter of 0.707, the lowest aspect ratio $Z/D = 2$, a large mass difference $\epsilon_a = 0.5$ (corresponding to a mixture of CO_2 and CH_4, for example) and for scaled secondary forcing as large as 0.2 in all cases. The leading-order solutions do capture the correct trends in all cases, but the magnitudes of the secondary flow are only a fraction (between 1/2 and 2/3) of the solutions correct to $O(\epsilon^2)$. This shows that the Onsager model, which was originally formulated for isotope separation where the mass difference is negligible, can be fruitfully extended using an expansion in the ratio of the mass difference and average mass, to

https://doi.org/10.1017/jfm.2014.365 Published online by Cambridge University Press

predict the secondary flow in binary mixtures with relatively large mass differences at low rotation speeds in systems of practical interest.

Acknowledgements

The authors would like to thank the Department of Science and Technology, Government of India, for financial support. We thank Dr A. Chandrashekara, Bhabha Atomic Research Centre, India, for his kind support during the completion of this work.

Appendix A. Expressions for the viscosity, thermal conductivity and diffusion coefficient

For a hard-sphere gas, the viscosity, thermal conductivity and diffusivity can be expressed as functions of the mole fractions of the two species as (Chapman & Cowling 1970)

$$\left.\begin{aligned} \mu &= \frac{N_1^2 R_1 + N_2^2 R_2 + N_1 N_2 R'_{12}}{(N_1^2 R_1/\mu_1) + (N_2^2 R_2/\mu_2) + N_1 N_2 R_{12}}, \\ K &= \frac{N_1^2 Q_1 K_1 + N_2^2 Q_2 K_2 + N_1 N_2 Q'_{12}}{N_1^2 Q_1 + N_2^2 Q_2 + N_1 N_2 Q_{12}}, \\ D_{12} &= \frac{3E}{2n(m_1+m_2)}, \\ k_T &= \frac{5CN_1N_2\,(N_1S_1 - N_2S_2)}{N_1^2 Q_1 + N_2^2 Q_2 + N_1 N_2 Q_{12}}, \end{aligned}\right\} \tag{A 1}$$

where μ_1 and μ_2 are the viscosities of the pure components at temperature $\bar{T}$,

$$\mu_i = \frac{5}{16 d_i^2}\sqrt{\frac{m_i k_B T}{\pi}}, \tag{A 2}$$

$\bar{K}_1$ and $\bar{K}_2$ are the thermal conductivities of the pure components at temperature $\bar{T}$,

$$K_i = \frac{75}{64 d_i^2}\sqrt{\frac{k_B^3 T}{\pi m_i}}, \tag{A 3}$$

and the coefficients in equations (A 1) are

$$M_1 = m_1/(m_1+m_2), \tag{A 4}$$

$$M_2 = m_2/(m_1+m_2), \tag{A 5}$$

$$E = \left(\frac{2k_B T(m_1+m_2)^3}{\pi m_1 m_2}\right)^{1/2} \frac{1}{2(d_1+d_2)^2}, \tag{A 6}$$

$$Q_1 = P_1(6M_2^2 + 5M_1^2 - 4M_1^2 B + 8M_1M_2A), \tag{A 7}$$

$$Q_2 = P_2(6M_1^2 + 5M_2^2 - 4M_2^2 B + 8M_1M_2A), \tag{A 8}$$

$$Q_{12} = 3(M_1-M_2)^2(5-4B) + 4M_1M_2A(11-4B) + 2P_1P_2, \tag{A 9}$$

$$Q'_{12} = \frac{30k_BE}{4(M_1+M_2)}[P_1 + P_2 + (11-4B-8A)M_1M_2], \tag{A 10}$$

https://doi.org/10.1017/jfm.2014.365 Published online by Cambridge University Press

$$P_1 = \frac{15k_BE}{4(m_1+m_2)K_1}, \tag{A 11}$$

$$P_2 = \frac{15k_BE}{4(m_1+m_2)K_2}, \tag{A 12}$$

$$S_1 = M_1P_1 - M_2[3(M_2-M_1)+4M_1A], \tag{A 13}$$

$$S_2 = M_2P_2 - M_1[3(M_1-M_2)+4M_2A], \tag{A 14}$$

$$R_1 = 2/3 + (M_1/M_2)A, \tag{A 15}$$

$$R_2 = 2/3 + (M_2/M_1)A, \tag{A 16}$$

$$R'_{12} = E/(2\mu_1) + E/(2\mu_2) + 2(2/3-A), \tag{A 17}$$

$$R_{12} = \frac{E}{2\mu_1\mu_2} + \frac{4A(m_1+m_2)^2}{3Em_1m_2}, \tag{A 18}$$

$$A = 2/5, \tag{A 19}$$

$$B = 3/5, \tag{A 20}$$

$$C = 1/5. \tag{A 21}$$

Appendix B. Conservation equations in cylindrical coordinates

The mass conservation equation for an axisymmetric flow in cylindrical coordinates at steady state is

$$\boldsymbol{\nabla}\cdot(\rho\boldsymbol{v}) = \mathscr{S}_m, \tag{B 1}$$

where $\mathscr{S}_m$ is the mass source (rate of addition of mass per unit volume per unit time). The radial, meridional and axial momentum conservation equations at steady state are

$$\rho\left(v_r\frac{\partial v_r}{\partial r} - \frac{v_\theta^2}{r} + v_z\frac{\partial v_r}{\partial z}\right) = -\frac{\partial p}{\partial r} + \left[\frac{1}{r}\frac{\partial(r\tau_{rr})}{\partial r} - \frac{\tau_{\theta\theta}}{r} + \frac{\partial\tau_{rz}}{\partial z}\right] + f_r, \tag{B 2}$$

$$\rho\left(v_r\frac{\partial v_\theta}{\partial r} + \frac{v_rv_\theta}{r} + v_z\frac{\partial v_\theta}{\partial z}\right) = \left[\frac{1}{r^2}\frac{\partial(r^2\tau_{r\theta})}{\partial r} + \frac{\partial\tau_{\theta z}}{\partial z}\right] + f_\theta, \tag{B 3}$$

$$\rho\left(v_r\frac{\partial v_z}{\partial r} + v_z\frac{\partial v_z}{\partial z}\right) = -\frac{\partial p}{\partial z} + \left[\frac{1}{r}\frac{\partial(r\tau_{rz})}{\partial r} + \frac{\partial\tau_{zz}}{\partial z}\right] + f_z, \tag{B 4}$$

where f_r, f_θ and f_z are the force densities (force per unit volume) in the r, θ and z directions, respectively. The energy conservation equation is

$$\begin{aligned}\rho C_v\left(\frac{\partial T}{\partial t} + v_r\frac{\partial T}{\partial r} + v_z\frac{\partial T}{\partial z}\right) = {} & -p(\boldsymbol{\nabla}\cdot\boldsymbol{v}) + \tau_{rr}\frac{\partial v_r}{\partial r} + \tau_{\theta\theta}\frac{v_r}{r} + \tau_{zz}\frac{\partial v_z}{\partial z} \\ & + \tau_{r\theta}\left(r\frac{\partial}{\partial r}\left(\frac{v_\theta}{r}\right)\right) + \tau_{\theta z}\left(\frac{\partial v_\theta}{\partial z}\right) + \tau_{rz}\left(\frac{\partial v_z}{\partial r} + \frac{\partial v_r}{\partial z}\right) \\ & + \frac{1}{r}\frac{\partial}{\partial r}\left(rK\frac{\partial T}{\partial r}\right) + \frac{\partial}{\partial z}\left(K\frac{\partial T}{\partial z}\right) + \mathscr{S}_e,\end{aligned} \tag{B 5}$$

where $\mathscr{S}_e$ is the rate of addition of energy per unit volume per unit time. Here,

$$\boldsymbol{\nabla}\cdot\boldsymbol{v} = \frac{1}{r}\frac{\partial(rv_r)}{\partial r} + \frac{\partial v_z}{\partial z}, \tag{B 6}$$

$$\tau_{rr} = \mu\left(2\frac{\partial v_r}{\partial r} - \frac{2}{3}\boldsymbol{\nabla}\cdot\boldsymbol{v}\right), \tag{B 7}$$

$$\tau_{\theta\theta} = \mu\left(2\frac{v_r}{r} - \frac{2}{3}\boldsymbol{\nabla}\cdot\boldsymbol{v}\right), \tag{B 8}$$

https://doi.org/10.1017/jfm.2014.365 Published online by Cambridge University Press

$$\tau_{zz} = \mu\left(2\frac{\partial v_z}{\partial z} - \frac{2}{3}\boldsymbol{\nabla}\cdot\boldsymbol{v}\right), \tag{B 9}$$

$$\tau_{r\theta} = \mu\left(r\frac{\partial}{\partial r}\left(\frac{v_\theta}{r}\right)\right), \tag{B 10}$$

$$\tau_{rz} = \mu\left(\frac{\partial v_r}{\partial z} + \frac{\partial v_z}{\partial r}\right), \tag{B 11}$$

$$\tau_{\theta z} = \mu\left(\frac{\partial v_\theta}{\partial z}\right). \tag{B 12}$$

Appendix C. DSMC simulation

Before proceeding to simulate the centrifugal separation of gas mixtures, we first compare the DSMC result for the viscosity and thermal conductivity of a gas mixture with the theoretical prediction of the Chapman–Enskog theory (Chapman & Cowling 1970) for a dilute gas for a plane Couette flow in order to validate the simulation procedure, and compare the transport properties with the theoretical expressions given in appendix C. The fluid is a hard-sphere gas mixture in which both species have equal molecular diameter $d = 5.5 \times 10^{-10}$ m, average molecular mass $m_{av} = (m_1 + m_2)/2 = 58.4426 \times 10^{-26}$ kg/molecule, specific heat ratio $\gamma = 1.66$ and average number density 1.4×10^{20} m^{-3}. The pressure is set equal to a constant value, $p = nk_BT = 0.5275$ N m^{-2}, throughout the simulations. Two different relative masses for the two components, $\epsilon_a = 2(m_1 - m_2)/(m_1 + m_2) = 0.2$ and 0.5, are used in the simulations. The DSMC simulations are performed with different mole fractions of component 1 (N_1), which is the lighter component, to predict the variation of transport properties with composition. The viscosity, thermal conductivity and diffusivity of pure components based on the Chapman–Enskog theory (Chapman & Cowling 1970) using the first two terms in the Sonine polynomial expansion, and from DSMC simulations are given for $\epsilon_a = 2\Delta m/(m_1 + m_2) = 0.2$ and 0.5 in table 1.

The computational domain consists of the flow between two parallel plates, in the x–z plane separated by a distance $L_y = 0.01$ m in the y direction (a specific aspect ratio $L_x : L_y : L_z = 2 : 1 : 1$ is chosen to facilitate the DSMC simulations), as shown in figure 12. One surface is stationary, while the other is moving with a velocity $v_x = 300$ m s^{-1} in the x direction. The surfaces are maintained at a constant temperature of 300 K. Periodic boundary conditions are used in the x and z directions, while the boundary conditions at the walls $y = 0$ and $y = L_y$ are diffuse reflection conditions with accommodation coefficient 1 (the post-collisional velocities of the molecules at the wall are chosen from a Maxwell–Boltzmann distribution with mean velocity equal to the wall velocity and temperature equal to the wall temperature). The number of cells along the x, y and z directions are 100, 50 and 50, respectively. There are eight subcells in each cell. The average number of simulated particles in each cell is 100. For the densities simulated here, the number of real molecules per simulated molecule varies between 10^{16} and 10^{18}. The cell arrangement is shown in figure 12.

The velocity, temperature and mole fraction profiles for plane Couette flow are shown in figure 13 for wall temperature 300 K. The viscous energy dissipation results in an increase in the temperature in the gas, and the maximum temperature of 428 K is observed at the mid-plane between the two walls. It should be noted that there is both a small velocity slip as well as a temperature slip at the wall. The pressure and shear stress are uniform throughout the gas, and the temperature variation leads to a variation in the density in accordance with the ideal gas equation

https://doi.org/10.1017/jfm.2014.365 Published online by Cambridge University Press

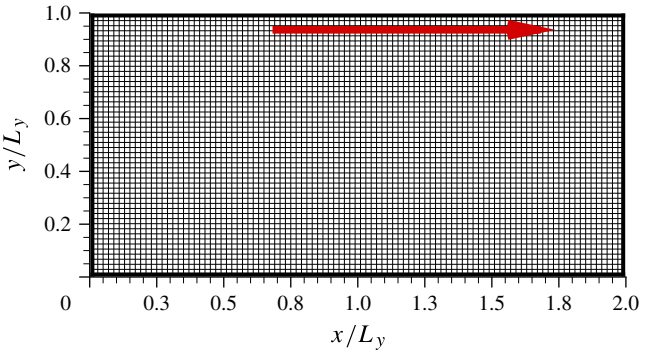


FIGURE 12. (Colour online) Computational domain and coordinate system for a plane Couette flow. The two parallel plates are separated by a distance $L_y = 0.01$ m in the y direction, and periodic boundary conditions are used in the x and z directions. The top plate velocity is $v_x = 300$ m s^{-1}, and the bottom plate is stationary. Both plates are at the same temperature $T_w = 300$ K. The average molecular mass $m_{av} = (m_1 + m_2)/2 = 58.4426 \times 10^{-26}$ kg/molecule, and average number density 1.4×10^{20} m^{-3}, with 50 % mixture.

Property	ϵ_a	Analytical	DSMC
μ_1	0.2	2.721×10^{-5}	2.717×10^{-5}
μ_2	0.2	3.007×10^{-5}	3.002×10^{-5}
μ_1	0.5	2.488×10^{-5}	2.484×10^{-5}
μ_2	0.5	3.202×10^{-5}	3.197×10^{-5}
$(nD)_1$	0.2	6.205×10^{19}	6.195×10^{19}
$(nD)_2$	0.2	5.616×10^{19}	5.610×10^{19}
$(nD)_1$	0.5	6.812×10^{19}	6.781×10^{19}
$(nD)_2$	0.5	5.261×10^{19}	5.257×10^{19}
$\bar{K}_1$	0.2	2.676×10^{-3}	2.660×10^{-3}
$\bar{K}_2$	0.2	2.422×10^{-3}	2.421×10^{-3}
$\bar{K}_1$	0.5	2.927×10^{-3}	2.918×10^{-3}
$\bar{K}_2$	0.5	1.932×10^{-3}	1.930×10^{-3}

TABLE 1. The coefficient of viscosity μ (kg m^{-1} s^{-1}), number density times diffusion coefficient nD (m^{-1} s^{-1}) and thermal conductivity $\bar{K}$ (W m^{-1} K^{-1}) of pure components, with average molecular mass $m_{av} = (m_1 + m_2)/2 = 58.4426 \times 10^{-26}$ kg/molecule, and with $\epsilon_a = 2\Delta m/(m_1 + m_2) = 0.2$ and 0.5 based on Chapman–Enskog theory (Chapman & Cowling 1970) and DSMC simulations at temperature 300 K. The system was discretized into 100 intervals in the flow direction and 50 intervals each in the other two directions, and there were 100 molecules per cell on average. Averages were obtained over 10^6 collisions per molecule.

of state. Since the number density is changing with position, there is a variation of mole fraction with position as well, as shown in figure 13. The results of the simulation are compared with the results of the continuum equations,

https://doi.org/10.1017/jfm.2014.365 Published online by Cambridge University Press

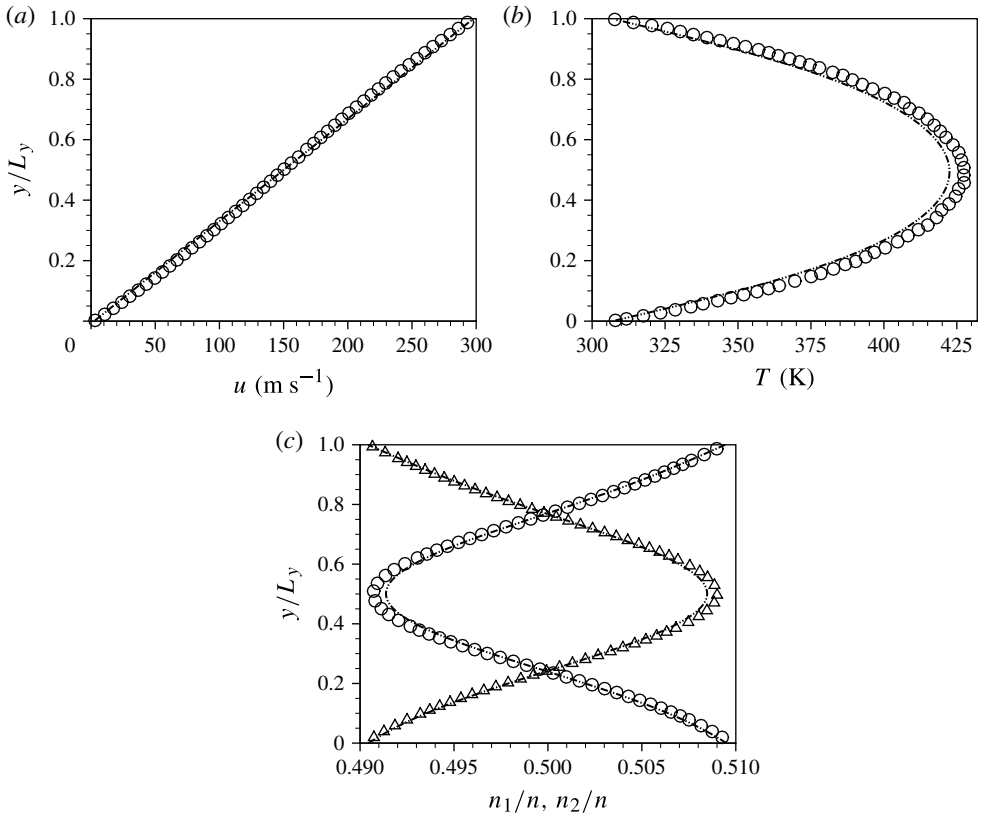


FIGURE 13. (*a*) The velocity, (*b*) temperature and (*c*) mole fraction profiles in the plane Couette flow of a binary mixture with average molecular mass $m_{av} = (m_1 + m_2)/2 = 58.4426 \times 10^{-26}$ kg/molecule, $\epsilon_a = 2\Delta m/(m_1 + m_2) = 0.5$. The symbols show the DSMC results for the velocity and temperature profiles in panels (*a*) and (*b*), and n_1/n (△) and n_2/n (◯) in panel (*c*). The line (– · · – · ·) shows the analytical solution for slip boundary conditions.

$$\tau_{xy} = \mu \frac{\mathrm{d}v_x}{\mathrm{d}y}, \tag{C 1}$$

$$\frac{\mathrm{d}}{\mathrm{d}y}\left(K\frac{\mathrm{d}T}{\mathrm{d}y}\right) + \mu\left(\frac{\mathrm{d}v_x}{\mathrm{d}y}\right)^2 = 0, \tag{C 2}$$

$$\frac{\mathrm{d}N_1}{\mathrm{d}y} + \frac{k_T}{T}\frac{\mathrm{d}T}{\mathrm{d}y} = 0, \tag{C 3}$$

where the mixture viscosity and thermal conductivity are given in (A 1) in appendix A. Equations (C 1)–(C 3) are solved with the boundary conditions for the velocity and temperature and no-flux conditions at the wall, and symmetry conditions at the axis, to obtain the final velocity and temperature profiles shown in figure 13(*a*,*b*). The mole fraction profiles, in figure 13(*c*), show the effect of diffusion due to a temperature gradient, where the lighter component diffuses towards the region of higher temperature, and the heavier component moves towards the region of lower

https://doi.org/10.1017/jfm.2014.365 Published online by Cambridge University Press

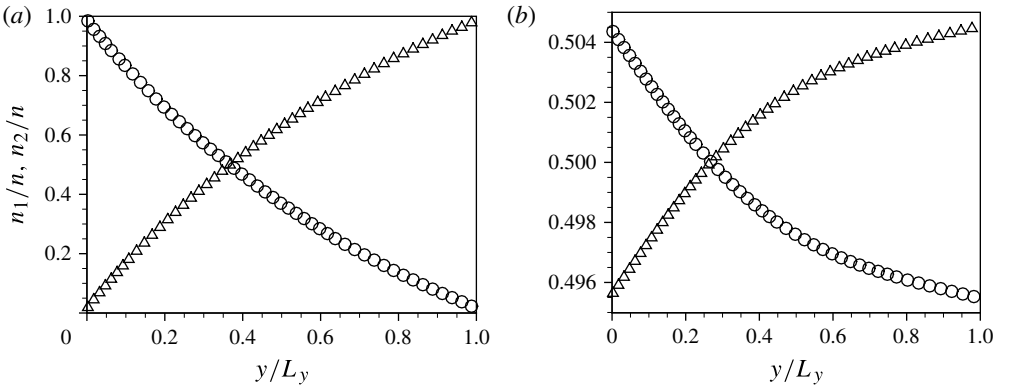


FIGURE 14. Mole fractions n_1/n (△) and n_2/n (○) as functions of position (y/L_y) for (*a*) concentration diffusion and (*b*) thermal diffusion for $\epsilon_a = 2\Delta m/(m_1 + m_2) = 0.5$.

temperature. In all cases, the simulation results are in quantitative agreement with the theoretical solutions of (C 1)–(C 3).

The mass and thermal diffusion coefficients for a binary mixture are studied using the same configuration as that in figure 12. For the mass diffusion, instead of using solid walls at $y = 0$ and $y = L_y$, we consider two pure component gases of species 2 at $y < 0$, and species 1 at $y > L_y$. The molecules are allowed to diffuse in the channel, with the restriction that there are only molecules of species 1 and 2 entering from $y < 0$ and $y > L_y$, respectively. The system is permitted to equilibrate until the concentration field is independent of time and the temperature is a constant. The results of the simulation are compared with the equation (Chapman & Cowling 1970)

$$\begin{aligned} \bar{\boldsymbol{c}}_1 - \bar{\boldsymbol{c}}_2 &= -\frac{n^2}{n_1 n_2} D_{12} \boldsymbol{d}_{12} - \frac{n^2}{n_1 n_2} D_T \nabla(\log_e(T)), \\ &= -\frac{D_{12}}{N_1 N_2} \left(\nabla N_1 + \frac{N_1 N_2 (m_2 - m_1)}{\rho k_B T} \nabla p + k_T \nabla(\log_e(T)) \right), \end{aligned} \tag{C 4}$$

where $\bar{\boldsymbol{c}}_1$ and $\bar{\boldsymbol{c}}_2$ are the species averaged velocities. Since the temperature and pressure are independent of position in the simulation, the diffusion coefficient can be evaluated as $D_{12} = -N_1 N_2 (\bar{\boldsymbol{c}}_1 - \bar{\boldsymbol{c}}_2)/(\mathrm{d}N_1/\mathrm{d}y)$. In order to determine the thermal diffusion coefficient, the walls at $y = 0$ and $y = L_y$ are maintained at two different temperatures, $y = 0$ at 300 K, and $y = L_y$ at 360 K. The system is equilibrated and the mole fractions of the two species are calculated. The thermal diffusion coefficient, $\alpha_T = k_T/N_1 N_2$, is then determined from (2.1) for the flux. The mole fraction profiles for mass and thermal diffusion are shown in figure 14(*a*,*b*).

A more microscopic comparison is provided by plotting ratios $\tau_{xy}/(T^{1/2}(\mathrm{d}v_x/\mathrm{d}y))$ and $q_y/(T^{1/2}(\mathrm{d}T/\mathrm{d}y))$ as functions of the mole fraction in figure 15(*a*,*b*). Here, the stress and heat flux are calculated from the second and third moments of the molecular velocity distributions (Chapman & Cowling 1970). Equations (A 1) in appendix A show that the mixture viscosity and thermal conductivity are proportional to the square root of the absolute temperature and independent of the number density, so the ratio $\tau_{xy}/(T^{1/2}(\mathrm{d}v_x/\mathrm{d}y))$ and $q_y/(T^{1/2}(\mathrm{d}T/\mathrm{d}y))$ are functions of only the mole fraction. Figure 15(*a*,*b*) shows that there is excellent agreement between

https://doi.org/10.1017/jfm.2014.365 Published online by Cambridge University Press

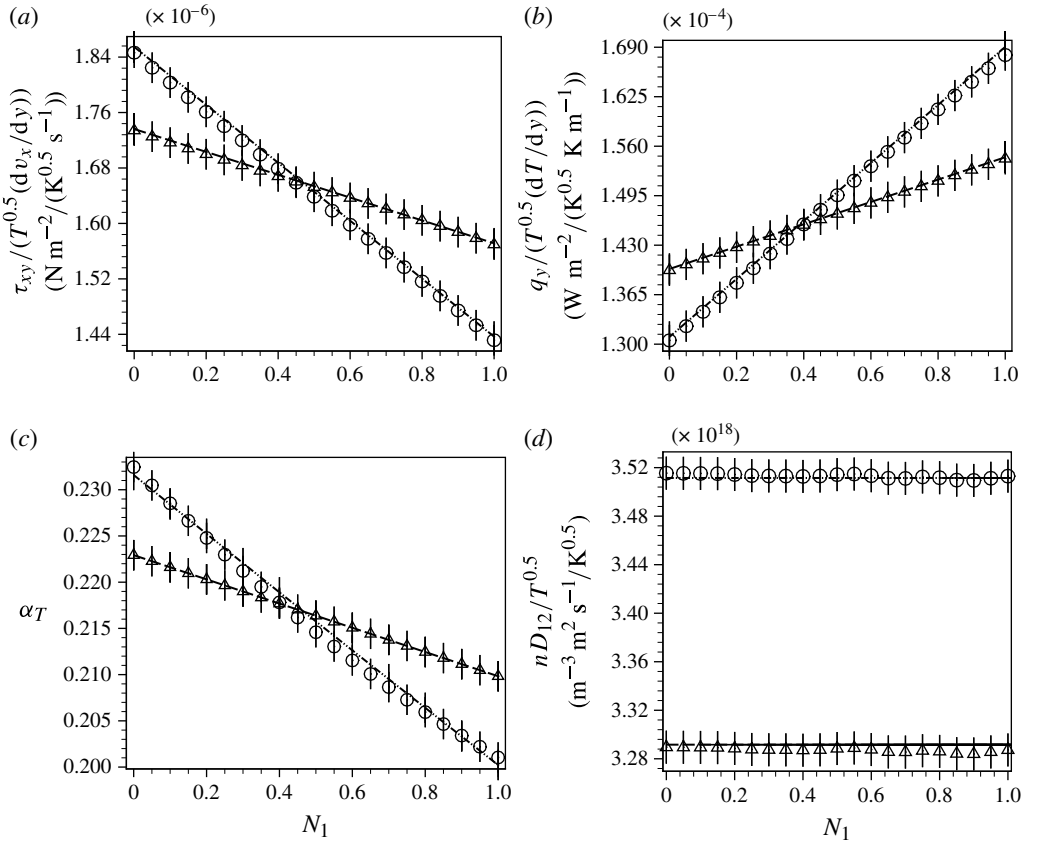


FIGURE 15. The ratios (*a*) $\tau_{xy}/(T^{1/2}(\mathrm{d}v_x/\mathrm{d}y))$ and (*b*) $q_y/(T^{1/2}(\mathrm{d}T/\mathrm{d}y))$, (*c*) the thermal diffusion factor $\alpha_T = (1/(N_1 N_2))k_T = (1/(N_1 N_2))\,(\mathrm{d}N_1/\mathrm{d}y)/(T^{-1}\mathrm{d}T/\mathrm{d}y)$ and (*d*) the ratio $nD_{12}/\sqrt{T}$ as functions of mole fraction of component 1 (N_1). The symbols show the DSMC results for $\epsilon_a = 0.2$ (△) and $\epsilon_a = 0.5$ (◯), and the lines show the analytical results for $\epsilon_a = 0.2$ (– – –) and $\epsilon_a = 0.5$ (– · · – · ·). DSMC results are shown at $y/L_y = 0.5$. The error bars show the standard deviation over four different DSMC runs carried out after equilibration, each for 10^6 collisions per molecule.

the theoretical predictions and the simulation results for the thermal conductivity and viscosity for hard-sphere gases. Next, we compare the results of (A 1) for the thermal diffusion coefficient k_T with experiments. The thermal diffusion coefficient is independent of temperature and number density, and is a function only of the mole fraction. It is more convenient to compare the thermal diffusion factor $\alpha_T = k_T/N_1N_2 = (1/N_1N_2)(\mathrm{d}N_1/\mathrm{d}y)/(T^{-1}\,\mathrm{d}T/\mathrm{d}y)$ as a function of the mole fraction of component 1 (N_1), as shown in figure 15(*c*). From (A 1), the diffusion coefficient is proportional to $\sqrt{T}/n$, and independent of mole fraction, while α_T is independent of number density and temperature. Therefore, α_T and $nD_{12}/\sqrt{T}$ are plotted as functions of mole fraction of component 1 (N_1) in figure 15(*c*,*d*). The error bars show the standard deviation over four different DSMC runs carried out after equilibration, each for 10^6 collisions per molecule. There is excellent agreement between the simulations and the Chapman–Enskog theory to within the error bars in the simulations.

https://doi.org/10.1017/jfm.2014.365 Published online by Cambridge University Press

REFERENCES

BERGER, M. H. 1987 Finite element analysis of flow in a gas-filled rotating annulus. *Intl J. Numer. Meth. Fluids* **7**, 215–231.

BIRD, G. A. 1994 *Molecular Gas Dynamics and the Direct Simulation of Gas Flows*. Clarendon Press.

CHAPMAN, S. & COWLING, T. G. 1970 *The Mathematical Theory of Non-Uniform Gases*. Cambridge University Press.

GUNZBURGER, M. D. & WOOD, H. G. 1982 A finite element method for the Onsager pancake equation. *Comput. Meth. Appl. Mech. Engng* **31**, 43–59.

GUNZBURGER, M. D., WOOD, H. G. & JORDAN, J. A. 1984 A finite element method for gas centrifuge problem. *SIAM J. Sci. Stat. Comput.* **5**, 78–94.

LAHARGUE, J. P. & SOUBBARAMAYER 1978 A numerical model for the investigation of the flow and isotope concentration field in an ultracentrifuge. *Comput. Meth. Appl. Mech. Engng* **15** (2), 259–273.

OLANDER, D. R. 1981 The theory of uranium enrichment by the gas centrifuge. *Prog. Nucl. Energy* **8**, 1–33.

PRADHAN, S. & KUMARAN, V. 2011 The generalized Onsager model for the secondary flow in a high-speed rotating cylinder. *J. Fluid Mech.* **686**, 109–159.

ROBERTS, W. W. 1985 Three dimensional stratified gas flows past impact probes and scoops: *N*-body Monte Carlo calculations. In *Proc. Sixth Workshop on Gases in Strong Rotation, Tokyo* (ed. Y. Takashima), p. 115.

ROBERTS, W. W. & HAUSMAN, M. A. 1988 Hypersonic, stratified gas flows past an obstacle: direct simulation Monte Carlo calculations. *J. Comput. Phys.* **77**, 283–317.

SOUBBARAMAYER & BILLET, J. 1980 A numerical method for optimizing the gas flow field in a centrifuge. *Comput. Meth. Appl. Mech. Engng* **24**, 165–185.

VIECELLI, J. A. 1983 Exponential difference operator approximation for the sixth order Onsager equation. *J. Comput. Phys.* **50**, 162–170.

WOOD, H. G., JORDAN, J. A. & GUNZBURGER, M. D. 1984 The effect of curvature on the flow field in rapidly rotating gas centrifuges. *J. Fluid Mech.* **140**, 373–395.

WOOD, H. G., MASON, T. C. & SOUBBARAMAYER 1996 Multi-isotope separation in a gas centrifuge using Onsager's pancake model. *Sep. Sci. Technol.* **31** (9), 1185–1213.

WOOD, H. G. & MORTON, J. B. 1980 Onsager's pancake approximation for the fluid dynamics of a gas centrifuge. *J. Fluid Mech.* **101**, 1–31.

WOOD, H. G. & SANDERS, G. 1983 Rotating compressible flows with internal sources and sinks. *J. Fluid Mech.* **127**, 299–311.

https://doi.org/10.1017/jfm.2014.365 Published online by Cambridge University Press